Reconstitution and functional characterisation of simple channel proteins in the planar lipid bilayer

Vom Fachbereich Biologie der Technischen Universität Darmstadt zur Erlangung des akademischen Grades eines Doctor rerum naturalium genehmigte Dissertation von

Dipl.-Biologen Michael Henkel
aus
Wiesbaden-Sonnenberg

Berichterstatter: Prof. Dr. Gerhard Thiel
Mitberichterstatter: Prof. Dr. Ralf A. W. Galuske
Tag der Einreichung: 22.06.2010
Tag der mündlichen Prüfung: 3.09.2010

Erscheinungsort: Darmstadt
Erscheinungsjahr: 2010

D17

Zusammenfassung

Die vorliegende Arbeit behandelt die elektrophysiologische Charakterisierung verschiedener primitiver kanalbildener Proteine bzw. Peptide.

Mithilfe der sogenannten `planaren Lipid Bilayer Technik`, welches ein maximal artifizielles System zur funktionellen Rekonstitution und zur Untersuchung von gereinigten Kanalproteinen darstellt, wurden protein-/ peptidvermittelte Einzelkanalströme gemessen. In Abhängigkeit von definierten Ionenkonzentrationen in den Badlösungen auf der cis- und trans-Seite einer Membran ließen sich die für die Proteine typischen Eigenschaften wie Strom/ Spannungs-Beziehungen, Offenwahrscheinlichkeiten, sowie Selektivitäten ermitteln.

Kapitel 2 behandelt den Wildtyp, sowie zwei unterschiedliche Mutanten von Kcv, einem tetrameren Kaliumkanal, welcher von dem *Paramecium bursaria Chlorella* Virus 1 (PBCV-1) kodiert wird. Die Daten zeigen, dass die subtile Mutation (T->S am Rest 63), einer zur Kavität des Kanals angrenzenden Aminosäure im Selektivitätsfilter, die Blockierbarkeit des Wildtyps durch Barium nahezu gänzlich aufzuheben vermag. Darüber hinaus verursacht die Mutation eine deutlich erhöhte Offenwahrscheinlichkeit des Kanals, wobei der Kanal jedoch nur selten die volle Leitfähigkeit erlangt; meist öffnet der Kanal nur zu verschiedenen Unterleitwerten. Wahrscheinlich reflektieren diese Unterleitwerte unterschiedliche kinetische Zustände des Kanals; Simulationen auf Grundlage von Markov-Modellen zeigen, dass ein sehr schnelles Gating, in Kombination mit einer limitierten Registrierung des Kanalschaltens, für apparente Unterleitwerte verantwortlich sein kann. Die Funktionsveränderungen müssen auf einer empfindlichen Änderung in der Struktur des Proteins beruhen, denn ein Austausch zweier benachbarter Aminosäuren an derselben Stelle (T->S am Rest 63 und S->T am Rest 62) führt dazu, dass der Kanal wieder wie der Wildtyp schaltet.

Kapitel 3 behandelt unterschiedliche synthetische Varianten des PB1-F2-Proteins, welches in vivo von verschiedenen Influenza-A-Viren kodiert wird. In der Literatur wurde bereits beschrieben, dass das Protein in der Lage ist, im planaren Lipid-Bilayer eine Leitfähigkeit zu vermitteln. Das Auftreten von diskreten Leitfähigkeiten jedoch, verbunden mit Schaltereignissen, die für eine Funktion als Einzelkanal sprechen, war für dieses Protein zuvor noch nicht beschrieben worden. In dieser Arbeit konnte der Nachweis für eine kanonische Kanalfunktion des Proteins erbracht werden. In Kombination mit fluorimetrischen Studien zeigen die elektrischen Daten, dass der PB1-F2-generierte Kanal zwei diskrete Leitfähigkeiten hat und unspezifisch Kationen und Anionen leitet.

Kapitel 4 befasst sich mit Phospholamban, einem Protein, dessen Funktion als Modulator der sarco-/ endoplasmatischen Ca-ATPase (SERCA) bereits früher beschrieben wurde. Bekannt war seit langem, dass Phospholamban in zwei gleich häufig verteilten strukturellen Konformationen vorliegt, nämlich als Monomer und als Pentamer, wobei letztere die deutlich stabilere von beiden darstellt. Sehr umstritten ist die Hypothese, dass das Pentamer eine Kanalfunktion besitzt. Impedanzmessungen an so genannten `supported nano-BLMs`, in denen das Phospholamban-Protein rekonstituiert ist, und die in Kooperation mit der Arbeitsgruppe Moncelli am Institut für Chemie der Universität Florenz durchgeführt wurden, zeigen, dass Phospholamban in der Tat eine Ionenleitfähigkeit in Membranen induziert. Die Rekonstitution von Phospholamban im planaren Lipid-Bilayer unterstützt die These einer durch Phospholamban vermittelten Kanalfunktion. Im Bilayer können durch Phospholamban induziert zwei diskrete kationenselektive Leitwerte von 16 pS und 27 pS registriert werden.

Summary

The present study describes the electrophysiological characterisation of different primitive channel-forming proteins, respectively peptides.

Using the so-called `planar lipid bilayer technique`, which is a maximally reduced system for the functional reconstitution and electrophysiological characterization of purified channel proteins, protein-/ peptide-mediated single channel currents were measured. Depending on defined ion concentrations in the bath solution on cis- and trans-side of a membrane, typical properties of the reconstituted channels such as current/ voltage relationships, open probability and selectivities could be determined.

Chapter 2 deals with the wildtype and two different mutants of Kcv, a tetrameric K^+ channel, which is encoded by the *Paramecium bursaria Chlorella* Virus-1 (PBCV-1). The data reveal that the subtle mutation of one amino acid (T->S of residue 63), which lies in the selectivity filter next to the cavity, almost completely reverses the ability of the wildtype to be blocked by Ba^{2+}. Furthermore, the mutation causes a considerable increased open probability, whereas the channel rarely reaches the maximal conductance level; mostly the channel opens to different subconductances. These subconductances probably reflect different kinetic states of the channel; simulations based on Markov models reveal that a very fast gating in combination with a limited registration of the channel gating can be responsible for apparent subconductances. The altered function of the mutant must be due a sensitive change in the protein structure because a mutation of a second, adjacent amino acid is able to recover the properties of the wildtype.

Chapter 3 deals with different versions of the PB1-F2 protein which are encoded by different Influenza A viruses. It was already described in literature that this protein is able to augment the conductance in the planar lipid bilayer. The absence of discrete conductance fluctuations suggested that PB1-F2 is not a canonical channel. However, the instant study shows that synthetic peptide analogues of PB1-F2

generate canonical channel function in the planar lipid bilayer. In combination with fluorometric studies, the electrical data reveal that the PB1-F2-generated channels possess two discrete conductance levels and unspecifically conduct cations and anions.

Chapter 4 deals with phospholamban, a protein whose function as modulator of the sarco-/ endoplasmatic Ca-ATPase (SERCA) was described already previously. For a long time it was known that the monomer of phospholamban is in equilibrium with the pentameric form, whereas the latter one is considerably more stable. It is a matter of discussion whether the pentamer has a channel function. Impedance measurements in so-called `supported nano-BLMs`, in which the protein was reconstituted and which were performed in cooperation with the group of Moncelli at the institute for chemistry of the University of Florence, show that phospholamban indeed induces typical ion channel fluctuations in membranes. The reconstitution of phospholamban in the planar lipid bilayer supports the hypothesis of a phospholamban-mediated channel function with two discrete cation-selective conductance levels at 16 pS and 27 pS.

Vorbemerkung

Die Ergebnisse dieser Dissertation aus den Kapiteln 3 und 4 wurden bereits wie folgt veröffentlicht:

Henkel M, Mitzner D, Henklein P, Meyer-Almes FJ, Moroni A, DiFrancesco ML, Henkes LM, Kreim M, Kast SM, Schubert U, Thiel G (2010) The proapoptotic Influenza A virus protein PB1-F2 forms a nonselective ion channel. PLoS ONE 5(6): e11112. doi:10.1371/journal.pone.0011112

Smeazzetto S, Henkel M, Ferri T, Thiel G, Moncelli MR (2010) Ion Channel Activity of Pentameric Phospholamban. Biophysical Journal, vol. 98, issue 3, pp. 328a-328a

Contents

Chapter 1: General Introduction

Each kind of life, throughout all domains (Eukarya, Bacteria, Archaea), depends on the availability of double-layered lipid membranes, (respectively mono-layered lipid membranes in Archaea), which separates cells and cellular organelles from their exterior environments. These biological barriers are necessary for the generation of electrochemical gradients which form the energetic basis for all biological processes. In principle, due to the nonpolar interior, such membranes are impermeable for most molecules with exception of small lipophilic but polar molecules like carbon dioxide, alcohols and urea that can diffuse through the membrane. In order to allow the selective passage of ions, bigger and also charged molecules, special transmembrane proteins have evolved that mediate their permeability. As their function is essential for all cells, it is plausible that such proteins occurred very early in the evolution and for this reason are present throughout all domains of life, Eukarya, Bacteria and Archaea. Moreover, also viruses, which are not considered as a life form, are suggested to possess such transmembrane proteins. Most of these proteins are highly selective for certain kinds of ions or molecules. Furthermore, they are highly regulated by physical or chemical signals.

Generally, transport processes across the membrane are distinguishable concerning their energy balance and their mode of action. If the electrochemical gradient is the only driving force for the passage of molecules, it is termed a passive transport; if it is connected with an expense of energy, an active transport. For the latter one ATPases, which pump ions like Na^+ against their electrochemical gradient across the membrane, demonstrate a typical example. The transport rates of such ion pumps lie under physiological electrochemical gradients in a range of 10^0 -10^2.

Passive transport is either mediated by carriers or by channels. The functional difference between carriers and channels is best reflected by the corresponding transport rates, which under physiological electrochemical gradients lie in a range of 10^2 – 10^4 for carriers and 10^6 – 10^8 for channels [1]. Carrier-coupled transport typically shows enzyme-like kinetics; carrier also possess substrate-specific binding

sites and they undergo conformational changes across the membrane before they release the according molecules on the other side of the membrane again; channels in contrast form water-filled pores which facilitate the free diffusion of molecules across the membrane. Nonetheless, although channels and carrier differ considerably concerning their transport rates, they are contrary recent presumptions, quite similar on the structural level. The CLC family of Cl^--transporting proteins includes both, Cl^- channels and Cl^-/ H^+ carriers. CLC-ec1 is a bacterial homolog of a Cl^-/ H^+ carrier. Recent studies revealed that the mutation of two amino acids of this carrier leads to properties that are untypical for carriers but typical for channels [2]. This also suggests that the strictly discrimination between channels and carriers is a simplification and describes two extreme modes; although most proteins which mediate passive transport can be assigned either to the group of carriers or the group of channels, there are examples which work in an intermediate form.

Channels are macromolecular pores that mediate usually a highly selective transport of one sort of ions across the membrane; other channels discriminate just between monovalent/ divalent anions/ cations or even just between anions/ cations. Most channels possess some kind of inner gate which fluctuates between discrete states, at least one open and one closed state. Such fluctuations underlie a stochastic behaviour which can be regulated by physical or chemical signals. Regulation in this context means that the probabilities to switch to certain states and their dwell times in one or the other state are influenced by these signals. This switching process, which is termed gating, can be modulated either by factors such as the membrane potential, mechanical pressure, or chemical binding of molecules. Some channels are also light-sensitive.

Channels are formed by an association of several transmembrane segments. These are arranged as either bundles of α-helices or β-strands and span the membrane, such that one end is in contact with the environment and the other end is located in the cellular interior. Transmembrane segments that are organized as β-strands are typical for a certain subclass of channels, termed porins. These are composed of β-barrels and occur in outer membranes of bacteria, chloroplasts and mitochondria.

Some of them, like VDAC (voltage dependent anion channel) are able to conduct large molecules (up to 5000 Da) while at the same time they show high selectivity for anions [3].

In contrast to porins, nearly all other channels are made of transmembrane segments that are organized as α-helices. These transmembrane segments are 15-20 amino acids in length and most of the amino acids are hydrophobic and poorly soluble in water. However, polar or even charged residues also occur and often play a structural or functional role. The transmembrane regions are connected by extramembrane segments that contain more hydrophilic amino acids. In contrast to the transmembrane segments, they vary considerably in length from channel to channel and can have regulatory influence. Although channels can also exist as monomers, the much more common forms are homomeric or heteromeric complexes. Thereby the number of subunits and the number of transmembrane segments per subunit generally differ but are constant within a channel family.

Very simple channels like the antibiotic peptaibol antiamoebin, that forms cation-selective pores, consist of an arrangement including a fixed number of small peptides, which possess just one transmembrane domain [4], [5], [6]. Nonetheless, although such channels are quite simple, they have properties which might suggest higher complexity. Beside selectivity, this includes some kind of channel gating and sensitivity for channel inhibitors, respectively channel blockers. However, not all channel-forming small peptides show discrete fluctuations like antiamoebin, which results from well-defined configurations of a fixed number of subunits.

The determination of several channel structures by x-ray diffraction shed light on their mechanism of function and revealed common principles of structural and functional design. In these terms one of the best understood K^+ channels is KcsA. K^+ channels represent a class of channels that occur in all organisms and the mechanism of their selectivity is conserved within the family. KcsA is built of four identical subunits. Each consists of three α-helices that form two funnel-shaped openings, one to the intracellular and one to the extracellular side. Near to the middle of the bilayer, they

surround a cavity which is lined by nonpolar residues. On the extracellular side there is a narrow fragment, approximately 12 Å long, that acts as selectivity filter and is formed by carbonyl oxygen atoms of a highly conserved amino acid sequence [7]. These partially negative charged oxygen atoms coordinate nearly perfectly two dehydrated potassium ions and by this mimic the electrostatic environment of their solvated state. In contrast, the affinity of sodium ions is several orders of magnitude smaller [8]. This explains the high selectivity of the channel for potassium. In presence of a sufficient ion concentration two of the four positions along the filter that can coordinate cations, are occupied by potassium. Thereby, the ions are separated by a water molecule. When a third ion enters, the electrostatic repulsion displaces a potassium ion from the opposite side [9].

Compared to cytosolic proteins, transmembrane proteins are much more homologue to each other and they show a higher structural simplicity. Thus, it is often possible to create high quality homology models of channels that have not yet been crystallized. Based on the structure of the bacterial potassium channel KirBac 1.1, such a model was developed for the Kcv channel [10]. Kcv is encoded by the *Paramecium bursaria Chlorella* virus-1 (PBCV-1) [11] and probably plays an important role during infection of host cells [12]. Like KirBac 1.1 it is a voltage-dependent potassium channel that also shares considerable structural similarities; particularly concerning the pore-forming domain which contains the highly conserved K^+ selectivity filter. The channel is also assembled into four subunits, each consisting of two transmembrane α-helix domains and it displays the same symmetries. However, in contrast to KirBac 1.1, whose subunits consist of 333 amino acids, Kcv is more reduced; each monomer is 92 amino acids in length. Because of the structural similarity of the pore domain - including filter region - to other K^+ channels and due to its structural simplicity, Kcv presents a suitable model for investigating channel properties like selectivity, gating and sensitivity against channel blockers. In chapter 1 heterologously expressed, isolated and purified Kcv wildtype (wt-Kcv) and two different mutant proteins were studied in the planar lipid bilayer system. The data reveal that a single very subtle and conservative mutation (threonine 63 against serine) within the selectivity filter considerably changes the sensitivity against Ba^{2+}. Wt-Kcv is nearly completely

blocked by Ba^{2+}; in contrast, the mutant (T63S-Kcv) is insensitive. Furthermore, the mutant exhibits numerous subconductances which represent the predominant states within the channel fluctuations. Although they differ with respect to their size, such subconductances can also be found in wt-Kcv. This shows that they are evoked by a mechanistic principle which is inherent to the channel and just enhanced by the mutation. Finally, both, the altered Ba^{2+} sensitivity and the different occurrence of substates can be explained by a modified affinity between the mutated selectivity filter and the conducted cations.

It is probably not surprising that the structure of potassium channels is highly conserved. However, interesting to note is that other channel-forming peptides which do not belong to the family of K^+ channels reveal the same overall architecture principles of K^+ channels. High-resolution structure of the oligomeric antiamoebin channel is not yet known, but a detailed, high quality model has been proposed, based on x-ray and nuclear magnetic resonance structures of a single antiamoebin helix [4], [5], [6]. Remarkably it displays high similarity with the structure of KcsA potassium channel [7]. It consists of eight transmembrane helices that are organized as parallel bundles, forming a water filled pore. This is shared by the KcsA channel, which is tetrameric, but also built of eight transmembrane helices, two contributed by each monomer. Carbonyl groups from amino acids, which are exposed to the lumen, play the counterpart to the cation-binding regions in KcsA that coordinate the dehydrated potassium ions. Furthermore, a ring of glutamine side chains achieves the same function of the water filled cavity of KcsA.

It is plausible to assume that precursors of small transmembrane peptides like antiamoebin emerged earlier during evolution than those of more complex channel proteins that possess multiple transmembrane domains [13]. These types of peptides already exhibit functional principles which are typical for more complex channels; they reveal moderate selectivity and gating. It is reasonable to assume that during evolution small changes in these primordial peptides were sufficient to create channels with a higher selectivity and gating behaviour.

Viruses are generally well known for their minimalist organisation. They are capable of limiting their genome and their structural proteins to the very essentials. In this context it is not surprising to find that also the structural complexity of channel proteins, which are encoded by viruses, belong to the most simple channel proteins.

Influenza A virus is a pathogen which infects not only birds and swine but also humans. Due to its strong enhancement of secondary infections of the respiratory tract and its contribution to lethal pneumonia by bacteria, it is of high relevance to human health [14]. In search of Influenza proteins, which are relevant for the pathogenicity of the virus, PB1-F2, an 87-amino-acids-long peptide was detected. This peptide is encoded by an alternative reading frame on the first genome segment of Influenza A virus [15]. The expression and secretion of the full-length sequence in host cells results in a depolarisation of the mitochondrial membrane voltage which then induces apoptosis and cell death of primarily macrophages and neutrophil granulocytes [16]. The PB1-F2 peptide has a structure, which is strongly depending on the environment. In water the peptide folds in a random fashion with no structured elements. In a hydrophobic, membrane like environment PB1-F2 exhibits at the C-terminal domain an α-helix; the N-terminus is, with the exception of two small helix domains, still unstructured. Interesting to note is that the C-terminal helix is long enough to span the membrane.

Until recently it was assumed that the PB1-F2 generated depolarisation of the mitochondrial voltage is evoked by the aggregation of PB1-F2 peptides and that these aggregates form nonselective lipidic pores which disrupt the inner and outer mitochondrial membrane. This view was based on the observation that in a previous study PB1-F2 was able to increase the membrane conductance of lipid bilayers without generating canonical single channel fluctuations. PB1-F2 was only found to evoke random noise like fluctuations of the membrane conductances; the latter was interpreted as a result of unstructured lipid pores. The data presented in chapter 2 shows that PB1-F2 is able to generate canonical channel like fluctuations and that this activity is associated with the helix forming part of the peptide. This functional

data together with structural considerations support a model according to which PB1-F2 is able to form transmembrane domains with channel conductance.

Mammalian cells also contain small transmembrane peptides. One example for such a protein is phospholamban. This 52-amino-acids-long integral membrane protein is involved in the contractility of cardiac muscle by regulating the intracellular calcium concentration of cardiac myocytes. Phospholamban regulates cardiac sarco-/ endoplasmatic Ca-ATPase (SERCA), a membrane protein occurring in the sarcoplasmic reticulum that causes a reduction of the intracellular calcium concentration by pumping Ca^{2+} into the sarcoplasmic reticulum. Unphosphorylated phospholamban inhibits SERCA, whereas the phosphorylated form releases SERCA inhibition and allows pumping of Ca^{2+} from the cytoplasm into the sarcoplasmic reticulum.

Recent studies revealed that phospholamban exists in equilibrium between monomeric and pentameric forms [17] wherein the stable pentameric form is 30 kDa in weight and each monomer (6 kDa) is composed by three domains: a helical cytoplasmic domain, a semi flexible loop and a helical hydrophobic transmembrane domain [18], [19]. However many points are still matter of debate: Whether the inhibition of the SERCA is mediated by the monomeric or pentameric form; what is the structure of the pentameric form; whether the pentameric form is an ion channel or simply a storage form. Although the monomer it is predominant hydrophobic, recently molecular modelling [20] and structural studies [17] supported the hypothesis that phospholamban has also ion channel activity and not only regulatory function.

In Chapter 3 phospholamban is reconstituted into planar lipid bilayers. The data reveal that this protein is able to generate distinct channel-like fluctuations. Together with structural data and with a new biometric method of impedance measurements these data support the idea that phospholamban is a channel-forming peptide.

The demonstration and detailed analysis of channel function of the aforementioned proteins relies in the present study on a reconstitution of the purified or of synthetic

proteins in planar lipid bilayers. In principle, there are several methods available for the recording of single channel activity. With the patch clamp technique it is possible to record channel activity directly in cells which naturally express a channel of interest or which serve as heterologous expression system for certain channels. While this method is suitable for channels within the plasma membrane it is in most cases not possible to use the patch clamp technique for recording activity of channels from endogenous membranes. In some cases it was shown that it is in principle possible to patch-clamp also membranes of some organelles like mitochondria. This, however, is connected to a high preparative effort and not practical in all cases. In order to circumvent this problem, the reconstitution of isolated and purified channel proteins in an artificial lipid membrane/ lipid bilayer offers a useful solution. The planar lipid bilayer system – as described by Mueller and Montal 1972 [21] - is a highly reduced setup consisting of two chambers which are filled with electrolytes and which are separated by a thin vertical orientated Teflon foil. This so-called septum exhibits a little hole, which is covered by lipid, e.g. α-phosphatidylcholine. Using the painting method [21] a thick drop of lipid is initially deposited in the hole. The lipid is then thinned out until it forms a lipid bilayer across the hole. This bilayer is equivalent to the membrane of cells. In this configuration the two chambers are electrically separated. Channel proteins of interest are first reconstituted into proteoliposomes before the liposomes are fused with the aforementioned bilayer. Each chamber is connected via silver chloride electrodes directly to the headstage of a patch clamp amplifier. If a channel protein is successfully reconstituted into the bilayer the current flow through a single protein can be recorded. For this purpose a voltage is applied across the membranes to generate a driving for the channel currents. In this way otherwise inaccessible channel proteins can be studied. In addition the technique offers a maximum in experimental simplicity. In the extreme case of synthetic channel proteins all the components of the system are chemically pure.

References Chapter 1

[1] Hille B (2001) Ionic Channels of Excitable Membranes. 3rd edition. Sinauer Associates Inc., Sunderland, MA. 607 pp

[2] Jayaram H, Accardi A, Wu F, Williams C, Miller C (2008) Ion permeation through a Cl^--selective channel designed from a CLC Cl^-/H^+ exchanger. Proc. Natl Acad. Sci. USA. 105, 11194–11199

[3] Komarov AG, Graham BH, Craigen WJ, Colombini M (2004) The Physiological Properties of a Novel Family of VDAC-Like Proteins from *Drosophila melanogaster* Biophys J. 86(1): 152–162

[4] Karle IL, Perozzo MA, Mishra VK, Balaram P (1998) Crystal structure of the channel-forming polypeptide antiamoebin in a membrane-mimetic environment. Proc. Natl. Acad. Sci. USA. 95:5501–5504

[5] Snook CF, Woolley GA, Oliva G, Pattabhi V, Wood SP, Blundell TL, Wallace BA (1998) The structure and function of antiamoebin I, a proline-rich membrane-active polypeptide. Structure 6:783–792

[6] Galbraith TP, Harris R, Driscoll PC, Wallace BA (2003) Solution NMR studies of antiamoebin, a membrane channel-forming polypeptide. Biophys. J. 84:185–194

[7] Doyle DA, Cabral JM, Pfuetzner RA, Kuo A, Gulbis JM, Cohen SL, Chait BT, MacKinnon R (1998) The Structure of the Potassium Channel: Molecular Basis of K^+ Conduction and Selectivity. Science Vol. 280. no. 5360, pp. 69 – 77

[8] Zhou Y, MacKinnon R (2004) Ion binding affinity in the cavity of the KcsA potassium channel. Biochemistry. 43:4978-4982

[9] Zhou Y, MacKinnon R (2003) The occupancy of ions in the K^+ selectivity filter: charge balance and coupling of ion binding to a protein conformational change underlie high conduction rates. J Mol Biol. 333:965-975

[10] Tayefeh S (2007) Computational study of the Kcv potassium channel. Dissertation, TU Darmstadt, 2007

[11] Plugge B, Gazzarrini S, Nelson M, Cerana R, Van Etten JL, Derst C, DiFrancesco D, Moroni A, Thiel G (2000) A Potassium Channel Protein Encoded by Chlorella Virus PBCV-1. Science 3 March 2000: Vol. 287. no. 5458, pp. 1641 – 1644

[12] Mehmel M, Rothermel M, Meckel T, Van Etten JL, Moroni A, Thiel G (2003) Possible function for virus encoded K+ channel Kcv in the replication of chlorella virus PBCV-1. FEBS Lett. 18;552(1):7-11

[13] Rode BM (1999) Peptide And The Origin Of Life. Peptides 1999, 20(6), 773-786

[14] McAuley JL, Hornung F, Boyd KL, Smith AM, McKeon R, Bennink J, Yewdell JW, McCullers, JA (2007). Expression of the 1918 influenza A virus PB1-F2 enhances the pathogenesis of viral and secondary bacterial pueumonia. Cell Host & Microbe 2: 240–249

[15] Chen W, Calvo PA, Malide D, Gibbs J, Schubert U, et al. (2001) A novel influenza A virus mitochondrial protein that induces cell death. Nat Med 7: 1306-1312

[16] Coleman (2007) The PB1-F2 protein of Influenza A virus: increasing pathogenicity by disrupting alveolar macrophages. Virology Journal 2007, 4:9

[17] Arkin I, Adams P, Brünger A, Smith S, Engelman D (1997) Structural perspectives of phospholamban. A helical transmembrane pentamer. Annu. Rev. Biophys. Biomol. Struct. 26, 157-79

[18] Zamoon J, Mascioni A, Thomas DD, Veglia G (2003) Phospholamban structural dynamics in lipid bilayers probed by a spin label rigidly coupled to the peptide backbone. Biophys. J. 85, 2589-2598

[19] Oxenoid K, Chou JJ (2005) Proc The structure of phospholamban pentamer reveals a channel-like architecture in membranes. Proc. Natl. Acad. Sci. USA;102:10870–10875

[20] Sansom M, Smith G, Smart O, Smith S (1997) Channels formed by the transmembrane helix of phospholamban: a simulation study. Biophys. Chem. 69, 269-81

[21] Montal M, Mueller P (1972) Formation of bimolecular membranes from lipid monolayers and a study of their electrical properties. Proc Natl Acad Sci USA 69:3561-3566

Chapter 2: Kcv

A single mutation in the selectivity filter of Kcv leads to a decreased Ba^{2+} sensitivity and an enhanced occurrence of subconductances

Abstract

The miniature K^+ channel Kcv proved to be a good model to investigate general properties of K^+ channels with respect to ion permeation and gating. Because Kcv represents effectively the common structural and functional core of all K^+ channels, its inherent mechanistic principles are suggested to have a universal character. The most conserved part of K^+ channels is the pore domain including the selectivity filter; for a long time it was thought that this domain is exclusively responsible for the selectivity. However, recent studies suggested that the selectivity filter can also function as a gate.

In this study we used the planar lipid bilayer technique to record the single channel activity of purified Kcv. The comparison of wt-Kcv and two filter mutants (T63S-Kcv and S62T/T63S-Kcv) underscores the function of the selectivity filter as a gate. The data reveal that the very conservative exchange of an amino acid at position 63 in the selectivity filter has a dramatic effect on the sensitivity of the channel against Ba^{2+}. The mutation furthermore favours a high open probability of the channel and is correlated with the occurrence of multiple substates. The latter is correlated with a modification of the gating properties resulting in fast gating. Altogether the data are consistent with a model in which the mutation lowers the affinity for K^+ and Ba^{2+} in a distinct site of the filter.

Introduction

Kcv is a homotetrameric miniature K^+ channel that is encoded by the *Paramecium bursaria Chlorella* virus-1 (PBCV-1) [1]. Each monomer is 94 amino acids in length. According to a homology model, which was based on the crystal structure of the KirBac 1.1 channel [2], the monomer of Kcv is build of two transmembrane α-helical domains, connected by a pore domain. This pore domain contains the highly conserved K^+ selectivity filter with the consensus sequence (TXXTXGY/FGD) found in all K^+ channels. Furthermore the protein possesses an extracellular turret domain and a very short intracellular helix at the N-terminus. The latter is equivalent to the slide helix of KirBac1.1.

The combination of a very small size together with a high degree of conservation of the selectivity filter makes Kcv a suitable model for analysing basic and general structure/ function-correlations of K^+ channels. Such a study can provide insights into structural features, which are underlying functional properties such as selectivity, gating and inhibition by blockers. One way to address these questions is by analysing the function of mutants in which critical amino acids have been modified experimentally [3] or by evolution [4]. In a recent study the approach of rational modifications of amino acids by single point mutations has been extended by an unbiased genetic approach. For this purpose a yeast complementation assay in the presence of the channel blockers Ba^{2+} or amantadine together with randomized mutagenesis of the filter domain of Kcv was employed. By this approach mutants were identified, which are resistant to Ba^{2+} and amantadine [4]. Further experiments in this study using a PCR-backcrossing procedure finally uncovered a single mutation, T63S that occurs in all these mutants and is responsible for both, the resistance against Ba^{2+} and amantadine. The critical position threonine 63 is part of the highly conserved selectivity filter of the channel and occupies a position that acts as a coordination site for cations. Kcv possesses 4 of these coordination sites and T63 forms the innermost one e.g. the site localized next to the channel´s cavity (Figure 2.1).

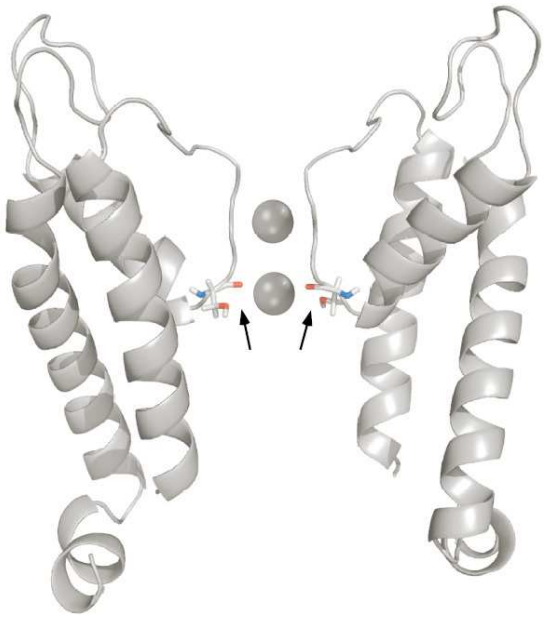

Figure 2.1 Cartoon illustration of the Kcv homology model, which is based on the KirBac1.1 crystal structure. For clarity only two of the four subunits are depicted. Spheres represent K^+ ions in the coordination sites 4 and 2 within the selectivity filter. The amino acids at position 63 are additionally depicted as sticks; the coordinating side chain oxygen atoms are marked by arrows.

Remarkably, this site is the only one in which the amino acid side chain coordinates the ion (within the filter); in the three remaining sites this coordination is achieved by the oxygen atoms of the amino acid backbone. Though it seems to be obvious that an exchange of this amino acid side chain affects blocking by Ba^{2+}, it is surprising to find that the subtle change T->S, which does not affect the coordinating side chain oxygen, shows such a strong impact on channel function.

Recently, also the electrophysiological properties of T63S-Kcv were studied in *Xenopus* oocytes by a two-electrode voltage clamp system. Titration with Ba^{2+} revealed that the mutant had a 100-fold increased K_d value for block compared with the wildtype-Kcv. This suggests that primarily a subtle single point mutation is responsible for the barium resistance. Interesting to note is that the introduction of the same T->S mutation in the human K^+ inward rectifier channel Kir2.1 also resulted in a decreased Ba^{2+} sensitivity, however, in Kir2.1 the mutation only resulted in a 12-fold

increased K_d value compared to the wildtype channel. The most striking difference between Kcv and Kir2.1, which might explain this difference of the K_d values, is the position 62 adjacent to position 63 of Kcv. The former is also part of the conserved selectivity filter and in Kcv it is made of a serine. The more common residue in K^+ channel filters however, which is also occurring in Kir2.1, is a threonine. Examination of a Kcv double mutant S62T/T63S, which resembles the background of Kir2.1, showed evidence for a negative coupling effect between the neighbouring residues at these two positions. The insertion of threonine instead of serine at position 62, resembling the filter sequence of Kir2.1, reduces the impact of the T63S mutation in Kcv. The resulting K_d value is 12-fold increased relative to wildtype, and consequently in line with that found for Kir2.1.

In addition to the altered Ba^{2+} sensitivity the analysis of channel currents revealed further differences between the wildtype and the mutant channel. One striking difference is that the wildtype channel (wt-Kcv) has a pronounced negative slope conductance at extreme negative voltages; this negative slope conductance is absent in the mutant T63S-Kcv. In the wildtype channel of Kcv this negative slope conductance is visible on the level of single channels when channel activity is measured in planar lipid bilayers or on the membrane of *Xenopus* oocytes [5], [6]. Detailed analysis of channel fluctuations at negative voltages revealed that this negative slope conductance can be explained by a fast gating process [6]. Fast gating in this context means that the open channel is frequently interrupted by very fast and short closures. These closures are faster than the recording system so that the macroscopic current only appears to be reduced.

From the absence of such a negative slope conductance in the macroscopic I/V relation of T63S-Kcv it was speculated that the mutation in the filter is also abolishing the fast gating component. The prove for this hypothesis on the single channel level is still missing because the single channel fluctuations of the mutant were so far not yet observed. Attempts to monitor single channel signals of the mutant in oocytes failed because the recordings only revealed noisy current traces without clear cut channel fluctuations (Abenavoli personal communication [6]).

In order to get an improved resolution of the mutant channel, here we used the planar lipid bilayer system as an alternative and suitable method to examine single channel properties of T63S-Kcv and S62T/T63S-Kcv in comparison to the wildtype channel.

The data show differences concerning conductivity and Ba^{2+} sensitivity between the three channel proteins. Further analysis of the beta distribution of the amplitude histograms uncovers some kinetic details that contribute to explain these differences.

Material and Methods

Escherichia coli strain Topo10F' (Invitrogen, California, USA) was used for subcloning and propagation of recombinant plasmids. Protease-deficient *Pichia pastoris* strain SMD1163 (his4, pep4, prb) (Invitrogen, California, USA) was used routinely for the expression of the K^+ channel gene. Enzymes for molecular biology were obtained from New England Biolabs (Ipswich, UK) or Stratagene (Santa Clara, California, USA). The detergent dodecyl α-D-glucopyranoside (DDM) was purchased from Glycon (Berlin, Germany). DNA sequencing was performed by MWG Biotech. All other reagents were obtained from Sigma-Aldrich Chemie Gmbh (Munich, Germany) or Merck GmbH (Darmstadt, Germany), unless otherwise stated.

Manufacture of wt-Kcv and Kcv-mutants expression constructs and *Pichia pastoris* transformation

Polymerase chain reactions (PCRs) employed either PfuI or the Taq Precision Plus System (Stratagene, Santa Carla, California, USA). The sequence of the synthetic gene of Kcv was designed and edited using RESTRI-software and synthesized by Entelechon GmbH (Regensburg, Germany) and inserted into the PCRtopo4 vector. The open reading frame encoding the Kcv synthetic gene was amplified from synthetic Kcv- PCRtopo4 by PCR (forward primer (F1), 5'GACGACGATGACAAGATAATGTTGGTCTTCTCC3'; reverse primer (R1), 5'GGAGAAGACCAACATTATCTTGTCATCGTCGTC3'), introducing a 5' BamHI restriction site and a 3' NotI restriction site. The PCR fragment was subcloned into BamHI-NotI-digested *Pichia pastoris* expression vector pPIC3.5K (Invitrogen, Karlsruhe, Germany), leading to the wildtype construct, which finally was confirmed by DNA sequencing. To aid purification, tag sequences were added to the 5' end of the synthetic Kcv coding region, to yield the following N-terminus: MAWSHPQFEKTRH(9)D(4)KI, including the Strep II tag, WSHPQFEKTR, followed by a nona-histidine tag and by the enterokinase cleavage site, DDDDK. *Pichia pastoris*

SMD1163 cells were transformed by electroporation with 15- 20 µg of PmeI-linearized vectors, using conditions recommended by the manufacturer.

To get the single mutant (T63S-Kcv) gene, the Kcv wildtype construct (wildtype gene subcloned in pPIC3.5) served as the DNA template for a PCR site-directed mutagenesis (QuikChange Site-Directed Mutagenesis Kit, Stratagene, California, USA) in order to exchange threonine 63 against serine (forward primer, 5'CCACCACCCACTCCTC CGTTGGTTTCGGTG3'; reverse primer, 5' CACCGAAACCAACGGAGGAGTGGGTG GTGG 3'). To eliminate the parental DNA, comprising the wildtype sequence, the products of each PCR site-directed mutagenesis were treated with DpnI (Stratagene), which digests exclusively the methylated DNA. XL1-Blue supercompetent cells were transformed with 1 µl of the PCR reaction. From the transformants the DNA was extracted with Quiafilter plasmid midi-kit (Quiagen, Hilden, Germany) and linearized with PmeI (NEB). 3 µg of linearized DNA was used to transform *Pichia pastoris* SMD1163 with the *Pichia* easycompt kit (Invitrogen).

To get the double mutant (S62T/T63S-Kcv) the single mutant construct again served as template for a further PCR site-directed mutagenesis leading to an exchange of serine 62 against threonine [forward primer, 5' GTCACCACCCACACCTCCGTTGGTTTC3'; reverse primer, 5'GAAACCAACGGAGGTGTGGGTGGTGAC3'].

Induction of K^+ channel production

Single colonies were grown at 30 ℃ overnight in MGY medium [0.34% (w/v) yeast nitrogen base, 1% (w/v) ammonium sulphate, 10-5% (w/v) biotin, and 1% (w/v) glycerol] to an absorbance at 600 nm (A600) of 2-6. After centrifugation at 1500*g* for 10 min, the pellet was resuspended to an *A*600 of 1.0 in MM medium (0.34% (w/v) yeast nitrogen base, 1% (w/v) ammonium sulphate, 10-5% (w/v) biotin and 0.5% (w/v) methanol) and grown for 48 h. Additional methanol was added after 24 h to a

final concentration of 0.5% (v/v), to maintain inducing conditions. Cultures were performed in a 2 l flask with 200 ml of MGY medium.

Pichia pastoris membrane preparation

Cells (4-10 g) were suspended in a final volume of breaking buffer (50 mM sodium phosphate (pH 7.6), 4% glycerol, and 1 mM EDTA) of 100 ml containing 0.1 mg/ml protease inhibitors of soybean trypsin inhibitor, 1 mM benzamidine, and 0.1 mM Pefabloc SC and resuspended using a Poltyron homogenizer (30 s at medium speed). An equal volume of ice-cold, acid-washed glass beads (0.25-0.5 mm diameter) was added, and the mixture was vigorously mixed for 3 min in a Beadbeater (Biospec Instruments). Glass beads, unbroken cells, and other cell debris were removed by centrifugation at 1500g for 10 min. The supernatant was removed and PEG 8000 (poly-ethylene glycol) (helps to precipitate the membranes) 10% W/V an NaCl 200mM were added to it and the mixture is incubated 20 min at 4℃ stirring. After 20 min the mixture was centrifuged at 18000 RPM (Sorvall ss34) for 45 min at 18℃. The resulting crude membrane pellet was suspended in breaking buffer (50mM NaH2PO4, 5% glycerol (w/W) NaOH pH 7.4, EDTA 1mM), and the protein content was determined using the DC protein assay (Bio-Rad). Membranes were diluted with breaking buffer to 20 mg of protein/ ml prior to freezing and storage at -80 ℃.

Purification of the Kcv-channel from *Pichia pastoris*

Membranes (3 ml) from cells expressing the synthetic Kcv gene construct were detergent-solubilised in buffer containing 50 mM imidazole (pH 7.4), 3% DDM, 600 mM NaCl, and 200 mM KCl for 1 h at 4 ℃ and cleared by centrifugation (100000g for 1 h). The supernatant was loaded (0.5 ml/min) onto 10 ml of resin sigma his-select nickel affinity; the latter was pre-equilibrated with solubilising buffer. The column was then washed at 1 ml/min twice with 10 ml of buffer containing 50 mM imidazole (pH 7.4), 0.1% DDM, 1 M NaCl, and 200 mM KCl and twice with 10 ml of buffer

containing 75 mM imidazole (pH 7.4), 0.1% DDM, and 200 mM KCl. To recover bound protein, the column was eluted at 0.3 ml/min with a buffer containing 300 mM imidazole (pH 7.4), 0.1% DDM, and 200 mM KCl.

Reconstitution of Kcv and electrophysiology

The Kcv-eluate usually had a protein concentration of 1mg/ml and was reconstituted into liposomes by the addition of 0.09% dodecyl α-D-maltoside (minimum of 99%, Biomol GmbH, Hamburg, Germany) and 10 mg/ml L-R-phosphatidylcholine [from soybean, type IV-S, g30% (TLC), Sigma, in 100 mM KCl and 10 mM Mops/Tris (pH 7.0)]. After 30 min incubation, the detergent was removed by the addition of BioBeads (SM2 Adsorbent, Bio-Rad). Kcv proteoliposomes were formed overnight at room temperature with one exchange of BioBeads. Experiments with planar lipid bilayers were performed as described by Schrempf et al. (1995) [7] by the Montal-Müller technique [8] with a 0.4 mg/ml solution of α-phosphatidylcholine (type IV-S >= 30 % TLC; Sigma-Aldrich (Steinheim, Germany) in n-decane (Carl Roth, Karlsruhe, Germany). The measurements were done in buffer containing 500 mM KCl, 10 mM Mops/Tris pH 7. The Ag/AgCl electrode in the trans-compartment was directly connected to the head stage of a current amplifier (EPC 7, List, Darmstadt, Germany); the electrode in the cis-compartment was connected to the ground. At positive potentials the electrode in the trans-compartment was positive and the electrode in the cis-compartment negative. In order to prevent surface-potential-effects, both electrodes were connected with the bath solution via an agar bridge (2% agarose in 2 M KCl). Currents were recorded and stored by an analog/ digital-converter (LIH 1600, HEKA electronics, Germany) at 4 KHz after low pass filtering at a frequency of 1 kHz. Data analysis was performed by Patchmaster-Software (HEKA electronics, Neustadt, Germany), QuB (University of Buffalo, Buffalo, USA, www.qub.buffalo.edu/wiki/index.php/Main_Page), Kielpatch-Software (University of Kiel, Kiel, Germany, www.zbm.uni-kiel/aghansen/software.html) and Excel (Microsoft, Redmond, USA) Before adding the protein to the trans chamber the bilayer conductance was recorded for some time in order to exclude artefacts evoked by

contaminations. Only perfectly silent bilayers were used for reconstitution of Kcv-proteins.

Data analysis

IV-curves were created by determining the apparent single channel currents by visual inspection with Patchmaster-Software.

Mean/ standard deviation plot was done using Excel-Software. Therefore, standard deviations of 20 recorded data points were plotted as a function of the averages of the same data points. This was done for every single data point which led to an overlap of the corresponding intervals; the first mean value was calculated from data points 1 to 20, the second one from data points 2 to 22, the third one from data points 3 to 23, etc.

In order to determine open probabilities amplitude histograms were created with QuB-Software (University of Buffalo, Buffalo, USA, www.qub.buffalo.edu /wiki/index.php/ Main_Page). Subsequently these histograms were fitted, whereas the positions of the peaks and the widths of the distributions were fixed manually. The resulting integrals of the Gaussian functions then constituted the basis for calculating each open probability, which were given by their magnitude relative to the whole area.

Evaluation of fast gating

The open state current of the studied channels display increased noise if gating is faster than can be resolved by the recording system, respectively the filter frequency. In this case, the value of the apparent single channel current, I_{app}, extracted from such data is smaller than the value of the “true” single channel current, I_{true} (which would be measured if the temporal resolution of the recording system was high enough). This effect is illustrated in Figure 2.2.

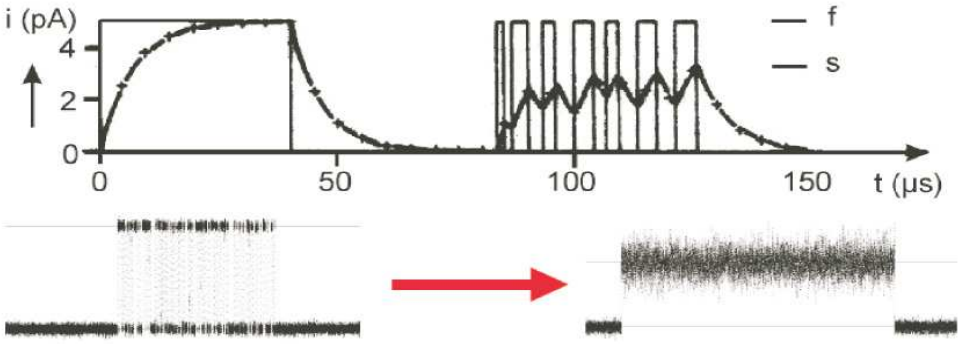

Figure 2.2 Reduction of the "true" current due to a limited sampling rate i.e. a too slow recording frequency. The apparent current is smaller and displays increased noise. The full value of the open state current is never reached, if the mean dwell time in a state is shorter than the rise time of the anti-aliasing filter.

The full value of the open state current is never reached if the mean dwell time in a state is shorter than the rise time of the anti-aliasing filter. Due to these conditions a noisy but reduced current-amplitude appears [9].

However, I_{true} can be retrieved by analysing the amplitude histograms. Base line drift and other artefacts would distort the analysis. Thus, all data had to be inspected closely and cleaned manually from sections showing these kinds of artefacts [10]. Sections of fast gating were extracted from the measured time series. These "cleaned time series" were used to generate the open point histogram (distribution-per-level, [11]) of the apparent open state. This was done with Kiel-Patch software using a Hinkley detector [12].

Determination of the true single channel current, I_{true}, and of the rate constants of an O-C model of fast gating

The open-state amplitude histogram of I_{app} as obtained from bursts of fast flickering is broader than that of the base line, and instead of Gaussian, the distribution may appear skewed [13], [14], [15]. These so-called beta distributions can be used to

reconstruct the “true” single channel current and the rate constants of the underlying gating process [9], [16], [17]. Schroeder and Hansen (2006) [9] have shown that it is sufficient to use a simple two-state Markov model for the analysis of the bursts in the time series.

The “theoretical” open point histogram obtained from the model was fitted with a Simplex algorithm [18], [19] to the open point histogram of the measured data. Simulations including noise and a low pass filter response equal to those in the experiment were employed to provide the theoretical curves; Figure 2.3 schematically illustrates this procedure. During fitting, the current was used as a fixed parameter which was changed stepwise in subsequent fits; this made the algorithm more stable. The simplex determined the best set of rate constants for each suggested current. From the resulting plot “error sum versus assumed I_{true}”, the minimum was taken as the “true” single channel current.

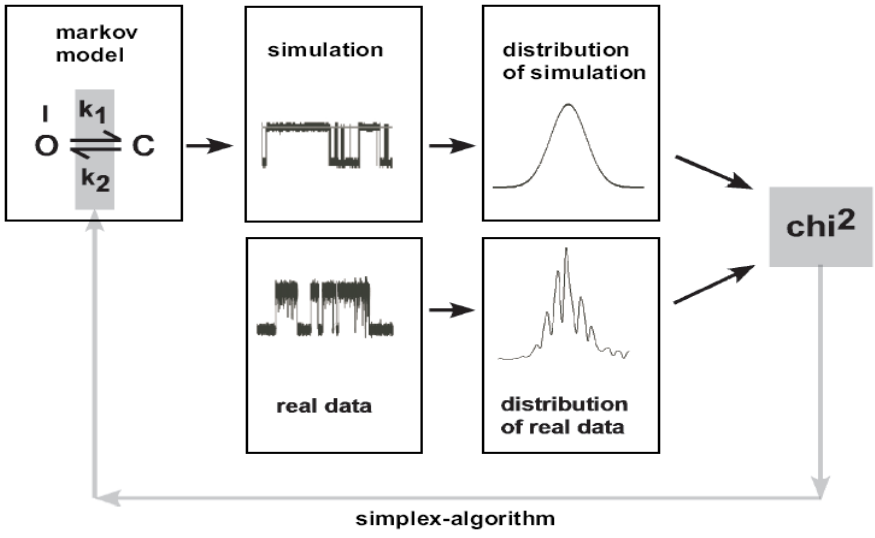

Figure 2.3 Schematic illustration of the procedure, which is used for reconstruction of the “true” current by analysing the amplitude distributions of the recorded apparent current. The “theoretical” open point histogram - obtained from time series which were simulated on basis of a Markov model - was fitted with a Simplex algorithm to the open point histogram of the measured data.

Experiments with Ba^{2+} block

To test the sensitivity of the channel proteins against Ba^{2+}, BaCl was added at a final concentration of 5 mM in both chambers and mixed. Usually, the signals of blocked channels were recognizable a few seconds after adding the blocker.

In a further step the reversibility of the Ba^{2+} block was tested. Therefore, Ba^{2+} was first added in order to block the channel and subsequently precipitated by adding and mixing 10 mM $NaSO_4$ to both chambers.

Results

General description of wt-Kcv, T63S-Kcv and S62T/T63S-Kcv

In order to investigate functional differences between wt-Kcv, T63S-Kcv and S62T/T63S-Kcv on the single channel level the purified proteins - each derived from a yeast expression system - were reconstituted in planar lipid bilayers. Shortly after adding the wt-Kcv protein at a final concentration of ≥ 30 µM into the bath solution of the trans-chamber (symmetrical 500 mM KCl, 10 mM Mops/Tris, pH 7.0), single channel fluctuations could be observed (Figure 2.4). Subsequently, currents across the bilayer in response to stepwise altering test voltages (from -80 mV to +80 mV) were recorded. In the same manner experiments were also done with proteins from the two mutants. Figure 2.4 shows exemplary time series of currents monitored in response to reconstitution of wildtype-Kcv (Wt-Kcv), T63S-Kcv and S62T/T63S-Kcv at test voltages of -80 mV and +80 mV.

The wt-Kcv signal displays at both voltages typical transitions between a closed state and one predominant open state (o_M), which is in accordance with the maximal unitary conductivity 250 pS of a single channel. Similar unitary current fluctuations with the same conductance were also described in previous studies with wt-Kcv [5], [20]. In comparison to the signal from wt-Kcv, the S62T/T63S-Kcv signal does not show any appreciable differences; this protein also generates typical unitary current fluctuations between a closed and one open state. The picture is very different in the case of T63S-Kcv. This channel shows primarily transitions between a closed state and many defined discrete substates (o_{SS}); in order to distinguish discrete sublevels, they are expressed as a percentage of the full open state. In the case presented in Figure 2.4 at least three substates are detectable; representative for all measurements the maximal open state is rarely achieved. The appearance of substates in T63S-Kcv seems to be voltage-independent. Figure 2.5 depicts time series for different positive and negative potentials, showing that numerous substates occur for all tested voltages.

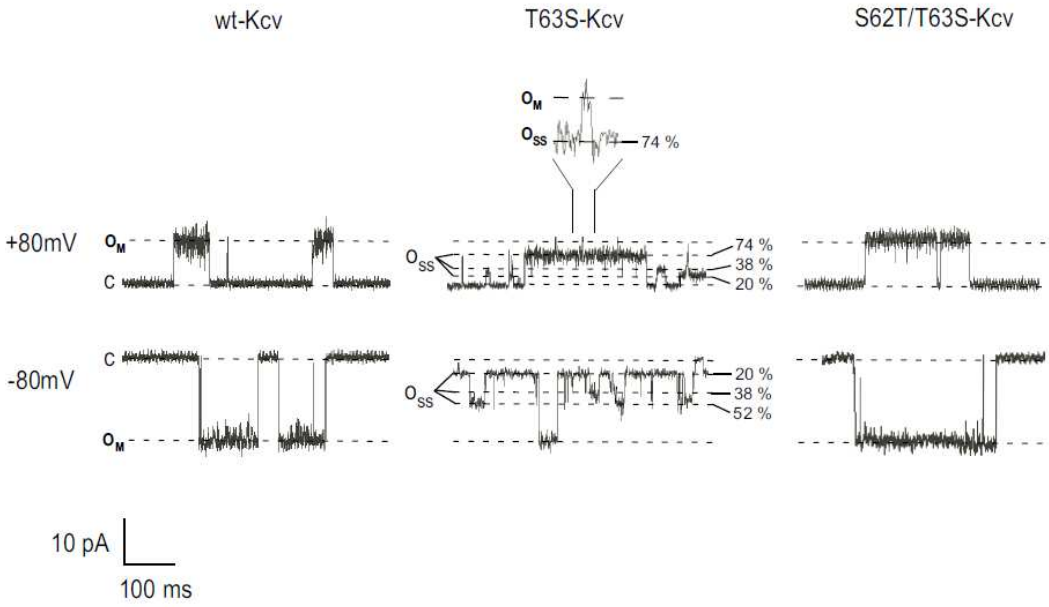

Figure 2.4 Exemplary time series of currents evoked by wt-Kcv, T63S-Kcv and S62T/T63S-Kcv at +/- 80 mV. A closer scrutiny to the time series of T63S-Kcv at +80 mV also reveals short occurrences of the maximal open state (O_M). Due to the high number of conductance levels in the case of T63S-Kcv, all substates are presented as percentage of the full open conductance.

The activity of T63S-Kcv with the predominant fluctuation between many substates is also associated with a highly increased open probability compared with channel activity generated by wt-Kcv and S62T/T63S-Kcv. We define here the overall open probability (p_o*) as the probability of the channel to leave the closed state to any of the conductance states. At +/- 80 mV T63S-Kcv has an open probability p_o* of 0.9. The open probability p_o* of Wt-Kcv and S62T/T63S is at the respective voltages only 0.04. The results of these experiments demonstrate that the mutation in T63S-Kcv does not only affect Ba^{2+} sensitivity (see also below), but also the gating properties of the channel. This observation does not disagree with macroscopic currents obtained by whole-cell measurements in oocytes, which reveal similar conductances for wt-Kcv and T63S-Kcv. On the single channel basis the elevated open probability could be compensated by a lower overall conductance of the prevailing open channel levels.

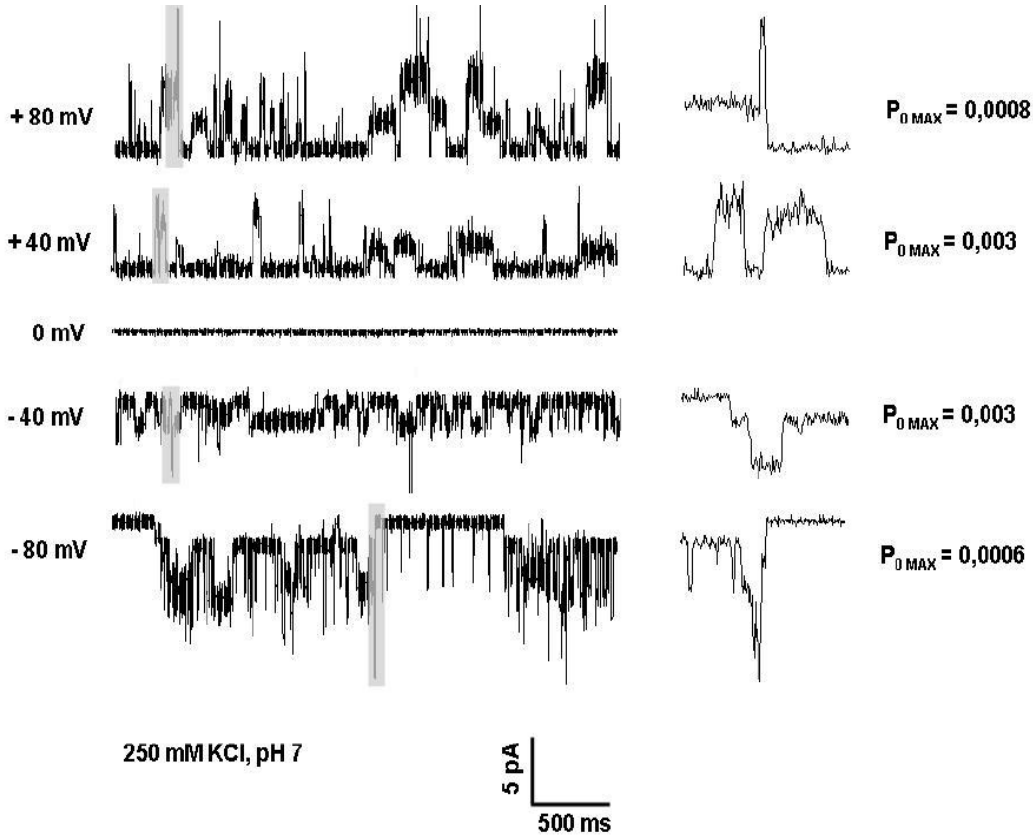

Figure 2.5 Time series of T63S-Kcv recorded at different positive and negative potentials. The records show numerous substates at all tested voltages. Grey colored sectors are shown enlarged in the right column.

Substates in wt-Kcv and T63S-Kcv

It has been reported previously that wt-Kcv also occasionally generates substates when reconstituted in planar lipid bilayers [5]. Such substates were also observed, albeit rarely, in the present study. Figure 2.6 shows exemplary time series of wt-Kcv and T63S-Kcv at -40 mV, each exhibiting diverse substates.

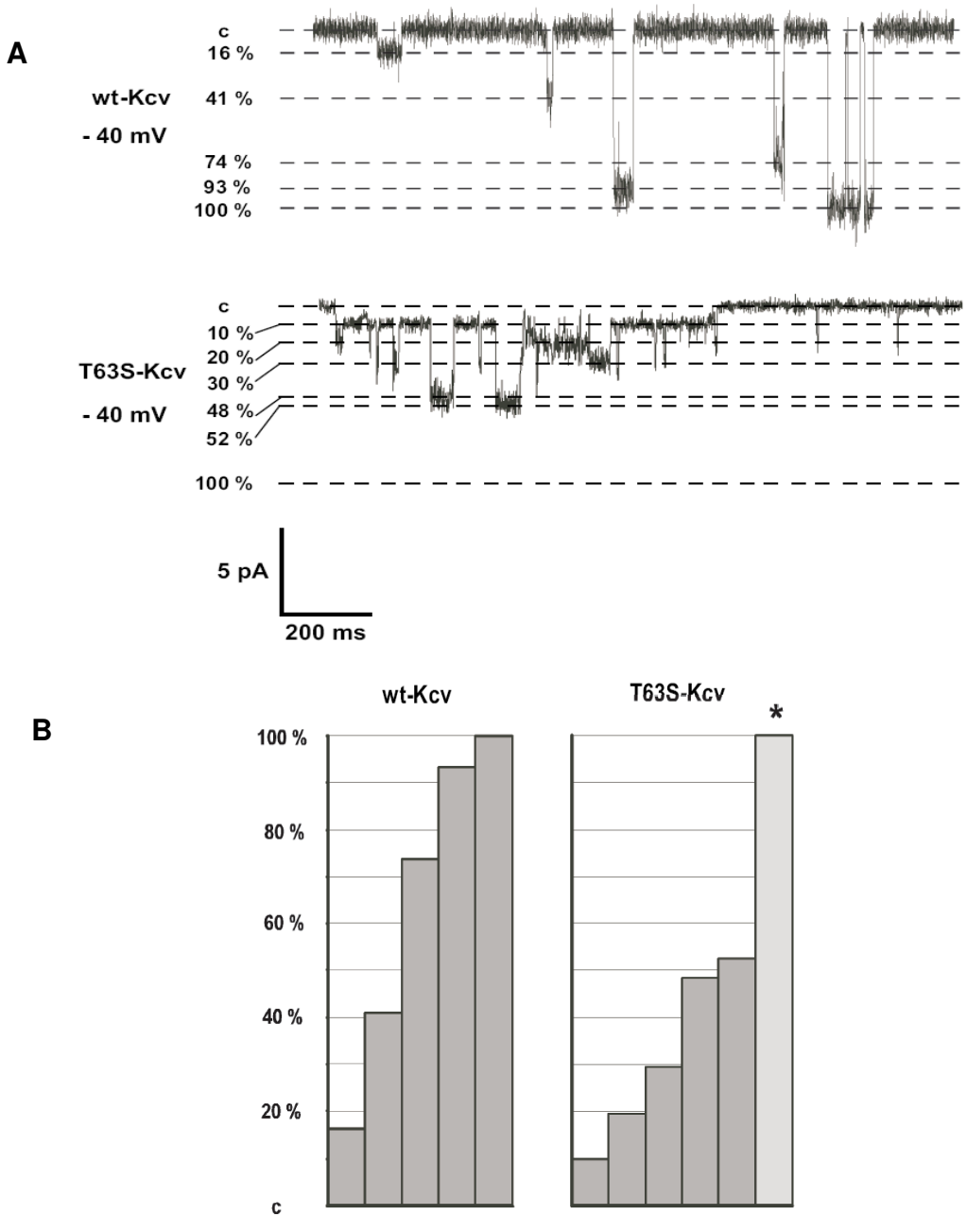

Figure 2.6 A Exemplary time series of wt-Kcv and T63S-Kcv recorded at -40 mV. Both channels exhibit numerous subconductances. **B** Comparison of conductance levels of wt-Kcv and T63S-Kcv as they occur in the time series above. Beside the full-open-conductance the time series of wt-Kcv exhibits 4 subconductances. The full-open-conductance (light grey bar marked by asterisk) is not reached in the time series of T63S-Kcv; the channel fluctuates between 5 different subconductances. The substates of the two channels do not directly correspond to each other and there is no systematic relation between them.

For wt-Kcv the 100 pS, respectively the 41% conductance level, is the predominant substate; with an even lower frequency also a few more substates can be seen, like the 16 %, the 74 % and the 93 % conductance levels. This demonstrates that substates are not per se a specific feature of T63S-Kcv; they can also occur, albeit, with a low frequency, in wt-Kcv. However, when we compare the substate levels of wt-Kcv with those of T63S-Kcv it becomes obvious that they are not identical; there is also no systematic relation between the different substates. Figure 2.6 **B** illustrates conductance levels of wt-Kcv and T63S-Kcv. Neither direct correlations of the substates nor fixed distances between them can be observed/ recognized.

I/V curves of wt-Kcv, T63S-Kcv and S62T/T63S-Kcv

To obtain the current voltage relation (I/V) of the three channels, the maximal unitary conductance level of wt-Kcv, T63S-Kcv and S62T/T63S-Kcv at all voltages was determined. From previous data it was already known that the I/V-relation of wt-Kcv is nonsymmetrical [5], [20]. This imposes a problem in the analysis because in bilayer reconstitutions the channel protein can in principle insert in one or the other orientation into the membrane. In >20 experiments with wt-Kcv we found that the I/V curve of this channel always showed a negative slope conductance at positive voltages when the protein was added to the trans-side of the membrane. The interpretation that the channel inserts with a biased orientation into the membrane is similar to a previous report on the reconstitution of Kcv in bilayers [5]. To further test this bias for insertion, we added protein in 5 other experiments to the cis-chamber. In these cases, the channel always generated an I/V curve with a negative slope at negative voltages. The results of these experiments demonstrate that the channel has indeed a strong tendency to insert in a prevailing orientation into the membrane. The site of the membrane to which the protein is added determines the orientation in the membrane. For further analysis, only experiments are considered in which the protein was added from the trans-side.

A plot of the maximal currents obtained under the aforementioned conditions as a function of voltage for wt-Kcv, T63S-Kcv and S62T/T63S-Kcv is shown in Figure 2.7.

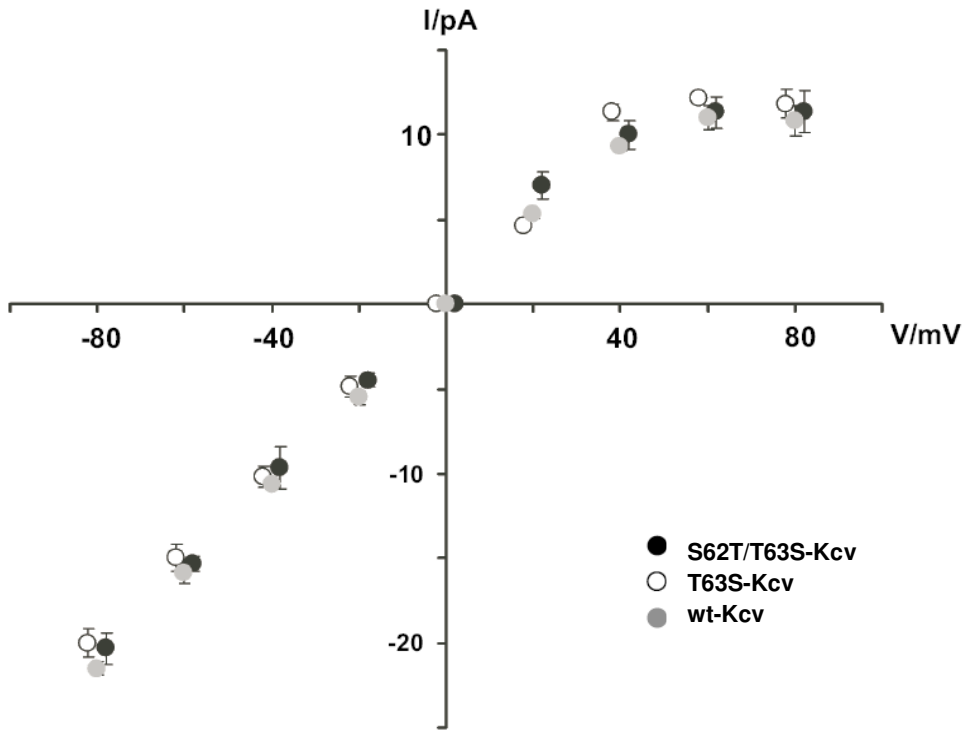

Figure 2.7 I/V relationships of maximal single channel conductance from wt-Kcv, T63S-Kcv and S62T/T63S-Kcv. Data are mean +/- SD from 5 measurements in symmetrical solution with 500 mM KCl, 10 mM Mops/ Tris, pH7.

The currents, which are averages from 5 measurements, give very similar I/V-relationships for all three channels. The plot is linear over a wide window of voltages (-80 mV to +40 mV); the slope conductance in the linear range (-80 to +20 mV) of all three channels is 250 pS. At positive voltages (>40 mV) a negative slope conductance can be observed for all three channels. The general shape of the I/V-relation as well as the conductance is similar to that reported previously for wt-Kcv [5], [20]. The results of these experiments mean that the mutations in the pore have no influence on the unitary conductance of the Kcv channel. In the case of S63T-Kcv, only the frequency with which the maximal conductance level is achieved is greatly reduced.

Transition probabilities between substates

The striking differences regarding the attendance of substates in T63S-Kcv compared with wt-Kcv can be further elucidated by a mean/ standard deviation plot of a typical time series, which is depicted in Figure 2.8.

For this analysis the standard deviation of 20 recorded data points (at +80 mV, symmetrical 500 mM KCl, 10 mM Mops/ Tris, pH 7.0) is plotted as a function of the average of the same data points. The x-coordinate represents the current and lines can be interpreted as transitions between different states; the more lines between two states the higher the corresponding transition probability. In the case of wt-Kcv mainly transitions between the closed (0 pA) and the maximal open state (12 pA) can be observed. The density of lines is higher in the range of the closed state; this is primarily because the noise of the closed state is smaller than that of the open state. In contrast the mean variance plot of T63S-Kcv is less defined, as expected from the time series. It reflects the rare attendance of the closed and maximal open state. In addition to the maximal open state, some other open states can be noticed. A small substate (0.8 pA corresponding to 10 pS), occurs to be the predominant conductance level. Most transitions start from or end at this state.

In comparison to T63S-Kcv the population of the closed state of wt-Kcv seems to be expanded. This could suggest that the channel rapidly fluctuates between a closed and a small conducting open state. A close scrutiny of the data, however, shows that the broad signal around the closed state in wt-Kcv is due to a higher noise level of the recording; it is not due to a substate.

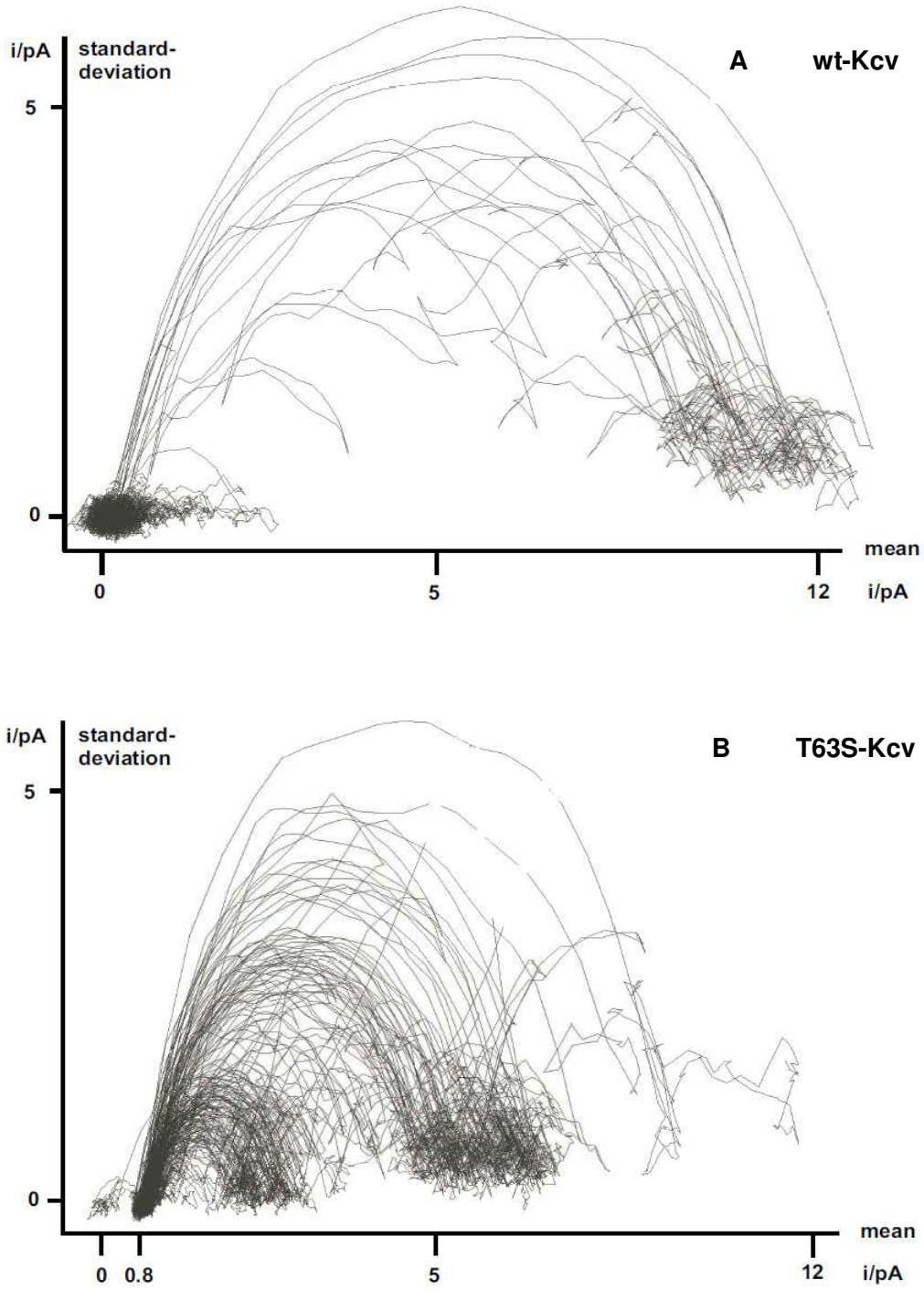

Figure 2.8 Mean/ standard deviation plots of **A** wt-Kcv and **B** T63S-Kcv reflect the conspicuous differences between the two channels concerning the occurrence of conductances. Lines represent transitions between states.

Contribution of fast gating to occurrence of substates

One of the most striking results of the present study is the observation that T63S-Kcv opens mostly only to distinct substates and only rarely reaches the full conductance level (O_M). In principle, these substates could reflect canonical substates i.e. conductance levels in which the channel is not fully conducting. Alternatively the substates could also be the result of kinetic modulations of the channel. If a channel opening is interrupted by very short closures, apparent substates could occur in channel recordings if these events are so fast that they are not resolved by the recording system.

The latter explanation for the substates in Kcv is not unrealistic: Firstly, in a previous study for a Ca^{2+}-activated K^+ channel from vascular smooth muscle cells it was shown, that at least some kind of substates can be considered as recording artefact induced by fast gating [21]. Secondly, a recent study gives evidence for the general occurrence of fast gating, also termed “flickering” in wt-Kcv [6]. Due to the limited resolution of the measuring system, respectively the low pass filter, this fast gating leads to the apparent negative slope conductance of the Kcv conductance at extreme voltages.

In contrast to I/V relations obtained from recordings in oocytes [4], not only wt-Kcv but also T63S-Kcv showed a negative slope conductance in the bilayer experiments presented here. This finding suggests that fast gating should also be present in T63S-Kcv. Furthermore, time series of wt-Kcv, T63S-Kcv and S62T/T63S-Kcv all display an increased asymmetric open-channel noise, which indicates a contribution of fast gating also for the mutants (Figure 2.4).

In order to test this suggestion, the “true” current (I_{true}) for T63S-Kcv was reconstructed using the procedure described in [9]. In summary, the low pass filter distorts the amplitude histograms of the current records. Instead of symmetric Gaussian distributions, they are comprised of skewed, so-called beta distributions [13]. The shape of these distributions allows under certain conditions the

reconstruction of the statistic properties of the undetected gating events, namely the true single channel current and the rate constants. Such beta distribution of amplitude histograms generated from single channel data were analyzed here.

Because T63S-Kcv signals display so many different conductance levels, only two predominant subconductances that also displayed a visibly increased open-channel noise (ca. 36 and 55% of maximal open conductance at +80 mV) were analyzed. The other subconductances had either very few data points or did not show increased noise, both features making beta analysis impossible.

As described in Materials and Methods, the amplitude distributions were fitted with different assumed currents. The one with the collective minimal error sum is assumed to represent the “true” current. An example of such a plot of chi square (the weighted error sum) as a function of I_{true} is depicted in Figure 2.9 for the 55% substate of T63S-Kcv at +80 mV.

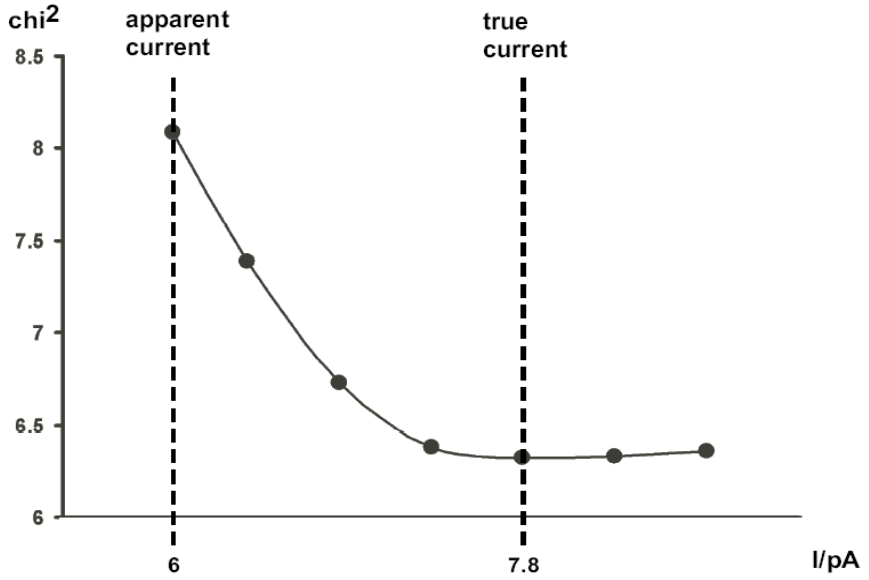

Figure 2.9 Plot of the weighted error sum as a function of I_{true} for one substate of T63S-Kcv (55% of the maximal open-conductance). The minimal error sum is correlated with the value which represents the “true” current.

The minimal error sum is given at a current amplitude of 7,8 pA, compared with the apparent current of 6 pA; the corresponding fit of distributions is illustrated in Figure 2.10.

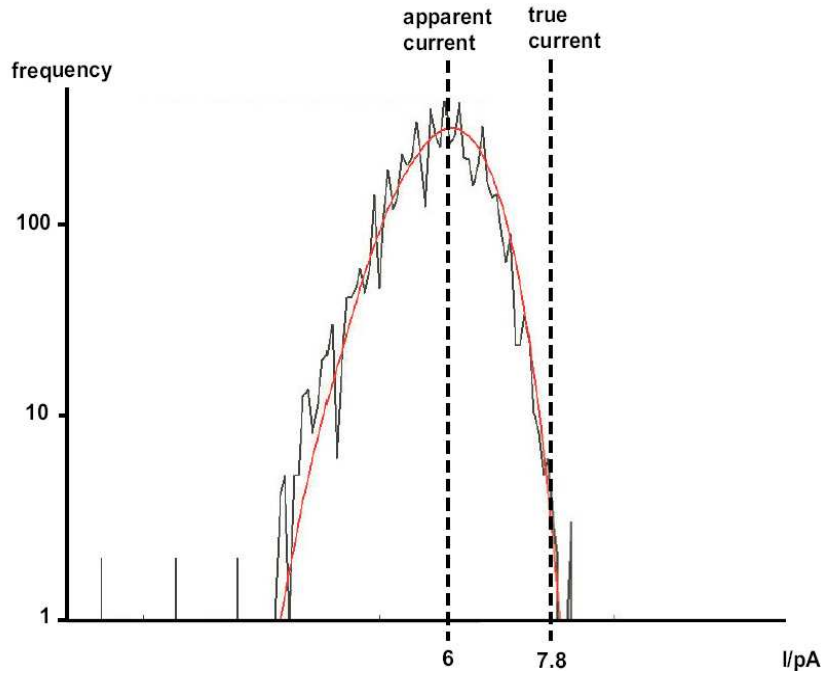

Figure 2.10 Fitted distributions (amplitude-histograms) of the measured current-signal (black curve) and the simulated signal (red curve). Dashed lines mark the apparent and "true" currents.

Figure 2.11 shows the I/V curves of the two selected substates (I_{app} 37% and 55%, grey lines) in comparison with the maximal open state I_{app} 100% (black line).

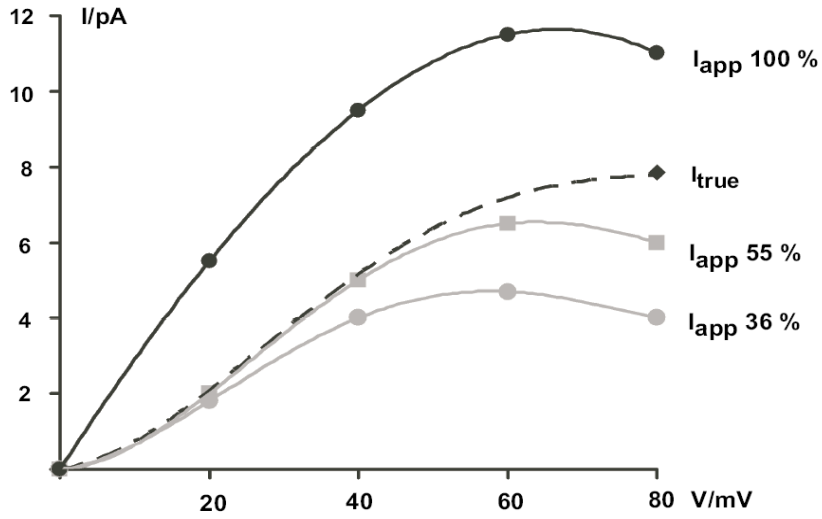

Figure 2.11 I/V curves of the two selected substates (I_{app} 37% and 55%, grey lines) compared to the maximal open state I_{app} 100% (black line). The negative conductance slopes of the apparent channel currents at high positive potentials reveal to be an artefact; the curve for reconstructed I_{true} current is higher and shows slight saturation. Although the conductance which corresponds to I_{true} is higher than the two apparent subconductances (36% and 55%) it is lower than the maximal conductance level.

Because the signal-to-noise ratio is a critical factor in beta analysis, the true current I_{true} for the two substates could only be reconstructed at +80 mV. Surprisingly, it was virtually identical for both the 37%-sublevel (7,79 pA) and the 55%-sublevel (7,8 pA). This suggests that possibly both substates are due to a fast block of one common conductance level; the recorded substate levels do not represent two distinct subconductance levels. The different apparent amplitudes of the currents arise from different rate constants, i.e. from different frequencies of fast gating. The dashed line for I_{true} is an estimation assuming that the behavior of the subconductances compared to the maximum conductance in T63S-Kcv is the same as in wt-Kcv. For the latter the relation was already well described by equation 2.1, which results from the depletion-theory [11].

Equation 2.1: $I_{true} = I_{app} * (1.2+0.09 \exp (x\ V / 34mV))$

Figure 2.12 depicts this principle schematically. The same true current I_{true} leads to two different apparent currents I_{app1} and I_{app2} depending on the frequency of fast gating.

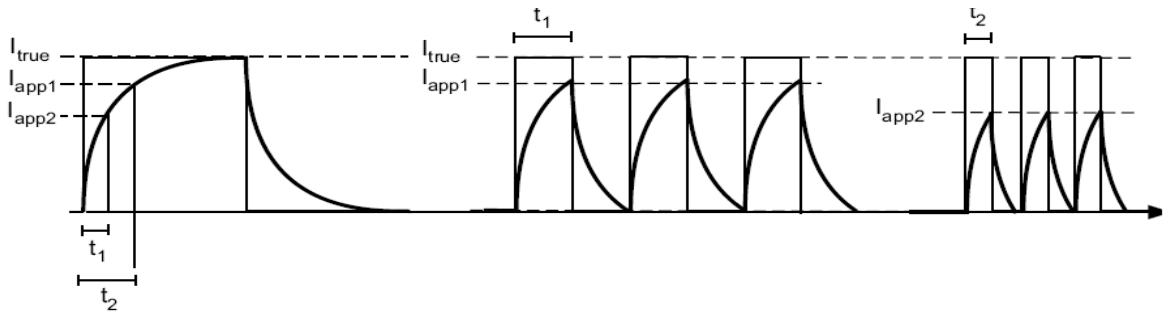

Figure 2.12 Schematic illustration of the relation between dwell times of the open state and the size of the apparent current amplitudes. Because of limitations of the measuring system an increase of the current signal is recorded with a delay. If this delay is slow relative to the dwell time of the open state, the full current amplitude is not detected, because the subsequent closing inverses the signal.

The data reveal that the reconstructed true current is larger than the measured current; however, I_{true} does still not reach the maximal channel amplitude. The data further show that in contrast to I_{app} the curve of I_{true} does not show a negative slope, but a moderate saturation, similar to the reconstruction of the true maximal current of Kcv-wildtype in Abenavoli et al. (2009). This suggests that also in the case of T63S-Kcv-substates the negative slope of I_{app} is evoked by fast gating. The rate constants are in a range of 10 to 40 kHz and hence too fast compared to the filter frequency of 1 kHz. For that reason I_{app} is an average over closed and open times at the input of the amplifier.

Altogether, the analysis of beta distributions supports the view that modulation of fast gating provides a suitable explanation for the occurrence of numerous substates. This could be shown for two of the many substates. Unfortunately, the same analysis could not be conducted for the remaining substates because their open dwell times

were too short. Nonetheless, it is reasonable to assume that also other substates are the result of fast gating events and hence caused by a kinetic effect. However, the calculated value for I_{true} did not correspond to the maximal open state. This implies that probably also a “real” reduction of the single channel current contributes to the occurrence of substates.

Differences in Ba^{2+} sensitivity

To test the three proteins for their sensitivity against Ba^{2+}, the blocker was added at a final concentration of 5 mM in both chambers. Soon after addition, currents of wt-Kcv and S62T/T63S-Kcv were blocked, whereas those evoked by T63S-Kcv seemed to be unaffected. Figure 2.13 shows a typical time series of currents from each protein in absence and presence of Ba^{2+}.

The block of wt-Kcv and S62T/T63S-Kcv turns out to be an extreme reduction of the open probability. A more detailed view of currents shows that the unitary channel amplitudes are more or less not affected by the blocker. However channel openings occur in the presence of Ba^{2+} as very short spikes implying that Ba^{2+} generates a strong decreased mean open dwell time. A similar effect of Ba^{2+} on the wt-Kcv channel was reported previously [5]. Figure 2.14 shows the Ba^{2+} block of wt-Kcv more detailed. A closer scrutiny of one of the spikes, recorded in the presence of Ba^{2+}, reveals that these events are still channel-like fluctuations with a full opening of the channel.

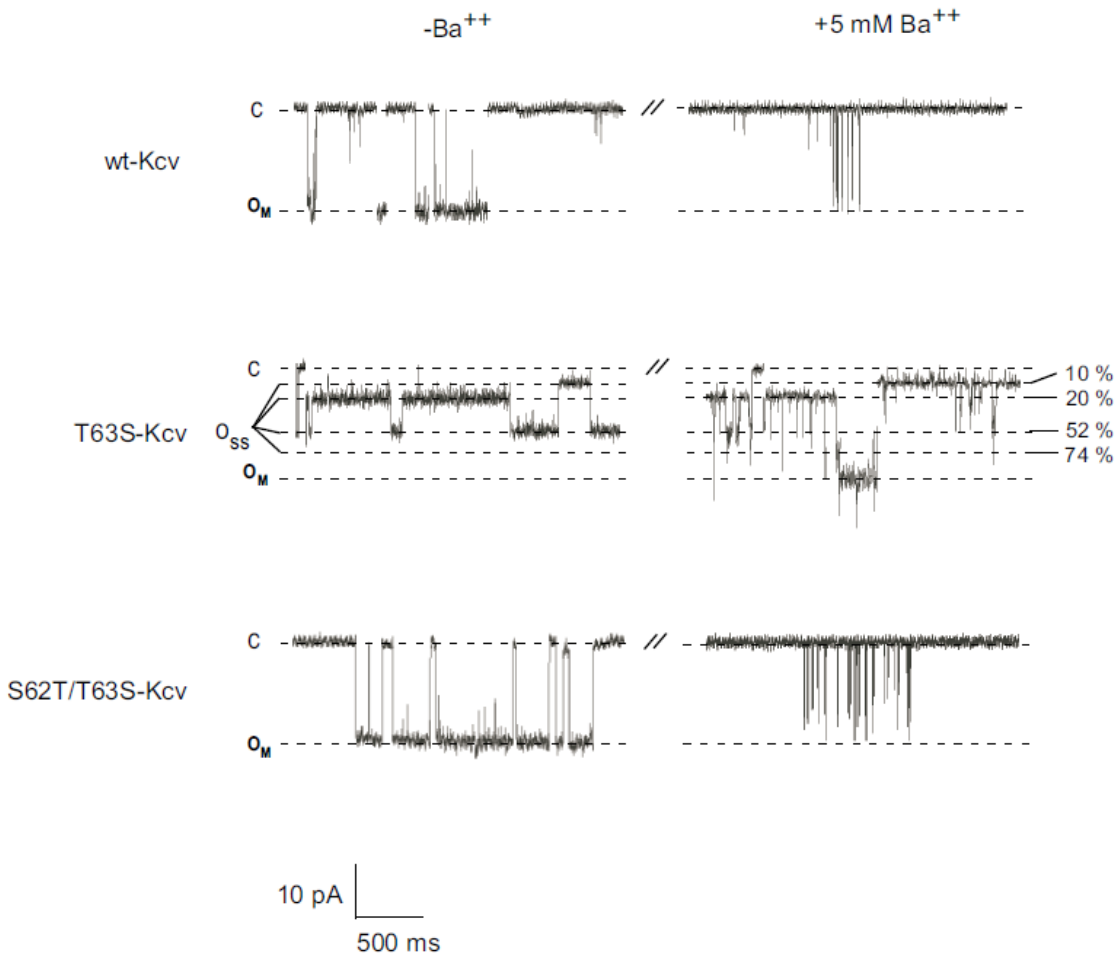

Figure 2.13 Time series of wt-Kcv, T63S-Kcv and S62T/T63S-Kcv before and directly after adding 5 mM BaCl2 to the cis and trans buffer. Wt-Kcv and S62T/T63S-Kcv are blocked nearly completely; the open dwell times are dramatically decreased. In contrast the single channel signal of T63S-Kcv exhibits no appreciable change in presence of Ba^{2+}.

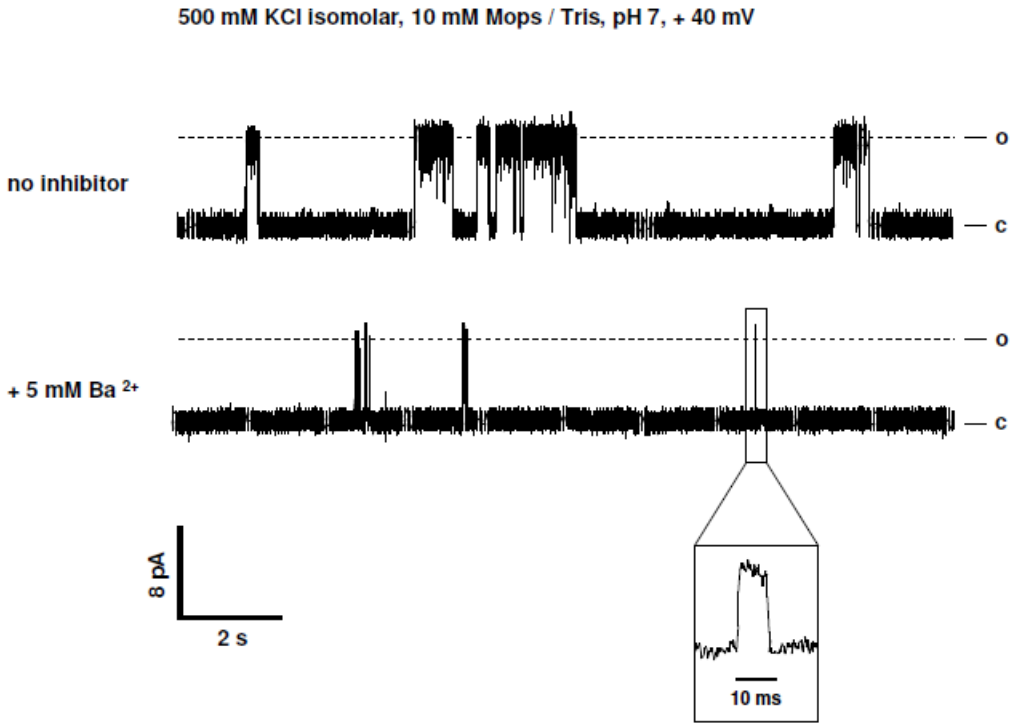

Figure 2.14 A Detailed view on time series of T63S-Kcv before and after adding 5 mM BaCl to cis- and trans-buffer. An enlargement of the marked sector in the lower row reveals that the little spikes actually are short discrete openings.

Properties of Ba^{2+} block

In order to further study the properties of the Ba^{2+} block, we tested whether it is reversible. Therefore, Ba^{2+} was first added in order to block the channel and subsequently precipitated by adding 10 mM $NaSO_4$ to both chambers. Figure 2.15 depicts an exemplary time series of wt-Kcv at -60 mV in absence (*), presence of 5 mM BaCl (**) and after further addition of $NaSO_4$ (***).

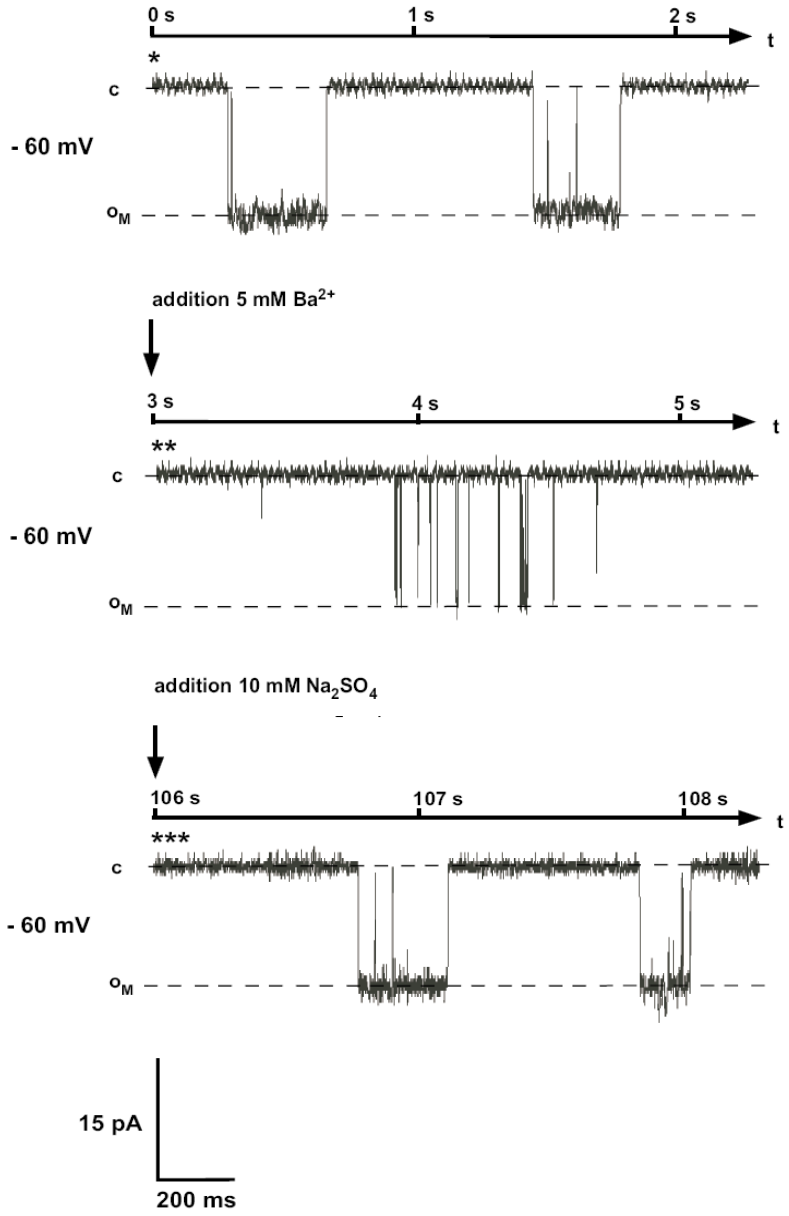

Figure 2.15 Reversibility of the Ba^{2+} block: upper row displays signal of T63S-Kcv at -60 mV before block. In the middle row the arrow on the left side indicates the point at which BaCl2 was added at 5mM to the cis- and trans-chamber; the channel is immediately blocked. In the lower row the arrow marks the addition of Na_2SO_4 at -60 mV to both chambers. Due to precipitation of Ba^{2+} the block is subsequently abolished.

Due to the precipitation of Ba^{2+}, the initial open probability is recovered suggesting that the Ba^{2+} block is completely reversible. The same effect can be observed for all potentials (data not shown).

Although Ba^{2+} appears to have no appreciable influence on T63S-Kcv, nonetheless, in one single measurement a short transient block was observed. Figure 2.16 depicts the respective time series.

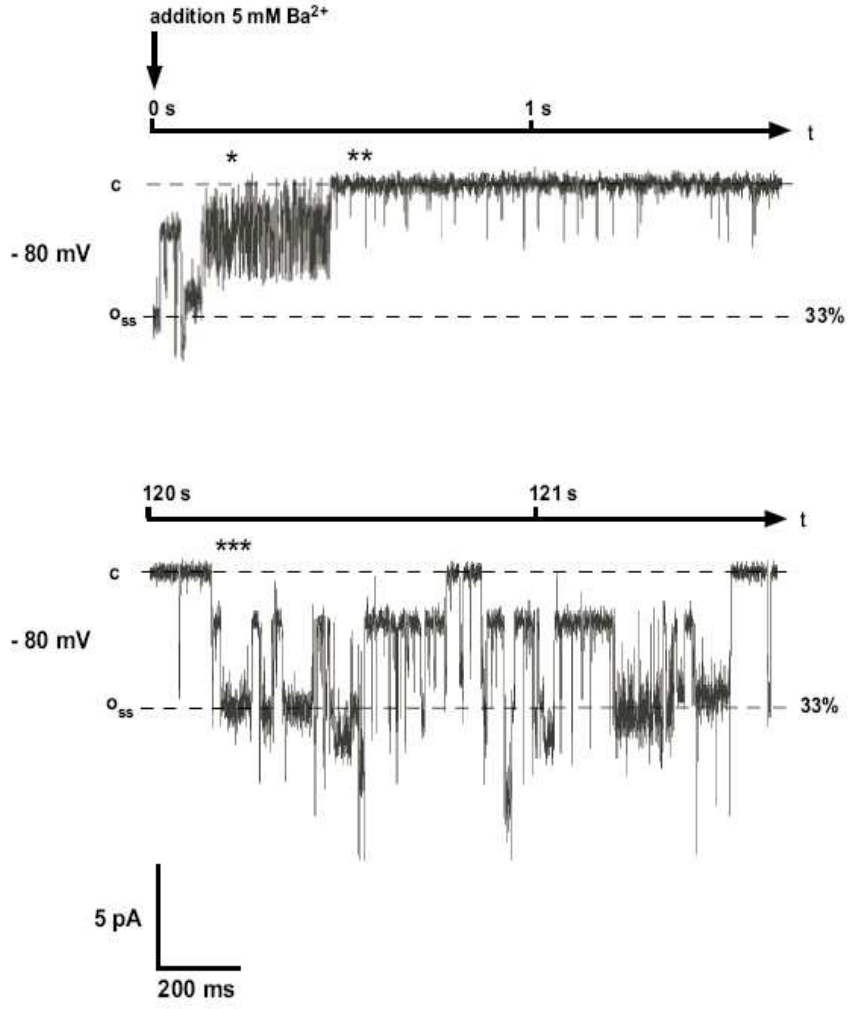

Figure 2.16 Time series of T63S-Kcv at -80 mV. Although the channel usually shows no effect upon the adding of BaCl, in one measurement the presence ob Ba^{2+} led to an extreme increase of noise, respectively flickering and a 40 sec long transient block. After that period the block disappeared again.

Immediately after adding BaCl to the cis- and trans-chambers the open channel noise increased (*) followed by a sudden block (**), which stayed for 40 sec before disappearing again (***). This observation reveals that also T63S-Kcv can in principle be blocked by Ba^{2+}. This block may not be stable because of the dramatically increased K_d value. An alternative explanation for this observation is that Kcv has two different open states and only one of them, the most frequently occurring state, is not Ba^{2+}-sensitive. This interpretation is also in line with the recent data obtained from whole cell recordings of T63S-Kcv in oocytes, which show that addition of Ba^{2+} leads to a modest inhibition in the mutant [4].

Influence of Ba^{2+} on open probabilities

In order to quantify functional differences between wt-Kcv, T63S-Kcv and S62T/T63S-Kcv, furthermore, the open probabilities in absence and presence of Ba^{2+} were analyzed. Therefore, histograms of amplitudes for each time series were created and fitted with multiple Gauss-functions. Afterwards, the open probabilities were expressed as ratios of the corresponding integrals. Due to the high number of substates in the case of T63S-Kcv, it was not possible to calculate open probabilities for each single conductance level. Hence, just the overall-open probability (p_o*) and the probability to achieve the maximum conductance level (p_o^M) were discriminated.

For wt-Kcv and S62T/T63S-Kcv these two different open probabilities are nearly the same, because when these channels open, they usually adopt the maximum open state; substates only rarely occur. Figure 2.17 shows open probabilities of the maximal open state as a function of voltage for wt-Kcv, T63S-Kcv and S62T/T63S-Kcv in absence and presence of Ba^{2+}.

Before adding $BaCl_2$, the overall open probability (p_o*) for T63S-Kcv is at + 80mV about 15-fold higher than the open probability for wt-Kcv and S62T/T63S-Kcv. Interesting to note is that the open probability of S62T has the same voltage dependency as the wt and the double mutant.

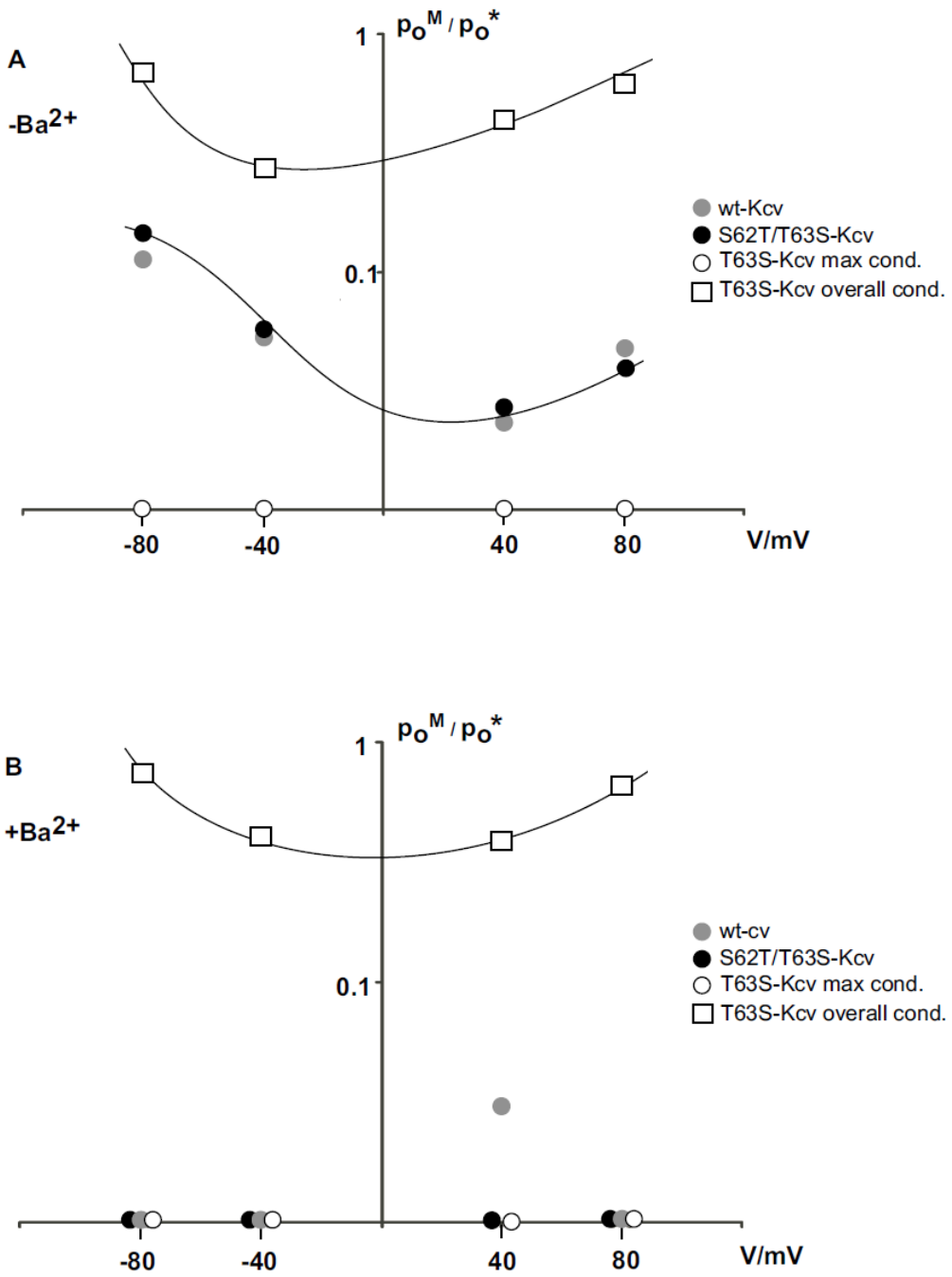

Figure 2.17 Open probabilities as functions of voltage for wt-Kcv, T63S-Kcv and S62T/T63S-Kcv before **A** and after **B** adding BaCl. Grey circles mark wt-Kcv, black circles indicate S62T/T63S-Kcv and white circles represents the probability for the maximal conductance of T63S-Kcv; the white squares mark the probability for the overall conductance of T63S-Kcv. This overall conductance includes the occurrence of all states apart from the closed state.

While the overall open probability of T63S-Kcv is higher compared to the two other channels, the open probability for the maximal conductance level of T63S-Kcv is dramatically lower than those from wt-Kcv and S62T/T63S-Kcv. Because of the rare appearance and the very short dwell times of the maximum open state of T63S-Kcv, it was not possible to achieve a statistically robust value; but it is clear that the value is at least a factor of 50 smaller than the corresponding values of the two other proteins.

In presence of Ba^{2+}, the open probabilities of wt-Kcv and S62T/T63S-Kcv also fall below this detection limit, e.g. they are much smaller than 0.01; the analysis does not allow to discriminate between wt-Kcv and S62T/T63S-Kcv. The overall-open probability P* of T63S-Kcv seems to be unaffected by Ba^{2+}.

Discussion

Electrophysiological recordings in *Xenopus* oocytes which express the wildtype of the potassium-selective Kcv-channel show that this channel is almost completely blocked in the presence of (>5 mM) Ba^{2+} or (>5 mM) amantadine [1]. By employing a yeast complementation assay mutants of Kcv, which were generated by randomized mutagenesis, were screened for Ba^{2+}- and amantadine-insensitive variants. A PCR-backcrossing procedure finally revealed the amino acid at position 63, which in wt-Kcv is a threonine, to play a crucial role for the sensitivity against the cationic blockers Ba^{2+} and amantadine [4]. In a further step, voltage clamp experiments with mutant-transfected *Xenopus* oocytes were carried out. Titration with Ba^{2+} revealed that an exchange of threonine at position 63 against serine leads to a 100-fold increase of the K_d value; and hence to an extreme reduction of the Ba^{2+} sensitivity.

Based on the deduced structural homology-model, it can be assumed that the amino acid at position 63 is involved in the coordination of both K^+ and Ba^{2+} within the selectivity filter [2]. Thus, also on the structural level it seems plausible that a mutation of this amino acid can affect the block by Ba^{2+}. The present experiments in which the mutant channel was reconstituted in planar lipid bilayer confirm this assumption. The analysis of channel fluctuations generated by the wt-Kcv protein show that Ba^{2+} blocks the K^+ channel. This block is mainly due to a decrease in the open probability because of a reduction of the open time; the number of opening- and closing events however is hardly influenced. In contrast, T63S-Kcv does not show an appreciable sensitivity against Ba^{2+}. The reduction of the open probability in the presence of Ba^{2+} is too small to discriminate it from the open probability in the absence of Ba^{2+}. The fact that Ba^{2+} exhibits no detectable effect on the activity of T63S-Kcv may indicate that the affinity to Ba^{2+} is even smaller in the bilayer system than in oocytes. Alternatively, it is also possible that small changes in the open probability after addition of Ba^{2+} are not detectable on a background of the statistic variability of the open probability in the absence of Ba^{2+}. At least in one experiment we were able to detect also with the mutant-channel a transient decrease in open probability. This means that the channel is, as expected from the expression studies in oocytes, still

sensitive to Ba^{2+}. In this context it might be possible that the mutant has different modes, which alternate between low and high Ba^{2+} sensitivity. The remaining sensitivity of the mutant in oocytes could be due to the statistically rare occurring mode of a higher Ba^{2+} sensitivity.

Although the present study gives clues about the site of block in the protein and some functional details of the Ba^{2+} block, it remains nonetheless surprising that the subtle change T->S displays such a strong impact on the channel function. Altogether, the selectivity filter of Kcv possesses 4 coordination sites. In this context threonine 63 is the only amino acid which is involved in coordination but which does not contribute to the coordination by ionic interactions between its backbone and the cation but between the side chain oxygen and the cation. However, this side chain oxygen is not affected by a mutation from threonine to serine. Hence we must assume that the altered Ba^{2+} sensitivity in the mutant is due to a steric modulation of this site.

An important result of the present experiments is that the T63S mutant is not only insensitive to Ba^{2+} but also generally fluctuates mostly between a closed and many different apparent substates. Altogether, the modified Ba^{2+} sensitivity and the difference in unitary channel fluctuations between wildtype-Kcv and T63S-Kcv find a coherent explanation in a simple drug-receptor-model [22]. In this model both, K^+ and Ba^{2+} represent the “drug” and the coordination site in the filter is the receptor. This is a valid assumption because both ions can be detected in the selectivity of the KcsA crystal. Ba^{2+} can be found in the 4^{th} site, i.e. the site at the border to the cavity [2]. The data imply that the mutation reduces the affinity between both K^+ and Ba^{2+} and the coordinating amino acids. As a result the residence time, respectively the dwell time of a K^+/ Ba^{2+} cations is independent of its concentration and only determined by the dissociation rate constant of K^+/ Ba^{2+} from the coordination site. The higher the dissociation rate constant is the smaller is the affinity and the dwell time of the cations. According to the model, the probability that a cation occupies the coordination site increases with its concentration and correlates with the association-rate-constant. The higher the Ba^{2+} concentration is the more closures take place.

This model is fully compatible with the present data. The long closures of wt-Kcv in presence of Ba^{2+} can be explained by a long dwell time of the cation in the coordination site; this corresponds to a high affinity of the site for Ba^{2+}. As a result of a decreased affinity in case of T63S-Kcv the duration of the closures decrease and the resulting current appears to be blocked less. In T63S-Kcv the affinity to Ba^{2+} becomes so low that the channel does not exhibit any more closures.

According to this model, also K^+ is binding to the same site; because of its high affinity we can assume that also K^+ results in short closures of the wt-channel. This assumption is reasonable assuming the evidence that the selectivity filter of K^+ channels, including that of Kcv, is contributing to gating [6], [23]. The mutation not only lowers the affinity of site 4 to Ba^{2+} but also to K^+. The shift from a high affinity to a low affinity binding has implications on the gating [22]. In this case, the channel conductance is expected to flicker as K^+ rapidly blocks and unblocks the channel. If this reduction of the affinity is very strong, the channel is expected to reveal only fast flickering activity. If this flickering is faster than the recording system, the closures and the openings can no longer be fully resolved [6]. As a consequence, channel fluctuations could appear as apparent substates. The predictions of this model are well supported by the present data. T63S-Kcv can open to the full unitary conductance level but exhibits mostly openings to various substates. An analysis of two of these substates implies that the reduced amplitude is not a canonical substate but due to a fast flickering block. This strongly supports a model according to which the mutation T63S alters the interaction between K^+ and the coordination site between a high affine to a low affine interaction. The different levels of substates may therefore reflect multiple binding affinities, which can occur between the respective site and Ba^{2+}. The latter analysis is not able to reconstitute the full opening from all the substate conductances. Hence, we can not exclude that some of the subconductances are indeed canonical substates. However, it is also possible that the low signal to noise ratio in the bilayer recordings is not sufficient for a full reconstitution of all the substates.

The existence of such a fast kinetic and its effect on single channel-signals in fact is plausible: In a previous study on Ca^{2+}-activated K^+ channels from vascular smooth muscle cells it was shown, that at least some kind of substates can be considered as recording artefact evoked by fast gating [21]. Further on, a recent study gave evidence that this fast gating or also termed “flickering” basically also exists in wt-Kcv; the negative slope conductance at extreme positive potentials could be explained as an artificial reduction of the “true” full-open current [6].

The aforementioned model implies that the wildtype-channel has in the selectivity filter a higher affinity to K^+ and Ba^{2+} than T63S-Kcv. This prediction of the model is also supported by the data. Western blots with the protein from the wt and the mutant channel revealed that the channel runs in an SDS gel as a tetramer. Previous data showed that the stability of the tetramer is maintained by the cations, which enter the channel pore [5]. The same analysis revealed that also Ba^{2+} is able to stabilize the tetramer meaning that Ba^{2+} and K^+ are able to enter the selectivity filter. Corresponding experiments with the mutant revealed that higher concentrations of K^+ or Ba^{2+} are required to stabilize the T63S-mutant tetramer [5]. The results of these experiments are consistent with the idea that the mutation has lowered the affinity of interaction of the selectivity filter for Ba^{2+} and K^+.

The only difference between wt-Kcv and T63S-Kcv is the additional methyl group at the C2 of threonine which is missing in serine. Because this subtle deviation is not implying any obvious difference for ionic interactions, we must assume that more diffuse interactions play a role in defining the different affinities between K^+/ Ba^{2+} and the coordinating amino acids. This hypothesis is also supported by two other observations. First, also the wt channel rarely reveals substates. If we are assuming that also these subconductance levels are due to a fast gating, we can speculate that the general mechanism of this kind of block is already present in the wt channel and only augmented by subtle changes in the mutation. Furthermore data from this and other studies show that the effect of T63S-Kcv is compensated by a double mutant S62T/T63S-Kcv [4]. Wt-Kcv has a serine at position 62 which is also part of the conserved filter-region. However, compared with most other K^+ channels this is

untypical. The insertion of threonine instead of serine at this position makes this domain more similar to the common filter-sequence of all K^+ channels. Recent voltage-clamp measurements of Kcv channels in oocytes showed that the double mutant severely lowers the effect of the mutation at position 63; while the single mutant T63S-Kcv exhibits a 100-fold increase of the K_d-value for Ba^{2+}, the double mutant S62T/T63S-Kcv shows only a 12-fold increase compared to the wildtype. Although the single channel-data from planar lipid bilayers experiments qualitatively reflect the different Ba^{2+} sensitivity of the two mutants, they do not show appreciable differences between the double mutant and the wildtype. In the presence of 5 mM Ba^{2+}, the open probability of the wildtype is considerably lower than 0,01 and can not be determined very accurately by the applied method. Probably a 12-fold shift of the K_d value, which would correspond to the expected value of the double mutant S62T/T63S-Kcv is too small to detect.

In the light of the aforementioned considerations, multiple kinds of chemical and structural interactions could be responsible for the strong effect of T63S-Kcv. One possibility could be an unspecific steric effect, which contributes to an altered orientation of the amino acid. This in turn could influence binding distances between the amino acid and K^+/ Ba^{2+}. Furthermore, the function of the amino acid could depend on a conformational stabilisation by the helical-structured TM2 domain of the channel which serves as backbone. Although such a stabilisation might also be disturbed by steric differences of the residues, in this context probably hydrogen bonds seem to play a more important role. Threonine 63 which occurs in wt-Kcv channel possesses an additional methyl group compared to serine. This methyl group can in principle form three hydrogen bonds with its environment. The necessity of such a stabilisation is not unrealistic, because in contrast to the transmembrane domains TM1 and TM2, the selectivity filter does not form a stable helical structure. The lack of stacking and hydrophobic effects does not prevent the torsion and flipping of the participated amino acids; however, a stable configuration of these amino acids is supposed to be a basic feature for their function as coordination sites and hence for the selectivity of the filter. A recent study addressed the question whether the selectivity filter itself could furthermore serve as an inner gate at the occupancy of

distinct stable conformational states (one open and one nonconducting state) of the selectivity filter [24]. Therefore, free energy molecular dynamics simulations of the bacterial K^+ channel KcsA were employed which are based on data of the according crystal structure. The transition between these conformational states is affected by a modest rearrangement involving two amide planes (Val76-Gly77 and Thr75-Val76) of one of the four subunits. The states are assumed to be strongly stabilized by hydrogen bonds between the involved amino acids of the selectivity filter and the helical TM2 domain.

Generally, the occurrence and the probability of a closed and multiple discrete open states can be reflected by a corresponding diagram which plots the free energy as a function of a conformational change. Such a conformational change can be considered as transition between discrete structures of the channel which causes different conductivities. Figure 2.18 compares diagrammatically the possible energy landscapes of wt-Kcv and T63S-Kcv as they would reflect the single channel signals; this includes also the relative probability of their occurrence. The minima of the curve represent more stable/ preferred conformations and the maxima unstable/ unfavorable conformations. The unstable/ unfavorable conformations form energetic barriers for transitions between the stable/ preferred conformations which represents the open and closed states. Figure 2.18A sketches the function as it might look like in the case of wt-Kcv. Two absolute free energy minima mark the closed (c) and the maximal open state (o_{max}) state; concurrently the minimal free energy implies a high probability for their occurrence. The dashed line describes a maximum between c and o_{max} which marks an unstable state and has to be overcome during the transition from the closed to the maximal open state. However, a closer scrutiny uncovers local minima which lie in between these states and represents substates (o_{ss}) of the channel. Because the free energy nonetheless, is relatively high, they rarely occur. On the left and right edge the curve increases exponentially; these regions reflect conformational states which are more or less “impossible”.

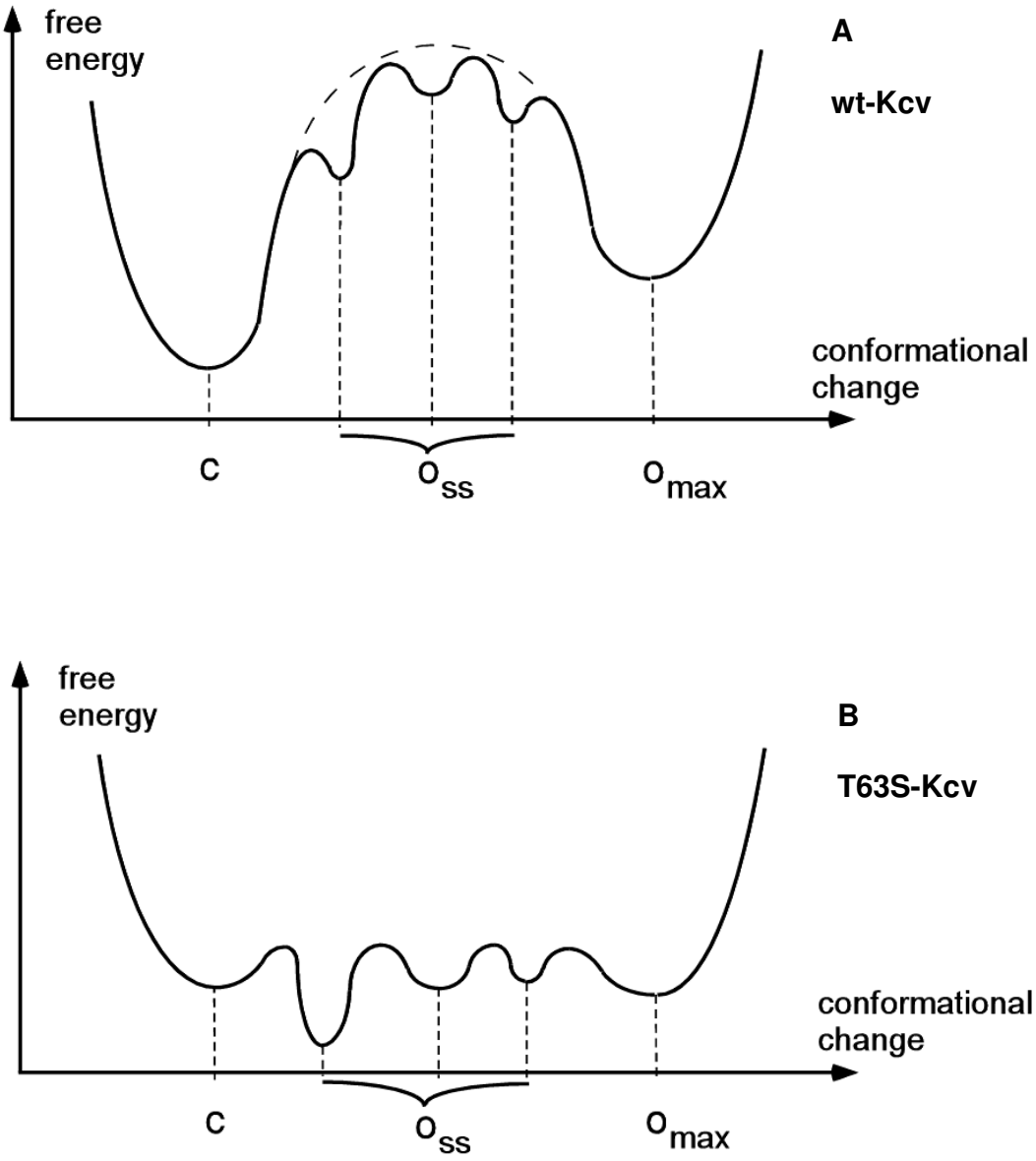

Figure 2.18 Schematic representations of energy-landscapes of **A** wt-Kcv and **B** T63S-Kcv (free energy of the channel are plotted as a function of conformational change). Minima represent stable states of the channels: closed (c), substates (o_{ss}) and full open state (o_{max}). Transitions between these states are accompanied by conformational changes of the channels; therefore local maxima have to be overcome. The free energy of each state is correlated with the relative occurrence of the according state.

Figure 2.18B sketches the according function of free energy as it could look like in case of T63S-Kcv. The energy landscape shows a different picture. Although, the position of the local minima concerning the x-coordinate is very similar compared to wt-Kcv the position along the y-coordinate and hence, the absolute free energy is shifted considerably. The values for all substates are considerably decreased. The free energy of the smallest substate is even lower than the free energy of the closed and the maximal open state; hence, it consequently represents the most occurring state. Furthermore, also in these free energy-diagrams it is obvious that the overall-open probability of the T63S-mutant is increased compared to wt-Kcv.

The data of the present study give evidence that the selectivity filter of Kcv works as gate. Different substates of the channel are characterized by a modulated affinity between certain amino acids within the selectivity filter and the conducted cations. As a result the change of affinity is mediated by very subtle alterations in the channel-structure. In contrary to general expectations the highly conservative exchange of the amino acid threonine 63 against serine displays a strong impact on the channel function. This demonstrates that even very small differences can influence considerably the affinity between channel and ion if they take place at a delicate position within the filter region. There they interrupt weak bonding forces, which are structurally and functionally important.

The present model in which the filter really fulfills the role of a gate is not unrealistic. A recent study pursued a theoretical approach and used Monte Carlo simulations in order to describe the coupling between gating and permeation [25]. Based on the structure of the KcsA K^+ channel the occurrence of substates in single channel signals could be well explained by a stochastically alternation between two conformations of the channel. These two conformations differ from each other just in their affinity between the selectivity filter and the conducted cations (K^+ and Na^+). The high affinity-conformation which corresponds to the closed state is coupled with high selectivity for K^+; the dissociation of K^+ is slow. The low affinity conformation which corresponds to the open state is coupled with low selectivity for K^+; the dissociation of K^+ is fast and there is no strong interaction between the filter and the cations. The

present single channel measurements in the planar lipid bilayer, especially experiments with the channel blocker Ba^{2+} are fully compatible with this model.

Furthermore, the coupling between the selectivity filter and gating was recently also shown experimentally [23]. Therefore purified channel proteins (of KcsA wildtype and KcsA mutants) were reconstituted in proteoliposomes and studied using a patch clamp setup. Mutations in the filter domain of KcsA, which affect the functional important interaction between glutamine 71 and asparagines 80, are associated with a considerably changed C-type inactivation of the channel and hence with an alternated kinetic. Single channel signals of KcsA wildtype and the KcsA mutants differ concerning the rate of their inactivation and their dwell times.

Both, the theoretical predictions from the Monte Carlo simulations and the patch-clamp-experiments with wt-KcsA/ KcsA mutants coincide with the data from the present study of wt-Kcv/ Kcv mutants concerning the role of selectivity filters for channel-gating. This strongly argues for a general functional principle which is inherent to all K^+ channels.

Altogether, the instant study demonstrates that Kcv is generally a suitable model-system for the investigation of ion-permeation and gating of channels.

References Chapter 2

[1] Plugge B, Gazzarrini S, Nelson M, Cerana R, Van Etten JL, Derst C, DiFrancesco D, Moroni A, Thiel G (2000) A Potassium Channel Protein Encoded by Chlorella Virus PBCV-1. Science 3 March 2000: Vol. 287. no. 5458, pp. 1641 - 1644

[2] Tayefeh S (2007) Computational study of the Kcv potassium channel. Dissertation, TU Darmstadt, 2007

[3] Hertel B, Tayefeh S, Mehmel M, Kast SM, Van Etten J, Moroni A, Thiel G (2006) Elongation of outer transmembrane domain alters function of miniature K^+ channel Kcv. J. Membr. Biol. 210:21-29

[4] Chatelain FC, Gazzarrini S, Fujiwara Y, Arrigoni C, Domigan C, et al. (2009) Selection of Inhibitor-Resistant Viral Potassium Channels Identifies a Selectivity Filter Site that Affects Barium and Amantadine Block. PLoS ONE 4(10): e7496. doi:10.1371/journal.pone.0007496

[5] Pagliuca C, Goetze TA, Wagner R, Thiel G, Moroni A, Parcej D (2007) Molecular properties of Kcv, a virus encoded K+ channel. Biochemistry. 2007 Jan 30;46(4):1079-90

[6] Abenavoli A, DiFrancesco ML, Schroeder I, Epimashko S, Gazzarrini S, Hansen UP, Thiel G, Moroni A (2009) Fast and slow gating are inherent properties of the pore module of the K^+ channel Kcv. JGP vol. 134no. 3219-229

[7] Schrempf H, Schmidt O, Kümmerlen R, Hinnah S, Müller D, Betzler M, Steinkamp T, Wagner R (1995) A prokaryotic potassium ion channel with two predicted transmembrane segments from *Streptomyces lividans*. EMBO J., 14, 5170–5178.

[8] Montal M, Mueller P (1972) Formation of bimolecular membranes from lipid monolayers and a study of their electrical properties. Proc Natl Acad Sci USA 69:3561-3566

[9] Schroeder, Hansen (2006) Schroeder, I., Hansen, U.P. 2006. Strengths and limits of Beta distributions as a means of reconstructing the true single channel current in patch clamp time series with fast gating. J. Membrane Biol. 210: 199-212

[10] Sigworth FJ (1985) Open channel noise. I. Noise in acetylcholine receptor currents suggests conformational fluctuations. Biophys J. 47(5):709-20

.

[11] Schröder I, Huth T, Suitchmezian V, Jarosik J, Schnell S, Hansen UP (2004) Distributions-per-level: a means of testing level detectors and models of patch-clamp data. J. Membrane Biol. 197: 49-58

[12] Schultze R, Draber S (1993) A nonlinear filter algorithm for the detection of jumps in patch-clamp data. J Membr Biol. 132:41-52

[13] FitzHugh R (1983) Statistical properties of the asymmetric random telegraph signal with application to single channel analysis. Math. Biosci. 64:75–89

[14] Yellen G (1984) Ionic permeation and blockade in Ca^{2+}-activated K^+ channels of bovine chromaffin cells. J Gen Physiol. 84:157-186

[15] Klieber HG, Gradmann D (1993) Enzyme kinetics of the prime K^+ channel in the tonoplast of *Chara*: selectivity and inhibition. J Membr Biol. 132:253-265

[16] Schroeder, Hansen (2007) Schroeder, I., Hansen, U.P. 2007. Saturation and µs-gating of current indicate depletion induced instability of the MaxiK selectivity filter. J. Gen. Physiol. 130: 83-97

[17] Schroeder I, Hansen UP (2008). Tl^+-induced µs-gating of current indicate instability of the MaxiK selectivity filter as caused by ion/protein interaction. J Gen Physiol. 2008 April; 131(4): 365–378

[18] Nelder JA, Mead R (1965) A simplex method for function minimization. Computer Journal, 1965, vol 7, pp 308–313

[19] Caceci, M.S. and W.P. Cacheris. 1984. Fitting curves to data - the simplex algorithm is the answer. *BYTE*. 5:340-362

[20] Shim, J.W., M. Yang and L.Q. Gu. 2007. In vitro synthesis, tetramerization and single channel characterization of virus-encoded potassium channel Kcv. FEBS Lett. 581:1027-1034

[21] Moss GW, Moczydlowski E (1996) Rectifying conductance substates in a large conductance Ca^{2+}-activated K^+ channel: evidence for a fluctuating barrier mechanism. J Gen Physiol. 107:47-68

[22] Hille B (2001) Ionic Channels of Excitable Membranes. 3rd edition. Sinauer Associates Inc., Sunderland, MA. 607 pp

[23] Cordero-Morales JF, Cuello LG, Zhao Y, Jogini V, Cortes DM, Roux B, Perozo E (2006) Molecular determinants of gating at the potassium-channel selectivity filter. Nat Struct Mol Biol.13:311-318

[24] Bernèche S, Roux B (2005) A gate in the selectivity filter of potassium channels. Structure. 13:591-600

[25] VanDongen AMJ (2003) K channel gating by an affinity-switching selectivity filter. PNAS vol. 101 no. 9 3248-3252

Chapter 3: PB1-F2

The proapoptotic Influenza A virus protein PB1-F2 forms a nonselective ion channel

Abstract

PB1-F2 is a proapoptotic influenza A virus protein of approximately 90 amino acids in length which is located in the nucleus, cytosol and in the mitochondria membrane of infected cells. Previous studies indicated that the molecule destabilizes planar lipid bilayers and has a strong inherent tendency for multimerization. This may be correlated with its capacity to induce mitochondrial membrane depolarization.

Here, we investigated whether PB1-F2 is able to form ion channels within planar lipid bilayers and microsomes. For that purpose, a set of biologically active synthetic versions of PB1-F2 (*s*PB1-F2) derived from the IAV isolates A/Puerto Rico/8/34(H1N1) (IAV_{PR8}), from A/Brevig Mission/1/1918(H1N1) (IAV_{SF2}) or the H5N1 consensus sequence (IAV_{BF2}) were used. Electrical and fluorometric measurements show that all three peptides generate in planar lipid bilayers or in liposomes respectively a barely selective conductance which is associated with stochastic channel type fluctuations between a closed state and at least two defined open states. Unitary channel fluctuations were also generated when a truncated protein comprising only the 37 C-terminal amino acids of *s*PB1-F2 was reconstituted in bilayers. Experiments were complemented by extensive molecular dynamics simulations of the truncated fragment in a lipid bilayer. The results indicate that the C-terminal region exhibits a slightly bent helical fold, which is stable and remains embedded in the bilayer for over 180 ns.

The data support the idea that PB1-F2 is able to form protein channel pores with no appreciable selectivity in membranes and that the C-terminus is important for this function. This information could be important for drug development.

Introduction

Influenza A Virus (IAV) is a permanent threat to humans and animals with the potential to cause disastrous pandemics which appeared periodically in the last century causing millions of fatal causalities [1], [2]. Aquatic birds are the primary reservoir of the virus. Some avian strains are able to infect other mammals or humans directly or after genetic reassortment caused by a process termed antigenic shift [3]. A major role is attributed to pigs which serve as “mixing vessel” that create avian-human reassortant strains, of pandemic potential. The recent flu pandemic caused by a influenza A virus strain of swine origin is of high interest to study the dynamics of virulence and viral spread. Though, much effort was made to unravel the precise mechanisms of IAV mediated pathogenicity in different host organisms leaving many questions to understand this complex process. Only a few years ago an 11th IAV gene product was discovered. The new protein, named PB1-F2 originates from an alternative open reading frame in the PB1 polymerase gene and it is present in most human and bird flu isolates [4], [5].

Recent work has established that PB1-F2 is an important pathogenicity factor, since it has the potential to augment the generation of fatal secondary bacterial pneumonia as it was demonstrated after the expression of the 1918 IAV PB1-F2 protein in infected mice [6]. Furthermore, a single amino acid exchange from Asn-66 to Ser-66 converted an H5N1 strain of moderate pathogenicity into a highly pathogenic virus. This mutation was also found in the PB1-F2 protein of the 1918 pandemic virus isolate [7]. Interestingly, H1N1 isolates of swine origin do not express functional PB1-F2, which might be a reason for the so far reported moderate pathogenicity of the new subtype variant [8].

The complete mode of action of PB1-F2 however is not yet fully understood. The protein exhibits a C-terminal mitochondrial targeting sequence (MTS) and is predominantly localized in the inner and outer mitochondrial membrane of IAV-infected or PB1-F2-transfected cells [9].

PB1-F2 is thought to initiate the intrinsic mitochondrial apoptosis pathway, presumably by depolarizing the mitochondrial membrane potential followed by subsequent Cytochrome c release [10], [11]. The mechanism by which PB1-F2 causes depolarization of the mitochondrial membrane potential is not yet resolved. This may be achieved either by an activity modulation of mitochondrial transport proteins, such as ANT3 and VDAC1 [10] and/ or by a direct interaction and consequent short circuit of the mitochondrial membrane with the viral protein [12].

Structural considerations [13] and functional assays [12], [14] suggest that the biological function of PB1-F2 indeed is related to its direct interaction with membranes. The NMR structure of the *s*PB1-F2 peptide derived from IAV_{PR8} reveals a strong tendency of the protein to undergo oligomerization mediated by two distinct domains in the N- and C-termini, respectively [13]. Comparative analysis of the peptide in aqueous versus lipid environment showed that the structure of PB1-F2 is strongly determined by the surrounding solvent [13], [14]. In an aqueous environment *s*PB1-F2 is mostly present as a random coil peptide. In a lipid-like environment the protein alters its structure revealing either a β-sheet or an α-helix rich structure. The NMR structure of the latter configuration reveals an α-helix at the C-terminal region between amino acid residues Ile^{55}-Lys^{85}. The length of this α-helix is sufficient for spanning a membrane. Although present in different cellular sites, its potential for forming an ion channel has not been investigated thoroughly yet.

Previous electrophysiological characterizations of *s*PB1-F2 derived from the isolate IAV_{PR8} revealed that the protein can form membrane pores in planar lipid bilayers resulting in a rapid elevation of a membrane conductance with a low ion selectivity [12]. Analysis of the currents elicited by sPB1-F2 exhibited only random fluctuations between multiple undefined conductance levels. Current fluctuations between a defined closed and open state, which are typical for the activity of channel forming proteins, were not observed. The absence of the latter type of channel like fluctuations fostered the speculation that the protein augments membrane conductance not by protein pores but partially by lipidic pores [12]. In the present study we further tested synthetic versions of PB1-F2 proteins derived from: i) the

A/Puerto Rico/8/34 (H1N1) (IAV_{PR8}) strain, ii) the spanish flu isolate A/Brevig Mission/1/1918 (H1N1) (IAV_{SF2}) and iii) the consensus sequence of PB1-F2 derived from 13 different bird flu virus strains (H5N1) (IAV_{BF2}) in planar lipid bilayers.

Reconstitution of all three PB1-F2 molecules resulted in an elevation of membrane conductance. Close examination of the PB1-F2 evoked currents revealed in all cases typical channel like fluctuation between two dominant conductance levels. The results of these experiments underscore that PB1-F2 from distinct isolates has the ability to form nonselective protein mediated channel pores in planar lipid membranes. Since a prerequisite for forming a well-defined pore is a stable protein fold in a lipid environment in contrast to an unspecific PB1-F2-induced membrane perturbation, we tested this hypothesis by extensive molecular dynamics (MD) simulations. To this end, the NMR structure of the truncated C-terminal fragment (PDB code 2HN8, [13]) was inserted into a POPC bilayer, solvated by 150 mM KCl aqueous solution, and observed and analyzed over 180 ns. The fact that the protein remained stable in a transmembrane orientation supports the hypothesis that PB1-F2 is able to generate canonical channel activity.

Material and Methods

Reconstitution & Electrophysiology

Experiments with planar lipid bilayers were performed as described by Schrempf et al. [29] by the Montal Müller technique [30] with a 0.4 mg/ml solution of α-phosphatidylcholine (type IV-S >= 30 % TLC; Sigma-Aldrich (Steinheim, Germany)) in n-decane (Carl Roth, Karlsruhe, Germany). sPB1-F2 was synthesized as described elsewhere [15, 31]. The measurements were done in buffer containing 500 mM KCl, 10 mM Mops/Tris pH 7. The Ag/AgCl electrode of in the trans compartment was directly connected to the head stage of a current amplifier (EPC 7, List, Darmstadt, Germany); the electrode in the cis-compartment was connected to the ground. At positive potentials the electrode in the trans-compartment was positive and the electrode in the cis-compartment negative. In order to prevent surface-potential-effects both electrodes were connected with the bath solution via an agar bridge (2% agarose in 2 M KCl). Currents were recorded and stored by an analog/digital-converter (LIH 1600, HEKA electronics, Germany) at 4 KHz after low pass filtering at 1 kHz. Data analysis were performed by Patchmaster-Software (HEKA electronics) and Igor Pro (WaveMetrics, Oregon, USA). Before adding the protein to the trans chamber the bilayer conductance was recorded for some time in order to exclude artefacts from contaminations. Only perfectly silent bilayers were used for reconstitution of PB1-F2 proteins.

Preparation of liposomes for the fluorescence assay

Lipid mixtures (100 mg / ml, S IV lipid, Sigma) were dried from CHCl3-methanol (1/1) solution under vacuum. Dried lipids were re-suspended in buffer (100 mM KCl, 10 mM Mops, titrated with Tris to pH 7.0) by vortexing; after addition of 20 µM fluorescence dye (Fluo-3, Invitrogen) liposomes were exposed to three freeze-thaw cycles. During thawing periods the liposomes were kept in an ultrasonic bath for 5 minutes. This procedure resulted in the loading of liposomes with dye. Finally the dye

was removed from the external buffer by precipitation; 1ml of the dispersion was therefore washed on sephadex® -columns (Sigma Aldrich, Steinheim, Germany). The liposomes were subsequently eluted from the column by Na^+ buffer (100 mM NaCl, 10 mM Mops/Tris pH 7.0). Immediately before an experiment, the eluate was further diluted 1/4 with the Na^+ buffer. The fluorescence signals (Figure 3.7 A,B) were measured with a fluorescence microplate-reader (NanoScan LF400, IOM, Berlin, Germany) or a fluorescence spectrophotometer (F-7000, HITACHI, Japan) (Figure 7C). In the microplate-experiments Fluo3 was excited at 488 nm and lucigenin at 456 nm. In both cases the emitted light passed through a 505 nm dichroic and a 520/10 band path filter. Fluo3 fluorescence measured in the fluorescence spectrophotometer was excited at 506$\pm$ 5 nm and at an emission wavelength of 526$\pm$ 5 nm.

MD simulation

The system was constructed using VMD [32] and described by with the CHARMM22 potential function for proteins [33], CHARMM27 for phospholipids [34], the TIP3P water model [35], and ion parameters developed by Roux [36]. All titratable residues were kept at their standard protonation states. The simulation has been performed with a modified version of the program NAMD 2.6 [37]. Starting with the experimental NMR structure [13], the protein was inserted into a pre-equilibrated POPC membrane by removing overlapping lipid molecules, leading to 26 and 28 POPC molecules in each layer. The system was solvated by ca. 150 mM aqueous KCl solution (15 K^+ and 6 Cl^- ions per 4050 water molecules), the positive net charge of the protein was therefore balanced by counterions. The total system contained 19641 atoms. The simulation time step was 2 fs, electrostatics were treated by the particle mesh Ewald method [38] on a 64x64x128 grid. Nonbonded real-space interactions were smoothly switched off over a range of 10-12 Å. Bond distances to hydrogen atoms were kept fixed. Production simulations were performed in the isothermal-isobaric (NpT) ensemble using the Langevin piston algorithm at 1 atm [39], [40] with an oscillation period of 800 fs and damping constant of 400 fs, and the Langevin thermostat with a coupling constant of 5 ps^{-1}. After minimization over 10000 steps we successively turned on the barostat and the thermostat over 0.182 ns, followed by 5 ns NpT

simulation with fixed protein backbone and 10 ns NpT simulation with c.o.m. constraint applied to the protein. Data for the fully free system were collected over 180 ns. The helicity of the protein backbone was analyzed with the STRIDE algorithm [41].

Results

Electrophysiology and single channel analysis

In order to examine the mechanism by which PB1-F2 augments membrane conductance we reconstituted the synthetic protein derived from influenza A virus strain A/Puerto Rico/8/34(H1N1) (sPB1-F2$_{pr8}$) in planar lipid bilayers. The amino acid sequence of the protein is shown in Figure 3.1.

```
PB1-F2pr8       MGQEQDTPWI LSTGHISTQK RQDGQQTPKL EHRNSTRLMG HCQKTMNQVV MPKQIVYWKQ 60
PB1-F2sf        MGQEQDTPWI LSTGHISTQK REDGQQTPRL EHHNSTRLMD HCQKTMNQVV MPKQIVYWKQ 60
PB1-F2bf        MEQEQDTPWT QSTEHINIQK RGNGQRTQRL EHPNSIRLMD HCLRIMSRVG MHKQIVYWKQ 60
                * *******   ** **. ** * :**:* :* ** ** ***. ** : *.:*  * ********

PB1-F2pr8       WLSLRNPILV FLKTRVLKRW RLFSKHE--- 87
PB1-F2sf        WLSLRSPTPV SLKTRVLKRW RLFSKHEWTS 90
PB1-F2bf        WLSLKNPTQG SLKTRVLKRW KLFSKQEWIN 90
                ****:.*     ********* :****:*
```

Figure 3.1 Alignment of predicted amino acid sequences of PB1-F2 proteins. The proteins from A/Puerto Rico/8/34 (H1N1) strain (PB1-F2$_{pr8}$), the Spanish flu isolate (PB1-F2$_{sf}$) and the bird flu virus (H5N1) (PB1-F2$_{bf}$) have an overall identity (*) of ca 60%. The domains, which are predicted by structural prediction algorithms to have a high propensity for α-helixes are marked in gray. The truncated peptide sPB1-F2$_{pr8}^{50-87}$ is underlined.

After adding the protein at a final concentration of 1 µM into the bath solution (500 mM KCl, 10 mM Mops/Tris, pH 7.0) the membrane conductance increased. Figure 3.2A shows exemplary currents across the bilayer in response to a voltage step from 0 mV to +80 mV before and after addition of the protein to the bath solution. In the case illustrated the viral protein evoked large current fluctuations with unresolved conductance levels; this observation is similar to that reported previously [12]. A close scrutiny of currents recorded in the presence of the sPB1-F2$_{pr8}$ protein however shows among many unresolved fast fluctuations also typical unitary channel opening/closing events (magnification in Figure 3.2A).

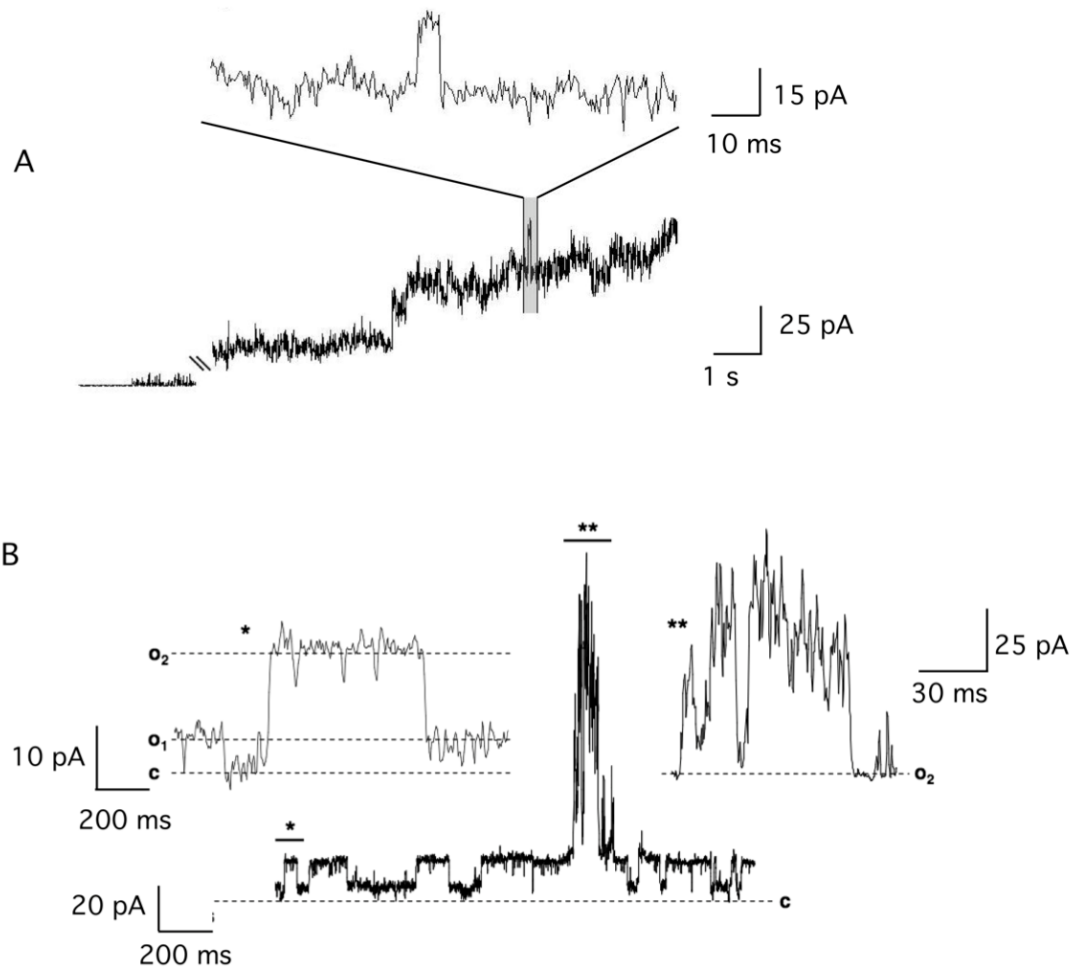

Figure 3.2 *s*PB1-F2 evoked membrane conductance. **A** Addition of *s*PB1-F2$_{PR8}$ protein at 1 µM to the trans-side of a planar lipid bilayer results in current fluctuations. In the present case only occasionally clear channel like fluctuations (see expanded trace) are resolvable on the background of many unresolved fluctuations. **B** In a majority of experiments the conductance fluctuates in a channel like manner between a closed (c) and two defined conductance levels o_1 and o_2. Transitions between the two conductance levels (*) are expanded in the left inset. The channel like fluctuations are occasionally interrupted by burst like events (**), which reveal also at higher magnification (inset on the right) no resolvable conductance levels.

In the majority of experiments we observed an overall low electrical activity after addition of *s*PB1-F2$_{pr8}$ at 1 µM. Figure 3.2B shows an exemplary recording with currents across a bilayer held at +80 mV; in this case the current frequently fluctuates

in an ion channel like manner between a closed state (c) and two defined conductance levels (o_1 and o_2); channel like activity is only occasionally interrupted by a burst of activity with no resolvable conductance levels. During the 12 min long recording the dwell time of burst like behavior was less than 10 % of the dwell time of channel type fluctuations. Worth noting is that the amplitude of the channel like fluctuations observed in this experiment (c -> o_2) is the same as that seen in recordings with high electric activity (e.g. magnification in Figure 3.2A).

Channel like fluctuations were observed in experiments with a protein concentration $\geq$20 nM. Independent on the concentration the two unitary conductance levels described in Figure 3.2 prevail along with some other more rare occurring conductance levels at all voltages. Figure 3.3A illustrates exemplary traces of unitary channel activity from an experiment with symmetrical 500 mM KCl. The two conductance levels are frequently achieved directly from the closed state. However the fluctuations illustrated in Figure 3.3B show that the channel can also reach the closed state from the high conductance level o_2 via an intermediate halt at the small conductance level o_1 (B); also partial closures in which the current decreases in step like fashion from o_2 can be observed (C). From these data we can conclude that the different conductance levels are causally related; they must be produced by the same protein or protein complex.

A plot of the two prevailing unitary current amplitudes from the closed level to o_1 and to o_2 as a function of voltages gives a linear current/voltage (I/V) relation for both levels of conductance in symmetrical 500 mM KCl (Figure 3.3D). The conductance of the large and the small unitary opening are 250 pS and 100 pS respectively. The same results were confirmed in 4 other reconstitution experiments using protein from two different preparations.

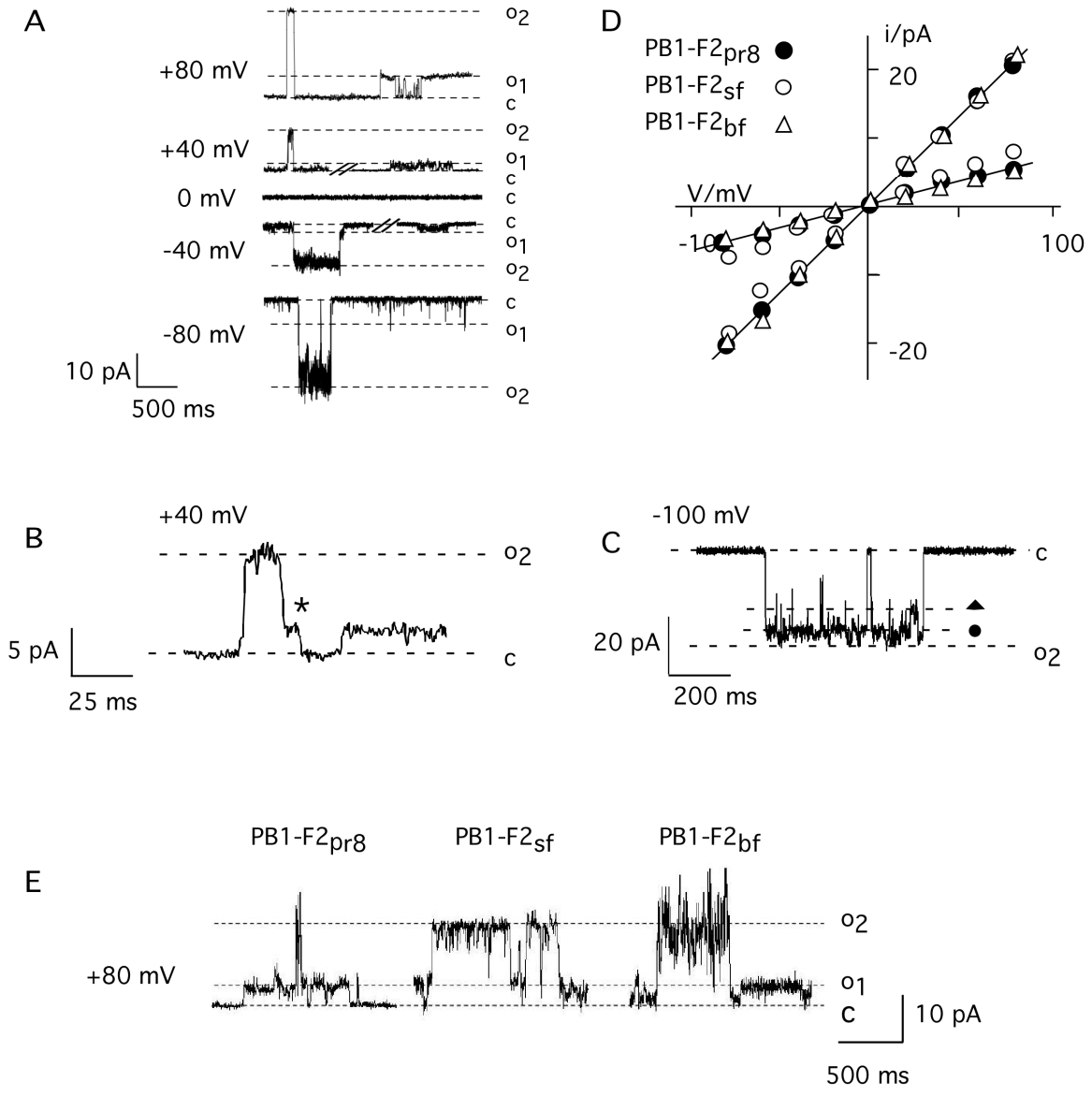

Figure 3.3 Unitary channel fluctuations and current voltage relation of sPB1-F2$_{pr8}$ generated conductance in planar lipid bilayer. Current fluctuates between a closed (c) and two (o_1, o_2) conductance levels **A**. Channel fluctuations recorded in symmetric 500 mM KCl in trans and cis chamber. **B** Example of channel opening in one step between closed (c) and maximal conductance (o_2) and closing with an intermediate rest at low conductance level (*). **C** Example of intermediate closures from maximal conductance (o_2) to subconductance levels, which are indicated by symbols (l,▲). **D** I/V relation of the small (o_1) and large current fluctuation (o_2). Experiments performed in symmetrical 500 mM KCl. The I/V relations in **D** were obtained from measurements of channel conductance evoked by peptide from *s*PB1-F2$_{pr8}$, *s*PB1-F2$_{sf}$ and *s*PB1-F2$_{bf}$. **E** examples of channel type current fluctuations between ->

the closed (c) and two conductance levels (o_1, o_2) evoked by *s*PB1-F2 peptide from influenza Puerto Rico strain (*s*PB1-F2$_{pr8}$), Spanish flu strain (*s*PB1-F2$_{sf}$) and bird flu strain (*s*PB1-F2$_{bf}$). Measurements in **A-C** were done in symmetric 500 mM KCl in trans and cis chamber at a voltage of +80 mV; all peptides were added to the buffer at final concentration of 1 µM.

To test whether the channel forming activity is unique to sPB1-F2$_{pr8}$ the same experiments were repeated with synthetic peptide analogs to PB1-F2 from the 'Spanish flu' virus (sPB1-F2$_{sf}$) and the bird flu virus (H5N1) (*s*PB1-F2$_{bf}$). An alignment of the three protein sequences shows that they are 60% identical (Figure 3.1). Direct comparison however also reveals deviations in the amino acid sequence throughout the protein; furthermore PB1-F2$_{bf}$ is at the C-terminus 3 amino acids shorter than the two analogs.

Figure 3.3E shows exemplary current traces at +80 mV from the three different peptides. The data reveal that all three peptides generate distinct channel fluctuations. In all cases the two dominant conductance levels o_1 and o_2 are again observable. The I/V curves obtained for *s*PB1-F2$_{sf}$ and *s*PB1-F2$_{bf}$ are indistinguishable from *s*PB1-F2$_{pr}$ (Figure 3.3D).

To test the selectivity of the *s*PB1-F2$_{pr8}$ generated channel for different ions the experiments were repeated under nonsymmetrical conditions. The I/V relations obtained in experiments in which KCl in the cis chamber was replaced by either NaCl or by K-gluconate were similar to those obtained with symmetrical KCl (Figure 3.4A). This means that the channel has no apparent selectivity; it neither discriminates appreciably between K^+ and Na^+ nor between Cl^- and gluconate.

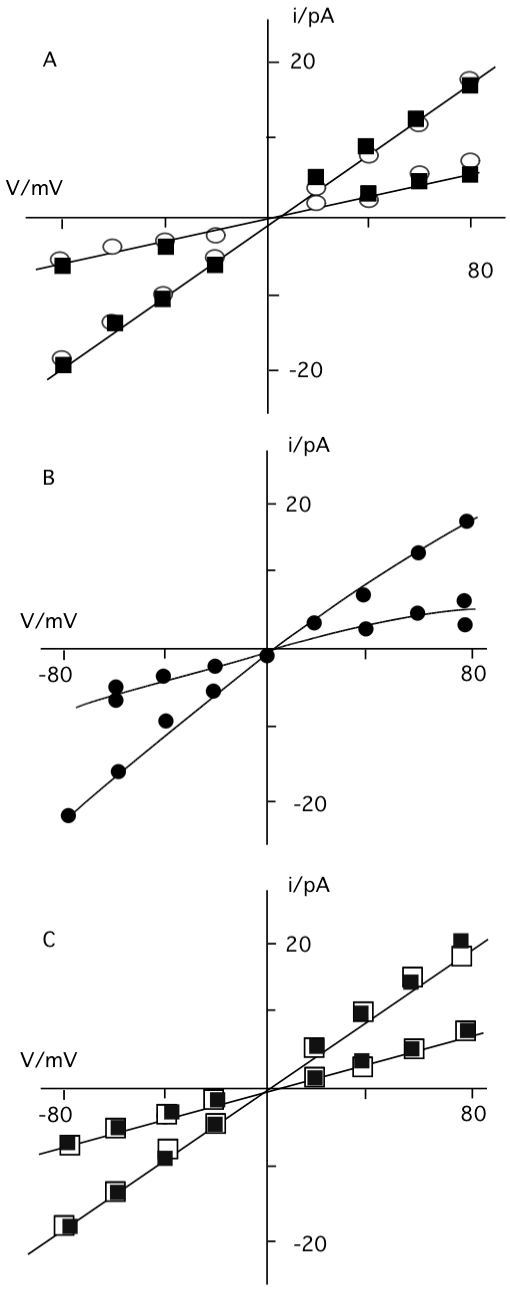

Figure 3.4 I/V relation of the small (o_1) and large (o_2) *s*PB1-F2 generated current fluctuation. **A** Unitary currents were recorded in bilayer with 500 mM KCl on *trans* side and 500 mM NaCl on trans (open circles) or with 500 mM KCl on cis and 500 mM K-gluconate on trans (filled squares). **B** I/V relation obtained with 500 mM KCl on trans side and 50 mM KCl on cis side. **C** I/V relation obtained with 500 mM KCl on cis and 500 mM $CaCl_2$ on trans-side. Currents were elicited upon adding *s*PB1-$F2_{pr8}$ (in **A-C**) and sPB1-$F2_{sf}$ (in **C**) to trans-side.

Further experiments were performed with a 10-fold concentration gradient of KCl across the bilayer. The current voltage relation obtained for *s*PB1-F2$_{pr8}$ under these nonsymmetrical conditions reverses close to 0 mV at ca +5 mV. This shift in reversal voltage is real because under nonsymmetrical conditions we were able to measure a negative current at 0 mV. The result of this experiment implies that the channel transports anions slightly better than cations.

In further experiments we tested whether the viral protein also transports divalent ions. For these experiments *s*PB1-F2$_{sf}$ or *s*PB1-F2$_{pr8}$ were reconstituted in a planar lipid bilayer with 500 mM KCl on the cis and 500 mM $CaCl_2$ on the trans-side. Also in these experiments we were able to detect distinct current fluctuations at positive and negative voltages (Figure 3.4C and inset). The results of these experiments show that the *s*PB1-F2 generated conductance is also permeable to Ca^{2+}.

During long observations it occurred that current fluctuations were more frequent at more extreme voltages than at moderate voltages. This suggested a voltage dependency of the *s*PB1-F2 generated conductance. In order to quantify the channel activity as a function of voltage we estimated the mean current generated by sPB1-F2$_{pr8}$ in a bilayer from n=25 voltage steps of 3 s duration from 0 mV to test voltages between +80 mV and -80 mV. The mean steady-state currents from 12 experiments recorded in symmetrical 500 mM KCl are plotted in Figure 3.5 as a function of voltage. They show a low activity at voltages around 0 mV. Towards both voltage extremes channel activity increases in a quasi-exponential fashion. Similar results were obtained with sPB1-F2$_{sf}$; also this protein exhibits a voltage dependent I/V relation of the mean current (Figure 3.5). The results of this analysis show that channel activity is irrespective of the viral origin of the sPB1-F2 protein favored by membrane voltage. It is not possible to say whether the proteins insert into the bilayer with respect to its orientation randomly or with a bias for one side over the other. Without this information it is not yet possible to discriminate whether the channel has an inverse bell shaped open probability or whether they function as a rectifier.

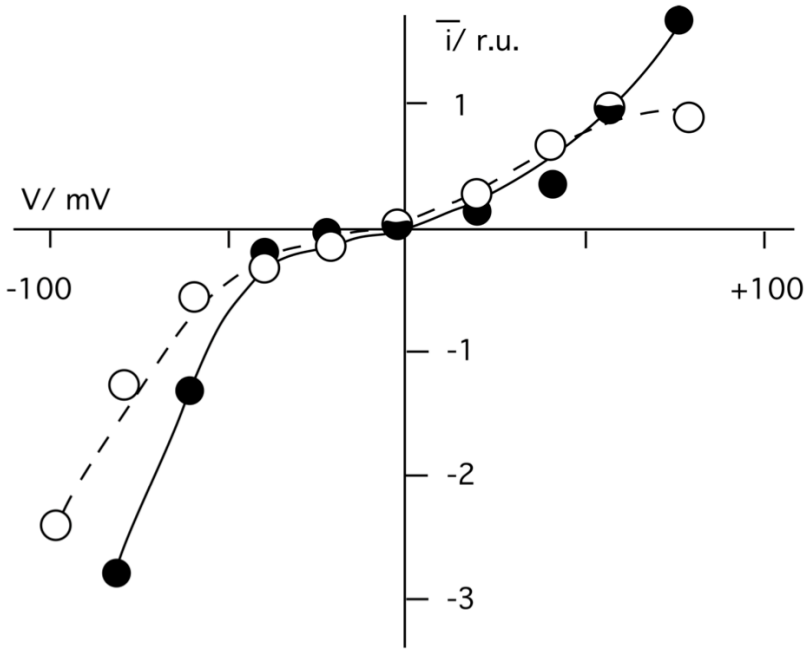

Figure 3.5 Mean current generated by *s*PB1-F2$_{pr8}$ (filled circles) or *s*PB1-F2$_{sf}$ (open circles) as a function of voltage. Channel activity was recorded in symmetrical 500 mM KCl. Peptide was added at 1 µM on trans-side. The current responses from n= 12, 3 sec long voltage scans at the respective test voltages were averaged.

The NMR structure obtained for sPB1-F2$_{pr8}$ implies a C-terminal α-helix, which is long enough to span a membrane [13]. In order to test whether this domain alone is sufficient for generating channel activity we produced a synthetic peptide, which is equivalent to the aa 50-87 of the full-length protein of PB1-F2$_{pr8}$ [15]. The peptide (sPB1-F2$_{pr8}^{50-87}$) was tested in planar lipid bilayer in the same way as the full-length protein. Figure 6 shows the result of a typical experiment with a symmetrical solution of 500 mM KCl; the membrane was clamped to +80 mV. Addition of the truncated peptide at a concentration of >200 nM to the trans-chamber generated a large conductance in the bilayer. The current generated by sPB1-F2$_{pr8}^{50-87}$ peptide showed mostly unresolved current fluctuations. But like in the experiment of Figure 2A it was also in these experiments possible to resolve channel like fluctuations between defined conductance levels (Figure 6). A plot of the resolvable channel like fluctuations reveals three distinct conductance levels with 330, 550 and 750 pS.

These conductance levels are not identical to those recoded with the full-length protein. Hence the putative α-helical part of the *s*PB1-F2 protein is sufficient to increase membrane conductance; it can even generate channel like activity. The difference in the resolvable conductance levels obtained with the full length compared to the truncated protein implies that the remaining n-terminal part of the protein has an influence on channel formation and unitary conductance.

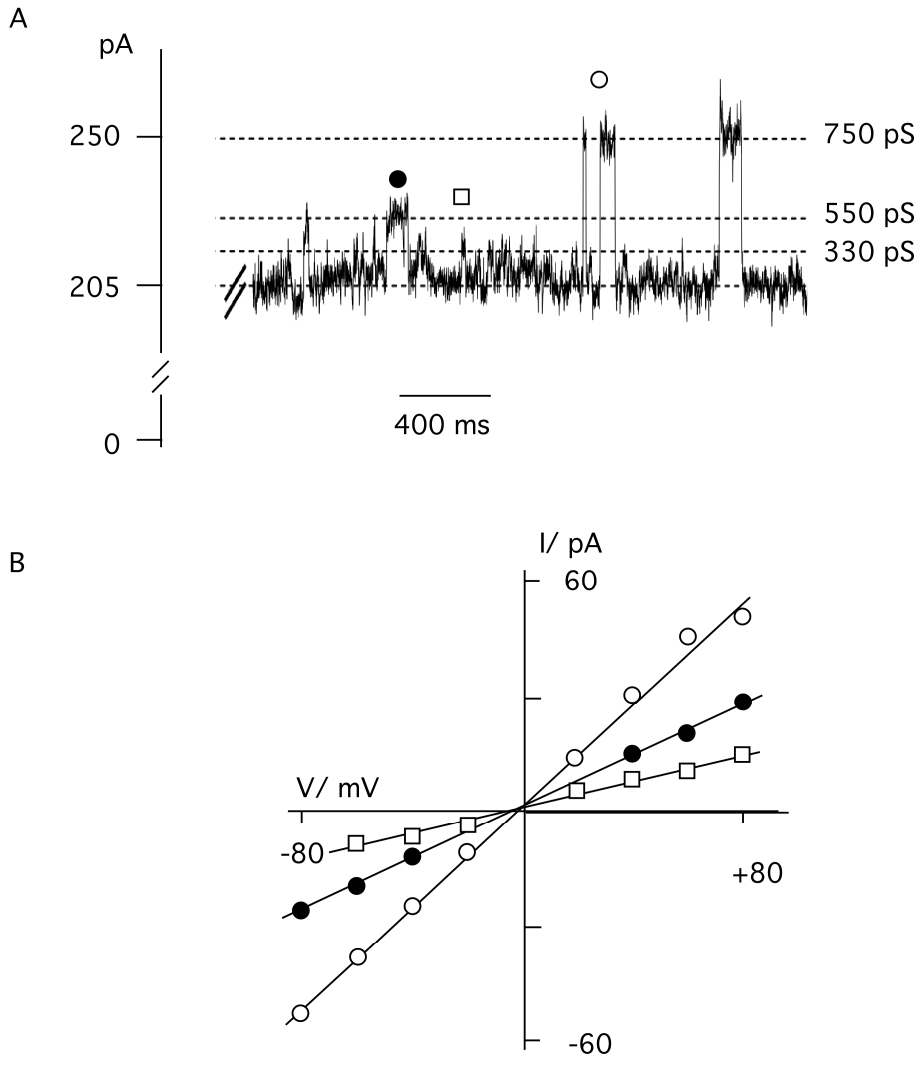

Figure 3.6 The truncated peptide *s*PB1-F2$_{pr8}^{50-87}$ generates an elevated membrane conductance. **A** Addition of *s*PB1-F2$_{pr8}^{50-87}$ protein to the trans side of a planar lipid bilayer evokes large currents across the membrane. On top of many unresolved current ->

fluctuations typical channel like opening and closing events are resolvable. In the example recorded at +80 mV three distinct current levels (indicated y different symbols) can be identified. **B** A plot of similar resolvable current levels as a function of voltage reveals three linear I/V relations with 330, 550 and 750 pS. The symbols in **A** cross reference with symbols in **B**. Measurements were done in symmetric 500 mM KCl with 200 nM peptide concentration.

Fluorescence assay

The electrophysiological data imply that the *s*PB1-F2 protein generates an unspecific conductance including permeation by Ca^{2+} and Cl^-. This offers the possibility to examine the transport properties of PB1-F2 also in an independent assay by fluorescence spectroscopy. To measure PB1-F2 generated Ca^{2+} fluxes we loaded liposomes with the Ca^{2+} sensitive dye Fluo-3. The fluorescence intensity of the dye remained constant under control conditions. Also addition of the K^+-selective ionophore Valinomycin had no appreciable effect on the Fluo-3 fluorescence. In contrast, addition of 1 µM *s*PB1-$F2_{pr8}$ resulted in a rise in Fluo-3 fluorescence indicating a net influx of Ca^{2+} into the liposomes (Figure 3.7). The sPB1-$F2_{pr8}$ generated fluorescence signal could be increased by adding the peptide together with Valinomycin (Figure 3.7). This enhancing effect of the ionophore on Ca^{2+} influx into the liposomes is expected because a K^+ efflux via Valinomycin provides a charge balance for Ca^{2+} influx. In this case the membrane of the liposomes is not building up a charge, which would hinder net Ca^{2+} influx.

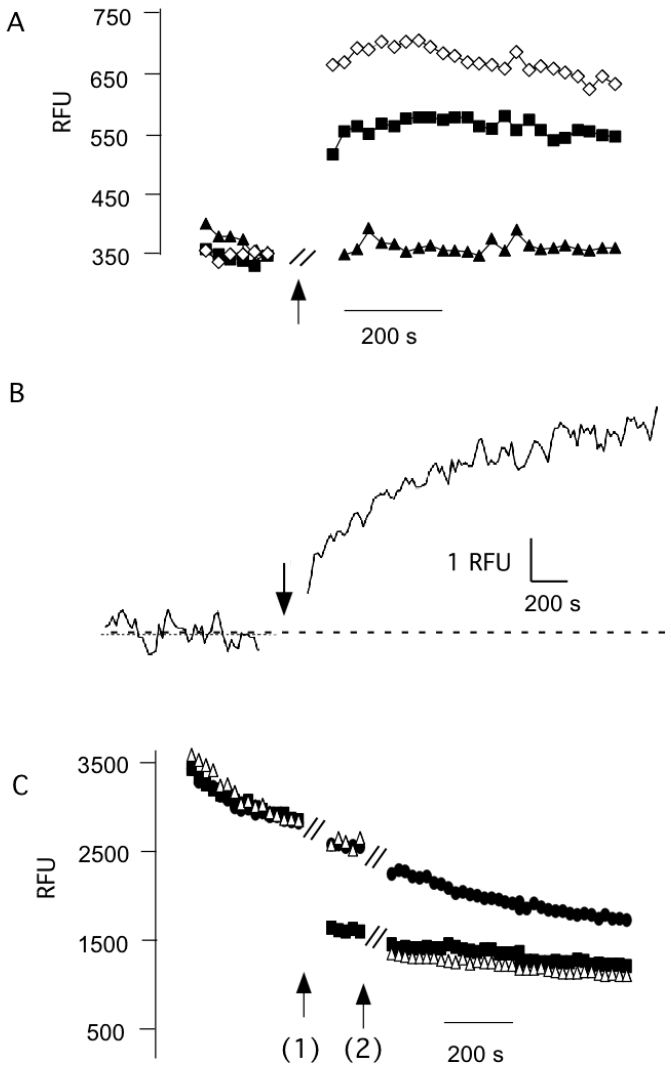

Figure 3.7 *s*PB1-F2 generates Ca^{2+} and anion fluxes into liposomes. **A** Fluorescence of liposomes with Ca^{2+} sensitive dye Fluo3 was recorded before and after adding (at arrow) ionophore Valinomycin (triangle), sPB1-$F2_{pr8}$ alone (filled squares) or together with Valinomycin (open squares). Peptide and ionophore were added during the time gap of ca. 1 min indicated in the graph. The presence of the peptide results in an increase in fluorescence indicating an influx of Ca^{2+} into the liposomes. The ionophore enhances Ca^{2+} influx because it prevents building up of a charge, which hinders net Ca^{2+} influx. **B** Fluorescence of liposomes filled with Ca^{2+} sensitive dye Fluo-3 before and after addition (at arrow) of 1 µM peptide to incubation medium. The truncated peptide sPB1-$F2_{pr8}^{50-87}$ results in a fast rise in Fluo3 fluorescence. **C** Fluorescence of liposomes filled with anion sensitive dye

lucigenin was measured before and after adding of anion specific ionophore TBT (filled squares, added at arrow 1), sPB1-F2$_{pr8}$ (open triangle, arrow 2). The control was left untreated (filled circles); the stepwise drop of the control signal is due to an unspecific drift of the signal. Both ionophore and sPB1-F2$_{pr8}$ generate a strong quenching of the lucigenin fluorescence well beyond the control indicating an influx of anions. Peptide and ionophore were added during the time gap of ca. 1 min indicated in the graph.

With a similar assay we also tested whether the truncated peptide sPB1-F2$_{pr8}^{50-87}$ is able to generate a Ca^{2+} conductance. For this purpose we loaded liposomes with Fluo-3 and measured the respective fluorescence before and after adding sPB1-F2$_{pr8}^{50-87}$ peptide to the incubation buffer. The exemplary data in Figure 3.7B show that the fluorescence signal was constant before addition of the peptide. The addition of sPB1-F2$_{pr8}^{50-87}$ at a final concentration of 1µM resulted in a quasi-immediate rise in Fluo-3 fluorescence reporting the influx of Ca^{2+} into the liposomes. The increase of relative fluorescence units (RFU) was 30 %. The same response with a mean rise of 28 $\pm$ 5 % in Fluo-3 fluorescence was observed in 3 other experiments.

In further experiments we also examined the ability of *s*PB1-F2$_{pr8}$ to stimulate Cl^- fluxes. In this case the liposomes were loaded with the anion sensitive dye lucigenin. Other than with Fluo-3 we observed in this type of experiments a non-specific drift of the fluorescence signal. But in spite of this shortcoming also this method could be used to demonstrate PB1-F2 generated anion fluxes. Figure 3.7C shows that addition of the anion specific ionophore TBT resulted in a strong quenching of the lucigenin fluorescence indicating the sensitivity of the system. A similar drop in fluorescence was obtained upon addition of *s*PB1-F2$_{pr8}$ at a concentration of 1 µM.

Collectively, the results of these experiments confirm the electrophysiological data in that the sPB1-F2 protein is able to generate a conductance without appreciable selectivity in lipid bilayers, which is able to conduct anions and divalent cations. The C-terminal domain of the protein with its putative α-helical structure seems to be sufficient for generating this conductance.

MD simulation

The electrical data imply that PB1-F2 is able to form with its C-terminus ion channels in membranes. A prerequisite for such channel formation is an insertion and a lasting transmembrane orientation of the C-terminus. To test the latter we examined the behavior of the peptide in its proposed α-helical form in a lipid environment at zero transmembrane voltage by molecular dynamics (MD) simulations. After a period with fixed center of mass of the C-terminal truncated fragment $sPB1\text{-}F2_{pr8}^{50\text{-}87}$ we observed the stability of the truncated protein by a number of quantitative measures over the last 180 ns after removal of the center-of-mass (c.o.m.) constraint. This constraint has been applied during pre-equilibration in order to fix the protein within the membrane. Quantitative results are shown in Figure 3.8. All quantities indicate a remarkable overall stability of the protein fold and of the transmembrane insertion geometry. Apparently, the protein structure fluctuates within expected margins, but there is no indication for a systematic long-term trend to escape from the bilayer or to switch to a different backbone fold.

While particularly the helical characteristic is preserved, we note a tendency to bend slightly in comparison with the NMR structure, most notable at around 70 ns where a slight step in the observables is visible. This process started shortly after removal of the c.o.m. constraint and is visualized in Figure 3.9 (note that the simulation box shrinks laterally even after long time, indicating that large time scales are required for reaching an equilibrium ensemble).

Bending is not unexpected since Pro^{67} is localized near the centre of the peptide. Interestingly, the Pro^{67} appears to be conserved within 263 bird flu sequences and all 20 of the H1N1 full length sequences analyzed by us so far (data not shown).

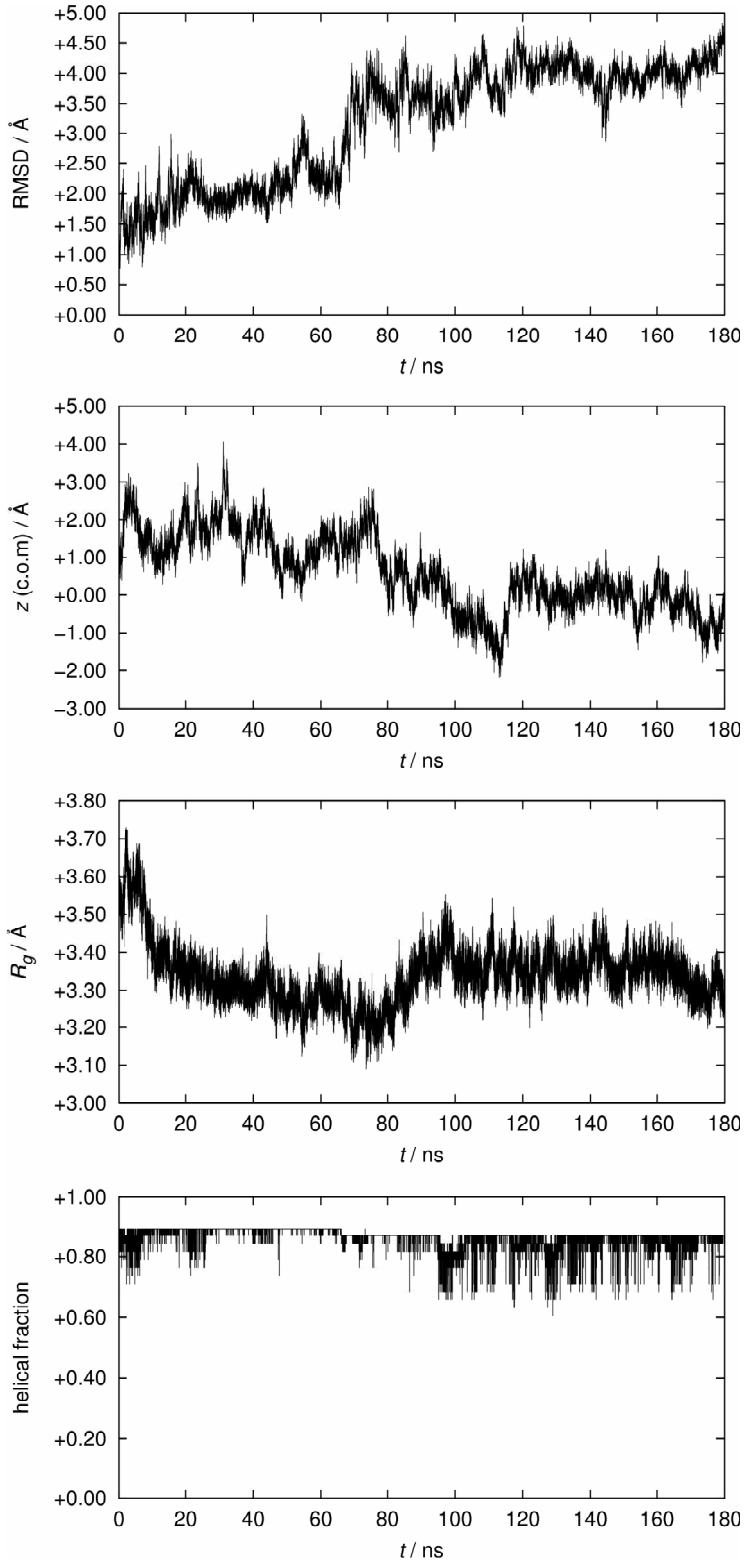

Figure 3.8 Dependence of various measures for protein stability over the simulation time after removal of the center-of-mass (c.o.m.) constraint (set to 0 ns). From top to bottom: ->

Root mean square deviation (RMSD) of the protein backbone, *z* coordinate (membrane normal) of the c.o.m. of the protein (corrected by removing the total membrane drift), the protein's radius of gyration (R_g), and the helical fraction recognized for the fold.

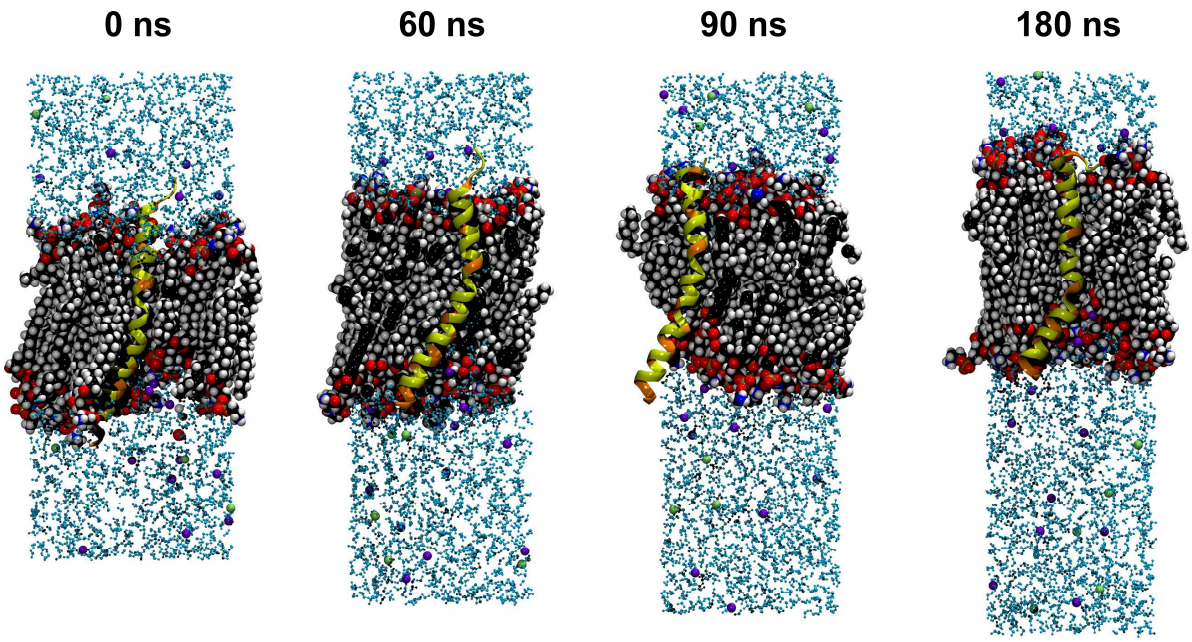

Figure 3.9 Snapshots of the simulation system after removal of the center-of-mass constraint (set to 0 ns). The protein is shown in cartoon representation with the location of positively charged amino acids marked by orange color. Potassium ions are shown in green, chloride ions in blue. The C-terminus is located on the bottom side.

However, the presence of a lipid environment apparently hinders the formation of a kink. The origin of this behavior is related to the presence of a large number of positively charged amino acids (all kept in the standard protonation state during the simulation) as illustrated in Figure 3.10. Arginine and lysine residues tend to "snorkel" into the direction of the membrane/solvent interface [16]. Close to the C-terminus (bottom side in Figures. 3.9 and 3.10) positive charges are clustered which leads to a net tendency to drag the protein in the direction of the C-terminus. In the presence of the c.o.m. constraint, this force is neutralized, whereas, in the absence of the constraint, the smaller number of positive charges on the n-terminal side is not sufficient to counteract fully. As a consequence, stabilization of the n-terminal side in

the interface decreases such that the influence of proline becomes more important which leads to the observed bending.

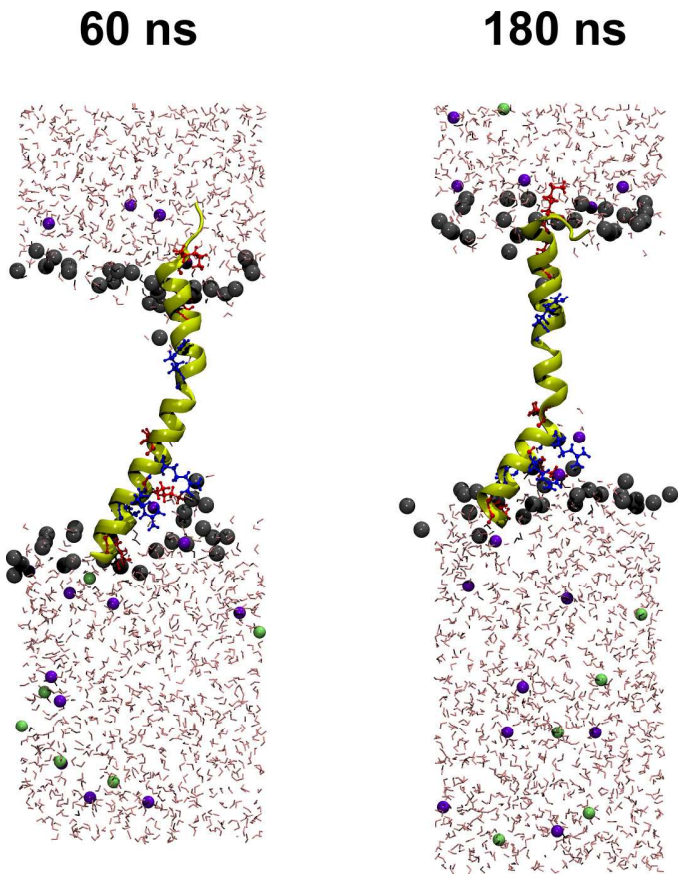

Figure 3.10 Snapshots of the simulation system after removal of the center-of-mass constraint (set to 0 ns). The protein is shown in cartoon representation with explicit depiction of positively charged residues (arginine: blue, lysine: red). Lipid molecules have been removed except for the head groups that are depicted as grey spheres. Potassium ions are shown in green, chloride ions in blue. The C-terminus is located on the bottom side.

It appears that the C-terminal cluster of positive charges leads to an accumulation of water and anions, which penetrate the lipid head groups. There is no indication of a persistent poration effect, however, which could be responsible for the measured channel currents. This observation requires further investigation in future work considering oligomers of the PB1-F2 peptide.

Discussion

Early studies described PB1-F2 as a proapoptotic protein, which was assumed to remove host immune cells responding to IAV infection [4], [11]. The molecular mechanisms of PB1-F2 induced apoptosis is still not totally understood, though recent results confirmed that its proapoptotic function is cell specific and related to PKC activation after infection of primary human monocytes [17]. However, since the protein is localized predominantly in the mitochondria of transfected or infected cells and found to alter the mitochondrial morphology [4] it was hypothesized that apoptosis induction occurs due to direct interaction with subunits of the mitochondrial PTPC or destabilization of the mitochondrial membrane by pore formation [10].

In previous experiments it has been demonstrated that PB1-F2 causes an elevation of membrane leakage [14] and increases the electrical conductance of membranes [12]. However, the currents elicited by the PB1-F2 protein were not showing defined conductance levels and channel like fluctuations. The results of these experiments therefore fostered the hypothesis that the PB1-F2 protein is not forming canonical protein mediated transmembrane pores. It was speculated that the protein may destabilize the lipid bilayer due to the formation of lipidic pores [12]. The question of how this protein destabilizes the mitochondrial membrane potential, by channel like or lipidic pore formation, is still under investigation.

The main observation of the present study is that the PB1-F2 protein is able to generate distinct opening/closing events between defined conductance levels; these events are typical for ion channel proteins [18]. Thus, it can be concluded that PB1-F2 can short circuit the mitochondria by inserting channel forming proteins into the organelle membrane. This finding might explain the property of PB1-F2 to disrupt the reticulotubular mitochondrial organization and to dissipate the inner membrane potential [4,10]. A similar strategy for inducing apoptosis is known from a number of other viruses [19]. In the case of PB1-F2 canonical channel activity is observed with the full-length protein but also with a truncated protein comprising only the putative C-terminal α-helix (from amino acid residues Ile^{55}-Lys^{85}). This together with the results

from MD simulations, which show that the truncated fragment is stable in the membrane, suggests that the C-terminus is part of the channel forming domain in the protein. But since the truncated and the full-length protein evoke different unitary conductances we must nonetheless assume that also the n-terminal part of the protein is involved in channel formation. Indeed the simulations show that the monomer alone leads to membrane denting, but is apparently incapable of inducing ion permeation; we did not find evidence for sufficient destabilization of the membrane to allow for passive ion translocation. Although we made no attempt to model a multi-protein complex, it is very likely that such a complex is necessary to facilitate ion transport. This hypothesis is supported by the finding that PB1-F2 has indeed the tendency to form oligomers. The latter involves distinct domains not only in the the C- but also in the N terminus [13] in line with the hypothesis, that both termini are important for the complete channel activity.

Our MD simulations imply that the C-terminus of PB1-F2 can maintain a transmembrane orientation and that this orientation is favored by positive amino acids at the membrane/water interfaces. The data however do not yet explain how a peptide with that many charges is able to insert into the membrane. In this context it is interesting to note that also many other short, highly cationic and hydrophilic peptides, including the voltage sensor of K^+-channels, are capable of inserting and in some cases even passing membranes [20], [21], [22]. The unusual behavior of these proteins can be explained by an interaction of the membrane with the distinct peptide structure; the charged amino acids in these membrane-inserting cationic peptides have to be evaluated in the overall context and their specific position in the entire peptide [20]. The structural and charge density features of the PB1-F2 protein are apparently similar to those of cationic peptides, which are able to insert spontaneously into membranes. Due to the large net charge it is very likely that the voltage dependency of the PB1-F2 conductance is related to a voltage-induced change of the positioning and orientation within the membrane. This issue needs further scrutiny by MD simulations employing an external transmembrane potential.

Both experimental and theoretical data support the view that channel activity is achieved by protein pores, which are formed by complex formation of the PB1-F2 protein. The importance of the C-terminus for channel activity is consistent with the finding that similar channel fluctuations are observed here with all three PB1-F2 analogs. The three proteins are variable in length with an overall identity of ca. 60%. Important in the context of structure/function correlates is that all three analogs contain a similar C-terminal domain with a putative transmembrane α-helix. Interestingly, all human H1N1 isolates circulating since 1950 were reported to code for a truncated PB1-F2 of 57 amino acids [5] lacking the C-terminal domain. Moreover, the current H1N1 swine flu isolates are not able to express any form of PB1-F2 since multiple Stop-codon mutations only allow the expression of the first 11 amino acids. This is consistent with initial findings that expression of PB1-F2 is species dependent and often interrupted in swine isolates [4]. Because of the missing C-terminal α-helix these proteins are therefore most likely unable to generate channel function.

The fact that the PB1-F2 peptides derived from different isolates were all able to generate similar channel like activity in planar lipid bilayers implies that the different PB1-F2 variants have the same potential of ion channel conductance within the mitochondria of infected cells. We can only speculate about the reasons why this channel type activity was recorded here but not in a previous study [12]. It is possible that the fusion efficiency of the peptides was in the present study lower than in a previous study. A lower number of proteins in the bilayer however can be beneficial for the resolution of single channel activity because individual events are not masked by the simultaneous activity of many channels. Also in the case of other pore forming peptides step like channel fluctuations can only be observed when the number of for proteins inserted into the bilayer is low [20], [23].

The analysis of PB1-F2 evoked unitary channel currents in buffers with different ion compositions reveals that the channel has two main conductance levels and both are nonselective; they transport cations as well as anions with a marginal preference for anions. The low selectivity of the channel and in particular the permeability to

gluconate implies a very simple and wide channel pore. The tendency of PB1-F2 to form oligomers [13] presumably results in a self-assembly of multiple monomers in membranes with a central water filled pore. Similar channel pores with low selectivity can also be formed by aggregation of small membrane proteins from other viruses [24], [25], [26] or by the aforementioned alamethicin [22].

One particular feature of the PB1-F2 induced channel activity is the occurrence of at least two defined conductance levels, which can be achieved directly from the closed state. This is not unique to PB1-F2 but can also be observed with other small channel forming membrane proteins such phospholamban [27]. Also the antibiotic peptide alamethicin generates multiple unitary current levels whose conductances obey a geometrical progression; each transition is thought to result from the uptake or release of an individual monomer within the conducting bundle [28]. This explanation however does not hold true for the PB1-F2 generated conductances because inspections of the current traces also revealed intermediate closures from the high conductance level to lower levels (see Figure 2C). Such behaviour cannot be explained by dynamic uptake or release of individual monomers from a conducting bundle. We must hence conclude that the low conductance level is a real substate of a channel protein build with a fixed number of monomers.

Recent data stress that PB1-F2 has the potential to modulate IAV virulence. A single amino acid exchange in the C-terminal region of the protein from Asn66 to Ser66 is sufficient to convert a virus of moderate pathogenicity into a highly pathogenic one [7]. It was also fund that the expression of the 1918 IAV PB1-F2 in mice enhanced secondary bacterial pneumonia [6]. This finding is important because most IAV related deaths are due to bacterial super-infection [6]. The present data show that the three PB1-F2 peptides from IAV of different pahtogenic potential have in spite of their sequence differences the same ability to generate ion channel activity. Hence the difference in biological function between the three PB1-F2 proteins must be due to other properties such as mitochondrial targeting or association with other proteins. Notably, the two PB1-F2 proteins, which were derived from the PR8 isolate and from the Spanish flu isolate, differ in amino acid 66, which is a Ser in IAV_{SF2} and an Arg in

IAV_{PR8} (Figure 1); this mutation, which accounts for the difference in pathogenicity [7], is within the mitochondrial targeting sequence [9].

Acknowledgments: Computer time was provided on the IBM Regatta system (Hessischer Hochleistungsrechner) at the Hochschulrechenzentrum Darmstadt.

References Chapter 3

[1] Lamb RA, Takeda M (2001) Death by Influenza virus protein. Nat Med. 7:1286-1288

[2] Yewdell J, Garcia-Sastre A (2002) Influenza virus still surprises Curr Opin Microbiol 5:414-418

[3] Webby RJ, Webster RG (2001) Emergence of Influenza A viruses. Philos Trans R Soc London B Biol Sci 356:1817-1828

[4] Chen W, Calvo PA, Malide D, Gibbs J, Schubert U, et al. (2001) A novel influenza A virus mitochondrial protein that induces cell death. Nat Med 7: 1306-1312

[5] Zell R, Krumbholz A, Eitner A, Krieg R, Halbhuber KJ, et al. (2007) Prevalance of PB1-F2 of influenza A viruses. J. Gen Virol 88: 536-546

[6] McAuley JL, Hornung F, Boyd KL, Smith AM, McKeon R, et al. (2007). Expression of the 1918 influenza A virus PB1-F2 enhances the pathogenesis of viral and secondary bacterial pueumonia. Cell Host & Microbe 2: 240–249

[7] Conenello GM, Zamarin D, Perrone LA, Tumpey T, Palese P (2007) A single mutation in the PB1-F2 of H5N1 (HK/97) and 1918 influenza A viruses contribute to increased virulence. Plos Pathogens 3: 1414-1421

[8] Schnitzler SU, Schnitzler P (2009) An updateon swine-origin influenza virus A/H1N1. Virus Genes. 39:279-292

[9] Gibbs, JS, Malide D, Hornung F, Bennink JR, Yewdell JW (2003) The Influenza A Virus PB1-F2 Protein Targets the Inner Mitochondrial Membrane via a Predicted Basic Amphipathic Helix That Disrupts Mitochondrial Function. J Virol 77:7214-7224

[10] Zamarin D, Garcia-Sastre A, Xiao X, Wang R, Palese P (2005) Influenza Virus PB1-F2 protein induces cell death through mitochondrial ANT3 and VDAC1. PLOS Pathogens 1:40-54

[11] Lowy RJ (2003) Influenza virus induction of apoptotic and extrinsic mechanisms. Int Rev Immunol 22:425-449

[12] Chanturiya AN, Basanez G, Schubert U, Henklein P, Yewdell J W, et al. (2004) PB1-F2, an Influenza A virus-encoded proapoptotic mitochondrial protein creates variably sized pores in planar lipid membranes. J Virol 78: 6304–6312

[13] Bruns K, Studtrucker N, Sharma A, Fossen T, Mitzner D, et al. (2007) Structural characterization and oligomerization of PB1-F2, a proapoptotic influenza A virus protein. J Biol Chem 282: 353-363

[14] Chevalier C, Al Bazzal A, Vidic J, Fevier V, Bourdieu C, et al. (2010) PB-1F2 influenza A virus protein adopts a beta-sheet conformation and forms amyloid fibres in a membrane environment. J Biol Chem (in press)

[15] Henklein P, Bruns K, Nimitz M, Wray V, Tessmer U, et al. (2005) Influenza A virus protein PB1-F2: synthesis and characterization of the biologically active full length protein and related peptides. J Peptide Sci 11: 481-490

[16] Killian JA, von Heijne G. (2000). How proteins adapt to a membrane-water interface. Trends Biochem Sci 25:429–434

[17] Mitzner D, Dudek SE, Studtrucker N, Anhlan D, Mazur I, et al. (2009) Phosphorylation of the influenza A virus PB1-F2 protein by PKC is required for effective virus propagation. Cellular Microbiology 1:1502-1516

[18] Hille B (2001) Ion channels of excitable membranes, Sinauer, Sunderland Massachusetts USA

[19] Madan V, Castelló A, Carrasco L (2008) Viroporins from RNA viruses induce caspase-dependent apoptosis. Cell Microbiol 10:437-451

[20] Hessa T, White ST, van Heijne G (2005) Membrane insertion of a potassium-channel voltage sensor. Science 307-1427

[21] Herce HD, Garcia AE, Litt J, Kane RS, Martin P, et al. (2009) Arginine-rich peptides destabilize the plasma membrane, consistent with a pore formation translocation mechanism of cell penetrating peptides. Biophys. J. 97:1917-1925

[22] Binder H, Lindbolm G (2003) Charge-dependent translocation of the Trojan peptide penetrating across lipid membranes. Biophys. J 85: 982-995

[23] Eisenberg M, Hall JE, Mead CA (1973) The nature of the voltage-dependent conductance induced by alamethicin in black lipid membranes. J. Membrane Biol 14: 143-176

[24] Fischer WB, Sansom MSP (2002) Viral ion channels: structure and function. Biochem Biophys Acta 152: 27-45

[25] Gonzales ME, Carrasco L (2003) Viroporins. FEBS Lett 552:28-34

[26] Nieva JL, Agirre A, Nir S, Carrasco L (2003) Mechanisms of membrane permeabilization by picornavirus 2B viroporin. FEBS Letters 552: 68-73

[27] Kovacs RJ, Nelson MT, Simmerman HK, Jones LR (1988) Phospholamban forms Ca^{2+} selective channels inlipid bilayers. J Biol Chem 263: 18364-18368

[28] Duclohier H, Wróblewski H (2001) Voltage-dependent pore formation and antimicrobial activity by alamethicin and analogues. J. Mmembrane Biol. 184: 1-12

[29] Schrempf H, Schmidt O, Kummerlin R, Hinnah S, Muller D, et al. (1995) A prokaryotic potassium ion channel with two predicted transmembrane segments from Streptomyces lividans. EMBO J 14: 5170-5178

[30] Montal M, Mueller P (1972) Formation of bimolecular membranes from lipid monolayers and a study of their electrical properties. Proc Natl Acad Sci USA 69:3561-3566

[31] Röder R, Brund K, Sharma A, Eissmann AA, Hahn F, et al. (2008) Synthesis of full length PB1-F2 influenza A virus proteins from ‘spanish flu’ and ‘bird flu’. J Peptide Science 14:954-962

[32] Humphrey, W., Dalke, A. and K. Schulten (1996) VMD - Visual molecular dynamics. J Molec Graphics 14:33-38

[33] MacKerell Jr A D, Bashford D, Bellott M, Dunbrack RL, Evanseck JD, et al. (1998) All-atom empirical potential for molecular modelling and dynamics Studies of proteins. J Phys Chem B 102:3586-3616

[34] Schlenkrich M, Brickmann J, MacKerell Jr AD, and Karplus M (1996) An empirical potential energy function for phospholipids: criteria for parameter optimization and applications. In Biological Membranes: A Molecular Perspective from Computation and Experiment. K. M. Merz and B. Roux, editors. Birkkäuser, Boston. 31-81

[35] Jorgensen L W, Chandrasekhar J, Madura JD, Impey RW, Klein ML (1983) Comparison of simple potential functions for simulating liquid water. J Chem Phys 79:926-935

[36] Roux Lab Home Page (2006) http://thallium.bsd.uchicago.edu/RouxLab/. Kale L, Skeel R, Bhandarkar M, Brunner R, Gursoy A, Krawetz N, Phillips J

[37] Shinozaki A, Varadarajan K, and Schulten K (1999) NAMD2: greater scalability for parallel molecular dynamics. J Comput Phys 151:283-312

[38] Essmann U, Perera L, Berkowitz ML, Darden T, Lee H , et al. (1995) A smooth particle mesh Ewald method. J Chem Phys 103:8577-8593

[39] Tu K, Tobias DJ, Klein ML (1995) Constant pressure and temperature molecular dynamics simulation of a fully hydrated liquid crystal phase dipalmitoylphosphatidylcholine bilayer. Biophys J. 69:2558-2562

[40] Feller SE, Zhang Y, Pastor RW, Brooks BR (1995) Constant pressure molecular dynamics simulation: the Langevin piston method. J Chem Phys 103:4613-4621

[41] Frishman D, Argos P (1995) Knowledge-based protein secondary structure assignment. Proteins. 23:566-579.

Chapter 4: Phospholamban

Ion channel activity of pentameric phospholamban

Abstract

Phospholamban (PLN) is involved in the contractility of cardiac muscle by regulating intracellular calcium concentration (Ca^{2+}_{cyt}) of cardiac myocytes. PLN is a regulator of sarco-/ endoplasmic Ca-ATPase (SERCA) but concerning its structure and activity many questions are still open. In the present paper we focused our attention on the main issue of whether the more stable pentameric form can be an ion channel. We used two different bio-mimetic systems namely supported nano-BLMs and traditional black lipid membranes, BLMs supporting the view that PLN works as an ion channel.

Introduction

Phospholamban (PLN) is a 52-amino-acids-long, integral membrane protein, which is involved in the contractility of cardiac muscle by regulating the intracellular calcium concentration (Ca^{2+}_{cyt}) of cardiac myocytes. PLN modulates Ca^{2+}_{cyt} by regulating the cardiac sarco-/ endoplasmatic Ca-ATPase (SERCA). This membrane protein in the sarcoplasmic reticulum (SR) maintains a low intracellular calcium concentration by pumping Ca^{2+} into the SR. Activity of SERCA is inhibited by the unphosphorylated PLN, whereas phosphorylated PLN releases SERCA inhibition and allows the pumping of calcium. The PLN monomer (6KDa) is in equilibrium with its pentameric form [1]; the more stable pentamer is a 30KDa-oligomer in which each monomer is composed of three domains: a helical cytoplasmic domain, a semi-flexible loop and a helical hydrophobic transmembrane domain [2], [3]. Various details on the structure of PLN and its activity are still a matter of debate. It is not known whether the interaction with SERCA is due to the monomeric or pentameric form [4], [5], [6]. Structural details of the PLN pentamer have also not yet been rectified and currently a so-called bellflower model [2] and a pinwheel model [7] of the pentamer are discussed in literature [2], [7], [8], [9].

In this paper we focused our attention on the main issue whether the more stable pentameric form is an ion channel or simply a storage form. A combination of functional studies [10], mutagenesis [11], [12], structural studies [2], [13] and molecular modelling [14] support the hypothesis that PLN can indeed have a transmembrane orientation with a hydrophilic central pore and that this complex can conduct ions. The channel forming hypothesis has been recently questioned by molecular dynamic simulations [15], [17]. Molecular dynamic simulations based on new high-resolution NMR structures show that the PLN forms a pore-like structure but that this pore is unable to conduct ions [16], [17]. Moreover, in a recent paper based on electrochemical measurements it was suggested that pentamer PLN displays just a storage form for monomer and does not generate any channel activity [16]. The authors observed no specific elevation of conductance in a tethered bilayer lipid membrane upon addition of $CaCl_2$ to the buffer solution [16].

In order to understand whether PLN pentamer can have ion channel activity, we have performed experiments by using two different bio-mimetic systems namely supported nano BLMs and traditional black lipid membranes (BLMs); both systems are characterized by the lipid bilayer membrane(s) separating two compartments (cis- and trans-chamber) containing aqueous solutions. These experimental systems are suitable for mimicking at the best the intra- and the extra-cellular sides of a biological membrane. In this paper the function of PLN pentamer was studied by conductivity measurements for the first time. This new approach allows to detect pore formation and to study directly the selectivity of ion channels. In order to confirm the results obtained from conductivity measurements, single channel recordings in traditional BLMs were carried out. Our results, which were obtained by two complementary approaches, show that PLN conducts ions across a lipid bilayer by an inherent ion channel activity.

Material and Methods

Nano BLMs

Nano BLMs consist of polycarbonate membranes (characterized by 1 μm diameter pores, pore density 10^5-10^8 pores*cm^{-2} according to pore size, Whatman Kent, England) covered by gold and octadecanethiol. For Au-covering a coating unit PS3 (Agar Aids, UK) was used. A self-assembled monolayer of octadecanethiol (ODT) (Sigma-Aldrich, USA) was obtained by spreading 3mM ethanolic solution of ODT on the gold layer. Subsequently, the ethanol was allowed to evaporate totally and the membrane was rinsed by a series of washing steps in ethanol, water and ethanol to eliminate ODT residues; at the end, it was totally dried. On the top of the gold-polycarbonate membrane, an octadecanethiol self-assembled monolayer (SAM-ODT) was formed. A lipid bilayer was formed on each pore of the polycarbonate membrane using dioleoylglycerophosphocholine (DOPC) (Avanti polar lipids, Alabaster, AL, USA) and cholesterol (Aldrich Chemical Co., USA), as described in Favero et al. [18], [19]. Experimental measurements were performed in a custom-made cell [18], [19]. The bi-cell, which was fabricated by G. Favero et al. [19], was modified including both, the two reference electrodes and the two Au-electrodes in the same working cell. Since conductivity measurements are temperature-sensitive (2% increase per one °C) the working cell was placed in a thermostated chamber kept at 25 °C. Solutions were injected into the chamber by using a peristaltic pump (ECONO PUMP, BIO RAD, USA), modified in order to keep the engine out of the Faraday cage.

The full-length wildtype phospholamban (PLN), obtained from Veglia's group, was embedded in the bilayer by fusing vesicles containing PLN at a 3:1:1 mass ratio mixture of DOPC: Cholesterol: PLN.

Electrochemical Impedance Spectroscopy (EIS) measurements were recorded by a PGSTAT12 Autolab potentiostat/ galvanostat (Eco Chemie), with an in-built frequency response analysis FRA2 module. The measurements were controlled by a personal

computer, using Autolab FRA software. Potentials were measured versus Ag/ AgCl electrodes. Impedance spectra were recorded within a frequency range of $5*10^{-3}$ - 10^{6} Hz and at zero offset potential.

Conductivity measurements were carried out by a 712 conductometer (Metrohm) modified with a resistance of 47KΩ in parallel to the working cell. The use of the peristaltic pump and the conductometer interfaced with the computer allowed to carry out measurements under constant perfusion of the bi-cells.

Traditional BLMs

Experiments with planar lipid bilayers were carried out as previously described [20] using the Montal-Müller technique [21] with a 0.4 mg/ml solution of L-α-phosphatidylcholine (type IV-S >= 30 % TLC; Sigma-Aldrich (Steinheim, Germany) in n-decane (Carl Roth, Karlsruhe, Germany). The measurements were performed in a buffer containing 500mM KCl, 10 mM Mops/Tris pH 7. The Ag/ AgCl electrode in the trans-chamber was directly connected to the head stage of a current amplifier (EPC 7, List, Darmstadt, Germany); the electrode in the cis-chamber was connected to the ground. At positive potentials the electrode in the trans-chamber was positive and the electrode in the cis-chamber negative. To prevent surface potential effects both electrodes were connected with the bath solution via an agar bridge (2% agarose in 2 M KCl). Currents were recorded and stored by an analog/ digital converter (LIH 1600, HEKA electronics, Neustadt, Germany) at 4 KHz after low pass filtering at 1 kHz. Data were analyzed by Patchmaster software (HEKA electronics, Neustadt, Germany) and Igor Pro (WaveMetrics, Oregon, USA). Before adding the full-length wildtype phospholamban (wildtype PLN) protein to the trans-chamber at a final concentration of ca. 0.3µM the bilayer conductance was recorded for approximately 1 hour in order to exclude artefacts from contaminations. Only bilayers without artefacts were used for reconstitution of PLN.

In order to further determinate the selectivity of the channel experiments were carried out in which K^+ in the cis-chamber was exchanged against Na^+. The value of the resulting shift of the reversal potential (E_{rp}) was used to calculate the relative permeability (α) of Na^+ compared to K^+ ($\alpha=P_{Na+}/ P_{K+}$). Therefore the Goldman-Hodgkin-Katz equation was transformed in a first step:

Equation 4.1 $$E_{rp} = (R*T / Z*F) * \ln (\alpha*([K^+]_{cis} / [Na^+]_{trans}))$$

Because the ion concentrations in the chambers $[K^+]_{cis}$ and $[Na^+]_{trans}$ were equal, the equation could be simplified and transformed in a second step:

Equation 4.2 $$\alpha = \mathrm{Exp} (E_{rp}*Z*F / R*T)$$

Results and Discussion

Nano BLMs

In the nano BLMs system, we first recorded specific resistance and specific capacitance values to verify the integrity of the membrane and incorporation of PLN. Subsequently, conductivity measurements were carried out on the same membrane, where PLN was successfully incorporated.

Specific resistance and specific capacitance values were recorded by performing EIS measurements. The respective values were obtained by fitting an equivalent circuit to the experimental data (Figure 4.1); the data obtained with and without PLN show the same order of magnitude for the specific capacitance (1.4 and 1.3 μFcm^{-2} for nano BLMs before and after PLN incorporation, respectively) and a decrease in the specific resistance by a factor of 10^4 after PLN incorporation (30.4 and $5.4*10^{-3}$ $M\Omega cm^2$ for nano BLMs before and after PLN incorporation, respectively). The equivalent circuit describes the electrical properties of the bilayer. The fact that approximately the same capacitance value was recorded in the presence and absence of PLN, proves the integrity of the membrane; the decrease in resistance associated with PLN suggests a successful incorporation of phospholamban and the presence of ion conducting pores. It is well known that channel formation by peptides or small proteins in bio-mimetic models causes specific resistance reduction [22], [23].

To perform conductivity measurements, we used the following protocol: a background electrolyte (10mM TRIS buffer, pH=7.5) was let to flow (2 ml/min) to both cell compartments. After a constant conductivity value was reached, this buffer was replaced by a solution containing the background electrolyte plus a fixed concentration (10mM and 20mM) of a suitable electrolyte, i.e. KCl, $NaClO_4$ and ChoCl (choline chloride).

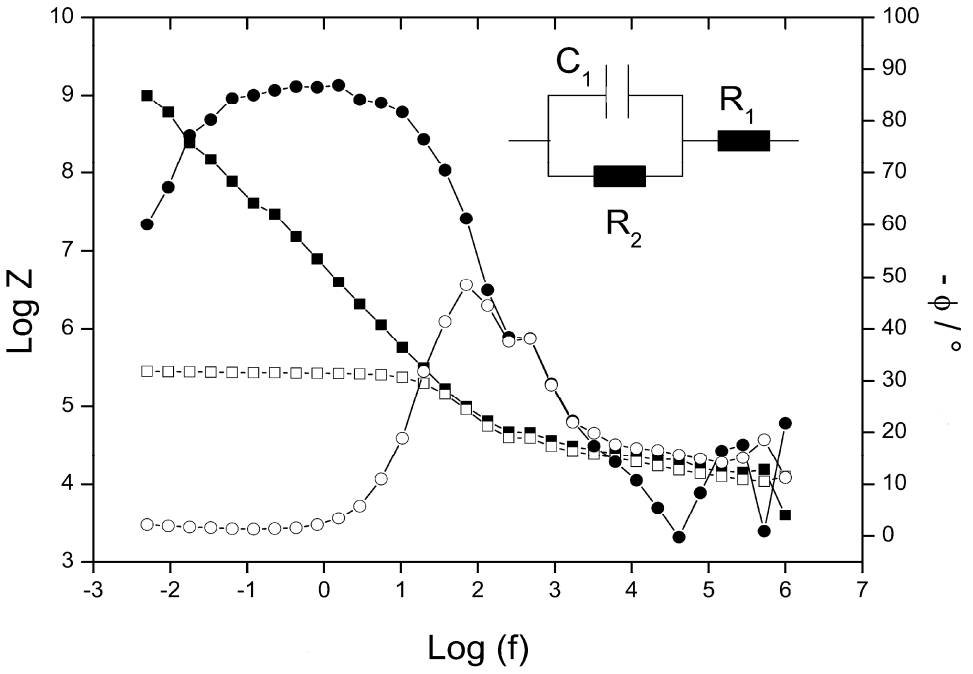

Figure 4.1 Logarithm of the impedance, Z (square symbol) and phase, (circle symbol) vs. logarithm of the frequency (f): curves recorded on nano BLMs (filled symbol) and nano-BLMs containing PLN (empty symbol). All data were obtained at zero offset potential. 10mM TRIS buffer pH=7,5 was present into working cell compartments. Inset: Equivalent circuit (C_1= bilayer capacitance; R_2= bilayer resistance; R_1=electrolyte resistance) used to fit the experimental data obtained from the Electrochemical Impedance Spectroscopy.

To check the system's reversibility after each electrolyte addition, the background solution was once again perfused into the bi-cell. Figure 4.2 reports the conductivity (κ) value vs. time for nano BLMs, embedding PLN in response to different electrolyte solutions. The data show that the conductivity value of nano BLMs containing PLN increased when different electrolytes were perfused through the chamber. Addition of electrolytes had no impact on the conductivity value in nano BLMs in the absence of PLN, meaning that the increase in conductivity is a property of PLN. The different tested electrolytes were chosen in such a way to make the contribution of different ions to the whole conductivity recorded evident. In particular, the different recorded conductivity between $NaClO_4$ and NaCl (at the same concentration) can be justified simply on the basis of equivalent conductance values of Cl^- and ClO_4^- (equivalent

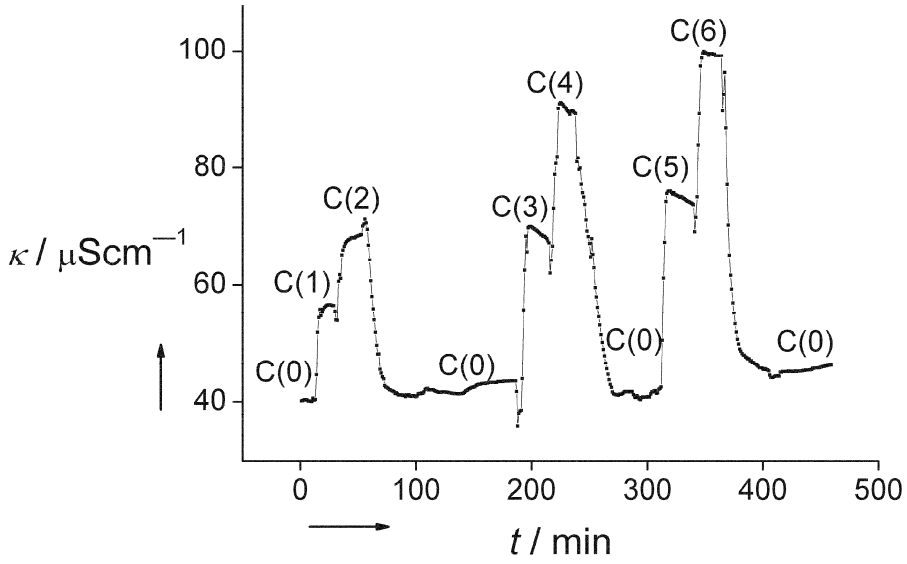

Figure 4.2 Conductivity (measured by conductometer) vs. time, recorded on PLN embedded in nano BLMs. Data were collected under constant perfusion (2 ml/min) of bicells. Experiment started with only TRIS buffer 10mM, pH=7,5 [C(0)] in the bicell. The solution was exchanged by flowing into bicell compartments TRIS plus one of the following electrolyte: ChoCl, $NaClO_4$ and NaCl at different concentration [C(1)=ChoCl 10mM, C(2)=ChoCl 20mM, C(3)= $NaClO_4$ 10mM, C(4)= $NaClO_4$ 20mM C(5)= NaCl 10mM, C(6)= NaCl 20mM] in TRIS-HCl buffer 10mM, pH=7,5.

conductance at infinite dilution is 76.3 and 67.3 Scm^2eq^{-1} respectively) since the Na^+ contribution is the same. Useful information about PLN may be obtained by comparing ChoCl and NaCl conductivity values. By considering the equivalent conductance at infinite dilution of NaCl (126.4 Scm^2eq^{-1}), Cl^- contributes for ca. 60% of the total recorded conductivity. Thus, for ChoCl the expected conductance is >60% of that of NaCl at the same concentration if also Cho^+ contributes to the signal. Since the conductance of ChoCl is around 60% of that of NaCl, it is evident that Cho^+ does not give an appreciable contribution to the whole recorded conductance signal. These results suggest that PLN is permeable only to relatively small ions as Na^+, Cl^- and ClO_4^- while bigger ions as Cho^+ are unable to pass trough.

The present data together with previous ones [2], [10], [24] are consistent with the view that the pentameric PLN can form nonselective ion conducting pores. Based on their model of a bellflower structure, Oxenoid and Chou suggested that many physiologically relevant ions such as Na^+, K^+, Ca^{2+} and Cl^- are small enough to pass through the narrowest part of the pentamer PLN (diameter ≈3.6Å). In agreement with the latter model the Cho^+ cation (radius 3.3Å [25]) was found not be conducted because it is larger than the estimated PLN pore [2].

Traditional BLMs

To further test the channel forming ability of PLN, the same protein was incorporated in traditional BLMs for single channel recordings. Figure 4.3A shows some representative recordings from these experiments revealing typical current fluctuations between a closed and a defined open state. Figure 4.3C illustrates a plot of the unitary open channel currents measured under symmetrical conditions (500 mM KCl) as a function of voltage. The I/V relation is linear, reverses at 0 mV and has a slope conductance of 27 pS. These data reveal that PLN has no apparent voltage dependency, meaning that it is potentially active at 0 mV. When the KCl solution in the cis-chamber was replaced with NaCl, the reversal voltage shifted negative by about 36 mV; thereby the cis-chamber was connected to the ground, which means that negative currents represent a flux of Na^{2+} from cis to trans and a positive current a flux of K^+ from trans to cis. The results of these experiments confirm the data of Figure 4.2 in that the protein conducts Na^+; the shift in reversal voltage, however, also means that the channel prefers K^+ over Na^+. By applying the Goldman-Hodgkin-Katz equation (Goldman, 1943) the relative permeability P_{Na+}/ P_{K+} could be determined as 0,25 which means that PLN conducts K^+ 4 times better than Na^+.

Altogether, these findings are in good agreement with data presented by Arkin (1995). He reported that PLN generated single channel fluctuations, which conducted equally well K^+ and Ca^{2+} and to a lesser extend also Na^+.

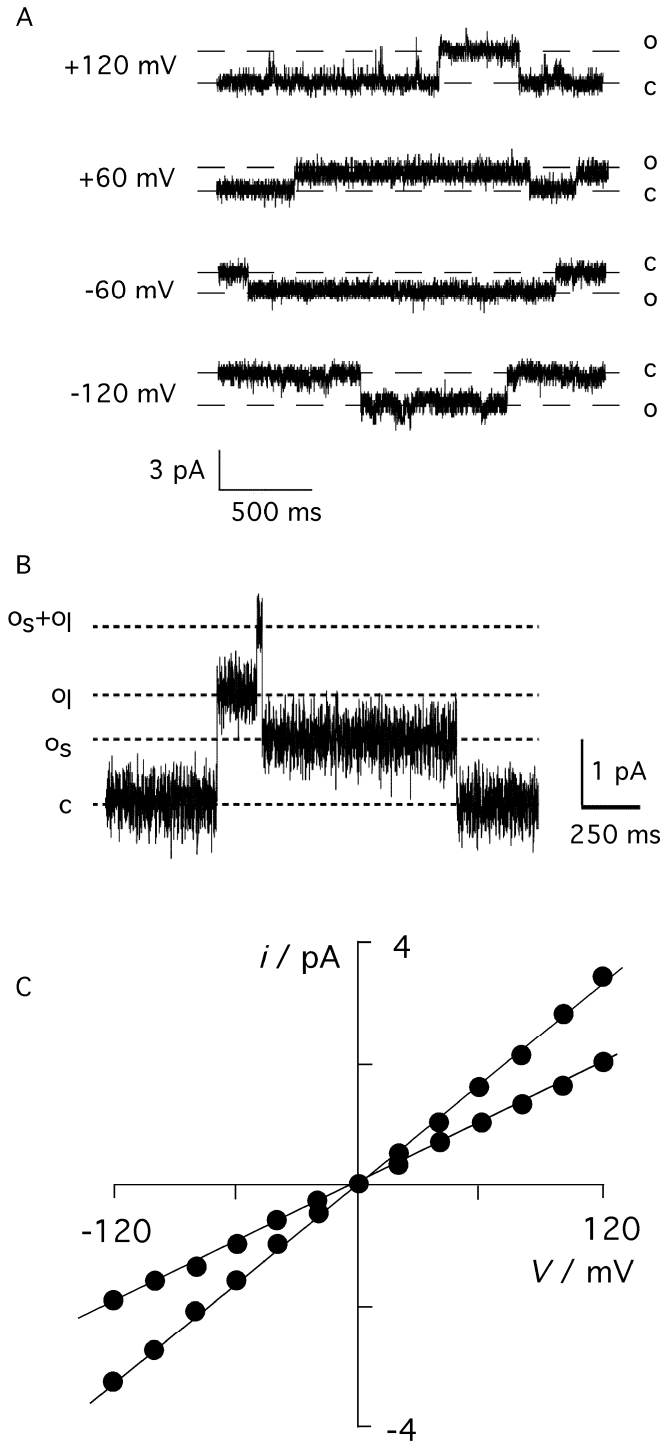

Figure 4.3 PLN generates single channel fluctuations in planar lipid bilayer. **A** Single channel activity recorded at different holding potentials, from -120mV to 120mV in symmetrical solution with 500mM KCl in 10mM MOPS/ TRIS (pH=7) buffer. c and o refer to the closed and open states of the channel, respectively. **B** Example of concomitant opening/ closing of large

conductance and small conductance. The two events are additive. First the large conductance opens (o_l) before also a lower conductance opens (o_s). Together the current reaches the sum of both amplitudes (o_l+o_s). Upon closing of the large conductance the current reaches the amplitude of the small conductance. Closing of the small conductance brings the current back to the baseline (c). **C** Current/ voltage relation (I/V curve) of large and small unitary currents obtained in same conditions as in **A** and **B**.

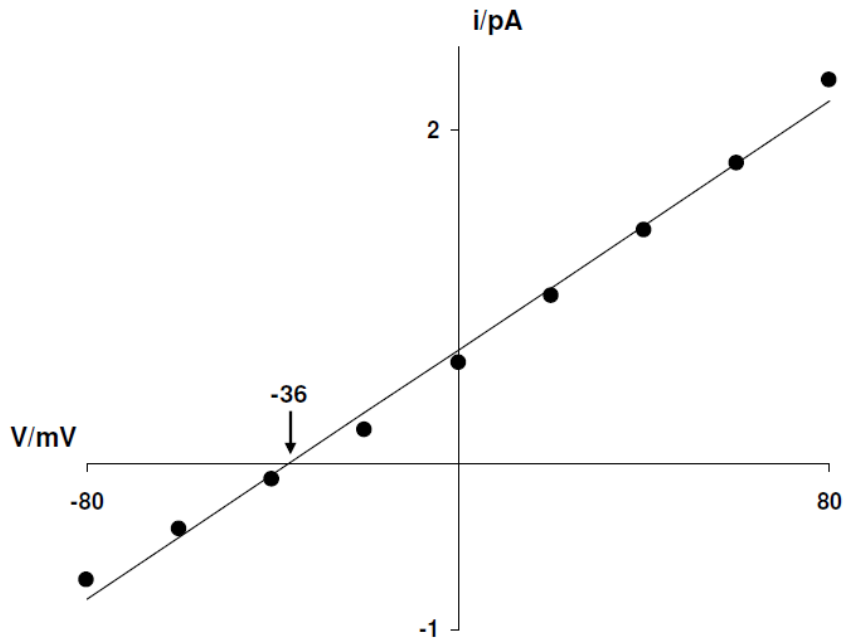

Figure 4.4 I/V curve of single channel fluctuations after the exchange of K^+ in the cis-compartment against Na^+ (conditions: 500 mM KCl trans, 500 mM NaCl cis, 10mM Mops/Tris, pH 7). The arrow indicates the reversal potential. The I/V curve section above the x-coordinate represents a net current of K^+ (from trans to cis), the section beneath a net current of Na^+ (from cis to trans). The electrochemical equilibrium at -36 mM shows that K^+ is preferred compared to Na^+.

In many bilayers an additional smaller conductance was found together with the larger 27 pS conductance. Figure 4.3B shows an example for the independent opening/ closing of the two distinctly different conductances. In the example trace, obtained at +60 mV holding voltage, the small conductance opens on top of the large conductance; both conductances close in opposite sequence. The fact that the two

conductances are like in the example always additive, means that the low conductance is not a subconductance level of the larger one. An I/V-plot (Figure 4.3C) of the small unitary channel fluctuations again reveals a linear relation, which reverses at 0 mV and has a conductance of 16 pS.

To obtain information on the basic functional parameters of the large and small conductance, the channel fluctuations were fitted by the QuB algorithm [26]. Good fits could be achieved assuming a simple o-c model. For a reference voltage of +80 mV this procedure yields an open probability (P_0) of 0.5 and 0.1 for the large and the small conductance, respectively. The mean open dwell times were 680 ms and 560 ms for the large and small conductance, respectively. The open probability and the relatively long open channel dwell times look similar to those reported previously for PLN channel activity [10].

Also in previous experiments [10], [24] small unitary channel fluctuations with two different conductances were observed upon reconstituting full-length PLN or the C-terminal fragment (amino acids 26-52) in lipid bilayers. Worth noting is that the present data and the previous recordings were obtained with different bilayer techniques and in different lipids [10], [24]; this stresses the fact that the channel events recorded with PLN are due to the protein and not a bilayer artefact.

Conclusions

In conclusion, the present results, obtained by two independent electrophysiological methods and previous works [2], [10], [24], support the view that PLN works as an ion channel. Unlike to what was predicted from some molecular models [15], [16], [17] the present experimental data show that the PLN pentamer can form a pore permeable to small ions; the protein exhibits gating, meaning that it fluctuates between an open and a closed state. In this context, it is reasonable to assume that the high-resolution NMR structure and the molecular models simply represent the channel in the closed state. The open/ closed dwell times of the PLN channel are in the ms range and

hence far too long for being detected in simulations. The present data also provide an explanation for the absence of a measurable Ca^{2+} conductance in a previous study. Since PLN generates a nonselective conductance, it is not surprising that an elevation of $CaCl_2$ against a 100-fold higher background of KCl was not generating a measurable current; the current was probably masked by the large KCl conductance. The present study does not bear a direct answer to the question on the physiological role of PLN. Nonetheless, the confirmation of PLN generated channel activity supports a previous model [10] according to which this protein generates a short circuit in the membrane.

The demonstration of channel function of PLN is of importance as it can be involved in the regulation of cardiac contraction/ relaxation. The voltage-independent activity of PLN suggests that it can be active at any prevailing membrane voltage of the sarcoplasmic reticulum. Activation of the channel could generate a futile cycle for the Ca-ATPase and thus regulate the latter. PLN generated channels could be a promising therapeutic target in heart failure and other cardiac diseases [27], [28]. The integration of both present experimental systems provides a strong tool for in-depth studies of PLN channel function with respect to selectivity and pharmacology.

Acknoledgments

We thank Prof. G.Veglia for providing phospholamban used in this work. The financial support from Ente Cassa di Risparmio di Firenze and Ministero dell'Istruzione, Università e Ricerca (PRIN project), is gratefully acknowledged.

References Chapter 4

[1] Cornea RL, Jones LR, Autry JM, Thomas DD (1997) Mutation and phosphorylation change the oligomeric structure of phospholamban in lipid bilayers. Biochemistry. 36, 2960-2967

[2] Oxenoid K, Chou JJ (2005) The structure of phospholamban pentamer reveals a channel-like architecture in membranes. Proc. Natl. Acad. Sci. USA;102:10870–10875

[3] Zamoon J, Mascioni A, Thomas DD, Veglia G (2003) Phospholamban structural dynamics in lipid bilayers probed by a spin label rigidly coupled to the peptide backbone. Biophys. J. 85, 2589-2598

[4] Kimura Y, Kurzydlowski K, Tada M, MacLennan DH (1997) Phospholamban Inhibitory Function Is Activated by Depolymerization. J. Biol. Chem. 272, 15061-15064

[5] Reddy LG, Jones LR, Thomas DD (1999) Co-reconstitution of Phospholamban Mutants with the Ca-ATPase Reveals Dependence of Inhibitory Function on Phospholamban Structure. Biochemistry 38, 3954-3962

[6] Stokes DL, Pomfret AJ, Rice WJ, Glaves JP, Young HS (2006) Interactions between Ca^{2+}-ATPase and the pentameric form of phospholamban in two-dimensional co-crystals. Biophys. J. 90, 4213-4223

[7] Traaseth NJ, Verardi R, Torgersen KD, Karim CB, Thomas DD, Veglia G (2007) Spectroscopic validation of the pentameric structure of phospholamban. Proc. Natl. Acad. Sci. U S A. 104, 14676-14681

[8] Tatulian S, Jones L, Reddy L, Stokes D, Tamm L (1995) Secondary structure and orientation of phospholamban reconstituted in supported bilayers from polarized attenuated total reflection FTIR spectroscopy. Biochemistry. 34, 4448-56

[9] Arkin IT, Rothman M, Ludlam CFC, Aimoto S, Engelman DM, Rothschild KJ, Smith SO (1995) Structural model of the phospholamban ion channel complex in phospholipid membranes. J. Mol. Biol. 248, 824-834

[10] Kovacs R, Nelson M, Simmerman H, Jones L (1988) Phospholamban forms Ca^{2+}-selective channels in lipid bilayers. J. Biol. Chem. 263, 18364-18368

[11] Simmerman HKB, Kobayashi YM, Autry JM, Jones LR (1996) A Leucine Zipper Stabilizes the Pentameric Membrane Domain of Phospholamban and Forms a Coiled-coil Pore Structure. J. Biol. Chem. 271, 5941-5946

[12] Arkin I, Adams P, MacKenzie K, Lemmon M, Brünger A, Engelman D (1994) Structural organization of the pentameric transmembrane alpha-helices of phospholamban, a cardiac ion channel. EMBO J. 13, 4757–4764

[13] Arkin I, Adams P, Brünger A, Smith S, Engelman D (1997) Structural perspectives of phospholamban. A helical transmembrane pentamer. Annu. Rev. Biophys. Biomol. Struct. 26, 157-79

[14] Sansom M, Smith G, Smart O, Smith S (1997) Channels formed by the transmembrane helix of phospholamban: a simulation study. Biophys. Chem. 69, 269-81

[15] Kim T, Lee J, Im W (2008) Molecular Dynamics Studies on Structure and Dynamics of Phospholamban Monomer and Pentamer in Membranes. Proteins 76, 86-98

[16] Becucci L, Cembran A, Karim CB, Thomas DD, Guidelli R, Gao J, Veglia G (2009) On the Function of Pentameric Phospholamban: Ion Channel or Storage Form? Biophysical J. 96, L60-L62

[17] Maffeo C, Aksimentiev A (2009) Structure, Dynamics, and Ion Conductance of the Phospholamban Pentamer. Biophysical J. 96, 4853-4865

[18] Favero G, D'Annibale A, Vampanella L, Santucci R, Ferri T (2002) Membrane supported bilayer lipid membranes array: preparation, stability and ion-channel insertion Anal. Chim. Acta. 460, 23-34

[19] Favero G, Campanella L, D'Annibale A, Santucci R, Ferri T (2003) Mixed hybrid bilayer lipid membrane incorporating valinomycin: improvements in preparation and functioning. Microchem. J 74, 141-148

[20] Schrempf H, Schmidt O, Kümmerlen R, Wagner R (1995) A prokaryotic potassium ion channel with two predicted transmembrane segments from Streptomyces lividans. EMBO J. 14, 5170–5178

[21] Montal M, Mueller P (1972) Formation of bimolecular membranes from lipid monolayers and a study of their electrical properties. Proc Natl Acad Sci USA 69:3561-3566

[22] Gallucci E, Micelli S, Picciarelli V (2003) in: Planar Lipid Bilayer (BLMs) and their applications. pp. 413 - 447 (Ottova-Leitmannova, A, Ed) Elsevier, Amsterdam

[23] Terrettaz S, Mayer M, Vogel H (2003) Highly electrically insulating tethered lipid bilayers for probing the function of ion channel proteins. Langmuir 19, 5567-5569

[24] Arkin IT, Rothman M, Ludlam CFC, Aimoto S, Engelman DM, Rothschild KJ, Smith SO (1995) Structural model of the phospholamban ion-channel complex in phospholipid-membranes. J. Mol. Biol. 248: 824–834

[25] Levitt DG, Decker ER (1988) Electrostatic radius of the gramicidin channel determined from voltage dependence of H^+ ion conductance. Biophys. J. 53, 33-38

[26] Qin F, Li L (2004) Model-based fitting of single channel dwell time distributions. Biophysical J. 87, 1657-1671

[27] Brittsan AG, Kranias EG (2000) Phospholamban and cardiac contractile function. J. Mol. Cell. Cardiol. 32, 2131-2139

[28] MacLennan DH, Kranias EG (2003) Phospholamban: a crucial regulator of cardiac contractility. Nat. Rev. Mol. Cell. Biol. 4, 566-577

Erklärung

Hiermit erkläre ich an Eides statt, dass ich die vorliegende Doktorarbeit selbstständig unter Anleitung meiner akademischen Lehrer angefertigt und keine anderen als die angegebenen Hilfsmittel benutzt habe. Die vorliegende Arbeit beinhaltet in den Kapiteln 3 und 4 Ergebnisse die in Kooperationen mit anderen Arbeitsgruppen/ Hochschulen entstanden sind. Einige der Experimente und Analysen wurden daher nicht von mir selbst durchgeführt. Diese betreffen die folgenden Abschnitte/ Abbildungen:

Kapitel 3:

Fluoreszensmessungen	Figure 3.7C	Meyer-Almes FJ	HDA Darmstadt
MD-Simulationen	Figure 3.8 Figure 3.9 Figure 3.10	Henkes L	TU Darmstadt

Kapitel 4:

Impedanzmessungen	Figure 4.1 Figure 4.2	Smeazzetto S	Univers. Florenz

Die Ergebnisse aus den Kapiteln 3 und 4 sind nach Absprache mit meinen akademischen Betreuern zur Veröffentlichung eingereicht worden. Die Doktorarbeit selbst hat aber noch nicht im Rahmen einer Prüfung vorgelegen. Des weiteren bestätige ich hiermit, dass ich noch keinen Promotionsversuch, weder an der Technischen Universität Darmstadt, noch an anderen Universitäten unternommen habe.

_____ Darmstadt, 15. Juni 2010

(Michael Henkel)

Lebenslauf Darmstadt, den 15.06.2010

Vorname, Name:		Michael Henkel
Anschrift:		Hahlgartenstr. 67, 64347 Griesheim
Geburtsdatum/-ort:		27.08.1979, Wiesbaden-Sonnenberg
Familienstand:		ledig
Staatsangehörigkeit:		deutsch
Schulausbildung:	1986-1990	Grundschule Geisenheim
	1990-1999	Rheingauschule Geisenheim
Abschluß:		Allgemeine Hochschulreife
Studium:	1999-2000	Maschinenbaustudium/ TU Darmstadt
	2000	Studienfachwechsel
	2000-2003	Grundstudium der Biologie/ TU Darmstadt Vordiplom
	2003-2005	Hauptstudium mit den drei Schwerpunkten Bionik, Pflanzenphysiologie, Zell-/ Entwicklungsbiologie
	1.-9.2006	Diplomarbeit in der Arbeitsgruppe „Membran-Biophysik“ von Herrn Prof. Gerhard Thiel mit dem Überthema „Aufbau eines Labors zur Rekonstitution von Ionenkanälen im planaren Lipid Bilayer“ und dem speziellen Thema „Funktionelle Rekonstitution des viralen Kaliumkanals MA-1D-Kcv“
Doktorarbeit:	2006-5.2010	Doktorarbeit in der Arbeitsgruppe „Membran-Biophysik“ von Herrn Prof. Gerhard Thiel, methodisch anknüpfend an die Diplomarbeit: Einzelkanal-Charakterisierung von verschiedenen

		viralen und tierischen Ionenkanälen im planaren Bilayer
	Seit 6.2010	Wissenschaftlicher Mitarbeiter von Herrn Prof. Ulrich Schubert am Virologischen Institut/ Klinische und Molekulare Virologie Erlangen
Weitere Tätigkeiten:	6.-8.1999	sechswöchiges Praktikum bei Sondermaschinenbau Beer/ Wiesbaden
	7.-8.2001	siebenwöchige Aushilfstätigkeit als Werkstudent bei HBM/ Darmstadt (Meßsysteme)
	7.-9.2002	achtwöchige Beschäftigung als Werkstudent bei Aventis Pharma in der Abteilung DI&A Biotechnologie (Functional Genomics)
	9.-12.2003	Mitorganisation eines Symposiums zur Biosensorik in Zusammenarbeit mit der Entwicklungsabteilung der Daimler Chrysler AG Frankfurt und der IHK Darmstadt
	3.-5.2004	zwölfwöchige Beschäftigung als Werkstudent bei Aventis Pharma in der Abteilung DI&A High Throughput Screening
	7.-8.2004	fünfwöchiges Praktikum am MPI für Biophysik/ Frankfurt in der Abteilung Molekulare Membranbiologie bei Herrn Dr. Ermler
	9.-10.2004	sechswöchige Beschäftigung als Werkstudent bei Aventis Pharma in der Abteilung DI&A High Throughput Screening
	3.-4.2005	sechswöchiges molekularbiologisches Praktikum am Paul-Ehrlich-Institut (Langen) in der Abteilung Medizinische Biotechnologie
	2005-2006	Betreuung von Praktika und Rechenübungen als Hilfswissenschaftler

Danksagung

Mein Dank gilt allen aktuellen und ehemaligen Mitgliedern der Arbeitsgruppe Membran-Biophysik von Herrn Prof. Dr. Gerhard Thiel für die gleichzeitig gemütliche und anregende Arbeitsatmosphäre. Darüber hinaus möchte ich folgende Personen dankbar erwähnen:

Gerhard Thiel, weil er mir stets ein äußerst verständnisvoller und lehrreicher Chef war, der zu jeder Zeit ein offenes Ohr hatte und mich für unsere Arbeit zu begeistern wußte.

Ulrich Schubert, dem ich mit den Umstand zu verdanken habe, auf ein hoch interessantes Thema gestoßen zu sein.

Indra, ohne die ich wohl den „wahren Wert“ so manch einer meiner Messungen nicht erkannt hätte.

Alle meine Freunde, mit denen ich die ganzen Jahre wundervolle Zeit verbringen durfte, ob auf dem Rad, im Wasser, beim Kaffeetrinken oder anderswo.

Kathrin, die sich trotz Bergen von zu korrigierender Klausuren die Zeit nahm, meine Arbeit zu lesen.

Meine Eltern und meine Familie, die mich immer bei allem was ich tat unterstützten.